WARWICK

The Selection and Tribological Performance of Coated/Non-coated Materials for High Temperature Tribological Systems for Turbomachinery

by

Raúl Francisco Chinchilla Adell

Innovation Report

Submitted to the University of Warwick for the degree of

Doctor in Engineering

Warwick Manufacturing Group

January 2019

Table of Contents

List of Figures

List of Tables

Acknowledgements

First, I would like to thank Prof. Barbara Shollock and Dr. Daniela Proprentner for all the support, help and time given to me. I Really appreciate.

I want to also thank Cummins Turbo Technology for their interest on the Project, specially to Dr. Michael Burkinshaw and Mr. Martin Lindsay for their help and patience. Finally, Mr. Alex Stelfox for all the work carried from a purchasing perspective.

I would like to thank Prof. Richard Dashwood for the oportunity given to go to America, it was very helpful and an unforgetable experience.

Dr. Evans Mogire and Mr. Lewis Curry for all the time we spent in the Metallography Lab and their unconditional help.

Dr. Geoff West and Samuel Marks for all their help and the good moments in the Microscopy laboratory and all their help.

To my family and Liz for the huge support during this four years, probably, the outcome will have not been the same, but just making the road less incline helped a lot during the walk towards the hill.

Declaration

The work submitted here and the submissions presented were produced by the candidate during the duration of the EngD. This is my own work and the innovation report and the submissions has not been submitted for a degree at another university.

Abstract

At the hot end of the turbocharger, there are components that undergo surface-related degradation mechanisms, which include the ones that arise when the components move against each other. Not only do these degradation mechanisms affect the long-term performance of the component, they could eventually lead to catastrophic failure of the entire turbocharger. In addition, future regulations dictate higher efficiency engine systems to meet emission restrictions. These require the turbocharger to run at higher temperatures and loads, leading to reduced service life of current components if new materials are not found. As conventional materials, like stainless steels, do not tend to provide adequate friction and/or wear behaviour and cobalt-based superalloys being expensive, alternative solutions need to be explored. As the dominant degradation processes are surface-related, treating or coating the material's surface to obtain the properties required for the application offers an alternative. As coating solutions will open a wide range of materials to investigate, a time efficient process needs to be implemented by industry in order to reduce the time in obtaining an appropriate solution. From an industrial perspective, the solution must not only fit with the required engineering requirements, it must also meet business and purchasing requirements.

The present study was conducted as a research and development project with Cummins Turbo Technologies (CTT) to implement new solutions for variable geometry (VG) turbochargers that will operate in increasingly aggressive conditions. A description of how sets of selected materials behaved at three critical temperatures for turbocharger operation is discussed in terms of microstructural, mechanical and chemical changes in order to understand their behaviour in the relevant environments. The fundamental degradation aspects of a range of coatings wear are compared to stainless steels and Co-superalloys, offering new scientific knowledge in high temperature dry wear of engineering alloys and coatings.

In order to understand the performance of the materials performace in the aggressive environments experienced a series of environmental tests were conducted and characterized before and after testing. A room temperature corrosion and high temperature oxidation test were done to obtain information about the material behaviour when the turbocharger is not or is in operation, respectively. A tribology test at different temperratures within the temperature range of operation of a VG mechanism were done in order to obtain information regarding their performance while in contact. A thermal shock test was done in order to understand whether or not the coating system is able to withstand high temperature changes.

Finally, an adhesion test was done in order to understand how to coating system will behave under overstressed conditions.

From Cummins's perspective, this knowledge was enhanced by the development of comprehensive selection methodology, which will be discussed and applied throughout this thesis. The methodology includes not only engineering requirements but also accounts for business requirements. This provides an innovative aspect to the research work that has been implemented by Cummin

1. Business case

1.1. Executive Summary

The development of new engine systems is driven by the increasing regulations related to the by-products created during the fuel combustion process, which are damaging to the environment and living organisms' health. In order to determine whether the emissions regulations are met by engine systems, three kinds of testing are carried out [1]:

- Steady-state cycle testing (SC) – Used to obtain engine performance at different set loads and revolutions
- Transient cycle testing (TC) – Tries to replicate the conditions experienced by the engine system under a real road situation
- Load response testing – Smoke is sampled and analysed under different speeds and loads.

The maximum values of different chemicals measured within diesel (compression ignition) and natural gas (positive ignition) exhaust gases in these tests are controlled by EU legislation Euro VI 'a', 'b' and 'c' [1] and are shown in the table below (ESC/TC= European SC/TC, WHSC/TC= World Harmonized SC/TC).

Euro VI emissions limits								
	Limit values							
	CO (mg/kWh)	THC (mg/kWh)	NMHC (mg/kWh)	CH_4 (mg/kWh)	NO_x(1) (mg/kWh)	NH_3 (ppm)	PM mass (mg/kWh)	PM (2) number (#/kWh)
ESC (CI)	1500	130			400	10	10	
ETC (CI)	4000	160			400	10	10	
ETC (PI)	4000		160	500	400	10	10	
WHSC (3)								
WHTC (3)								

Note:
PI= positive ignition
CI=compression ignition
(1) The admissible level of NO2 component in the NOx limit value may be defined at a later stage
(2) A number standard is to be defined at a later stage and no later than 1 April 2010
(3) The limit values relating to WHSC and WHTC, replacing the limit values relating to ESC and ETC, will be introduced, at a later stage, once correlation factors with respect to the current cycles (ESC and ETC) have been stablished, no later than 1 April 2010.

Table 1.1. Emission limits for different tests carried out on engine systems (adapted from [1]).

The upcoming Euro VII is expected to further reduce these limiting values of the different chemicals found in heavy-duty exhaust gases. Limiting values for NO_x are expected to be reduced

by half and NO_2 shall be added to the recorded values. Maximum size of particles will be reduced from 23nm to 10nm [2]. These tighter limits that will enforced by the Euro VII legislation will affect the development of not only materials of components, such as cylinder heads and pistons, but also the aftertreatment, such as filters, sensor technology and power train technology or hybridisation [2].

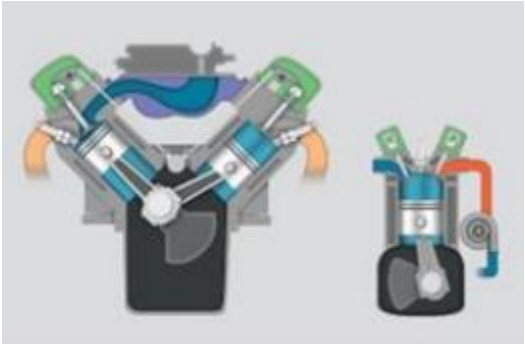

Figure 1.1. Schematic representation of engine downsizing [3].

One of the trends to achieve the ever more restrictive regulations is engine downsizing, illustrated in Figure 1.1. This is defined by the use of a smaller sized engine which nevertheless provides the same power output as its bigger version [3]. When downsizing, engine systems add turbomachinery to improve engine efficiency and power output. This improves fuel combustion efficiency due to higher amounts of available oxygen for combustion, resulting in an increase of engine power [4]. Turbocharging is considered a standard technology in the heavy-duty vehicle sector. The main reason of the boom of turbomachinery in engine systems was the need to achieve highly conflicting requirements [4]:

- Low-speed torque
- High-speed power
- Faster engine response during system changes
- Increased boosting
- Lastly, as previously mentioned, the highly demanding regulations in the reduction of exhaust chemicals exhaust after fuel combustion.

The principle of operation of a turbocharger is the exploitation of the kinetic energy of a turbine wheel driven by the hot exhaust gas coming from the engine, which is compressed at the turbine house. The exhaust gas energy is transfer to the turbine wheelthat rotates. The turbine wheel is connected to a compressor wheel by a shaft, from which the kinetic energy is transferred. As the compressor wheel rotates, air is sucked in and redirected to the engine using an outlet in the compressor housing that also compresses the air. In order to offer more control over the

amount of exhaust gas reaching the turbine to obtain better performance at different engine speeds, components like the Variable Geometry (VG) and Wastegate (WG) mechanism were developed [5].

The Cummins Turbo Technologies (CTT) VG mechanism, as shown in Figure 1.2, is composed of a fixed shroud plate and nozzle ring with extended blades, which slides using a pneumatic or electric actuator. By this movement, the pressures at the turbine wheel can be changed by reducing or increasing the exhaust gas flow area. This allows higher boost at low engine speeds, and reduce the back-pressure and turbine speed, and increase the back-pressure for braking purposes. The WG mechanism is a bypass valve that opens in order to reduce the exhaust gas flowing towards the turbine wheel, allowing the usage of a smaller housing, and wheel to achieve higher boost at lower engine speeds [6].

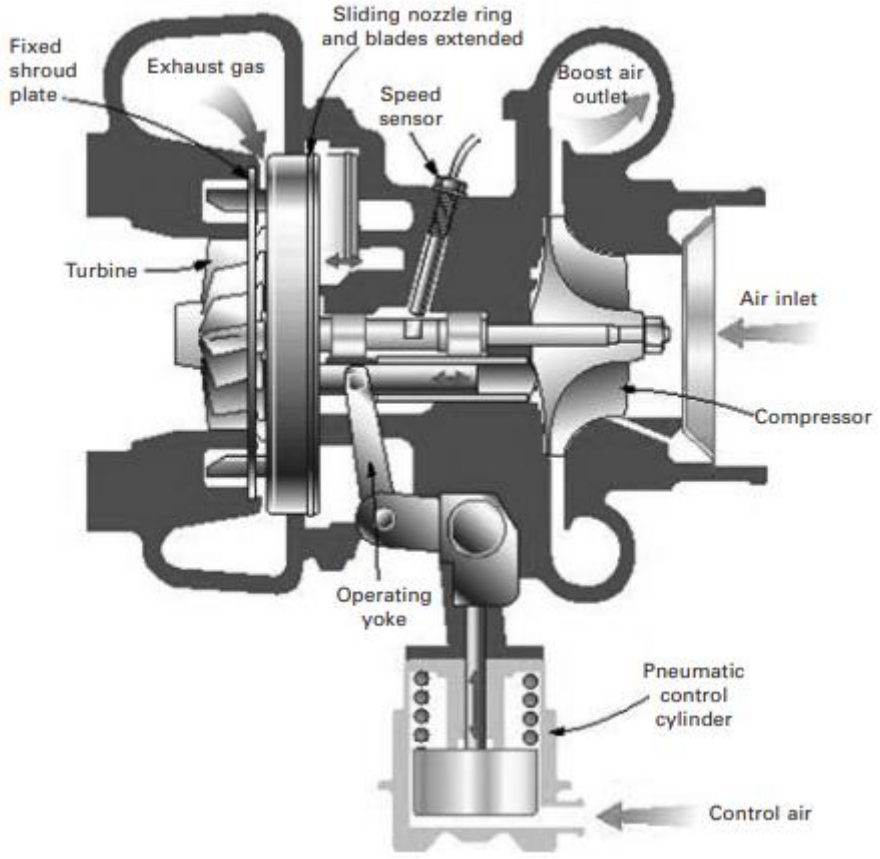

Figure 1.2. Schematic representation of a CTT VG turbocharger [6].

As these components are in the turbine housing, they already perform in a high temperature oxidative and corrosive environment. Additionally, all parts of these components are in contact with each other, which causes them to undergo tribological mechanisms that will degrade the components reliability, durability and performance over time. Further, future applications of these components will be subjected to wider temperature ranges and higher contact stresses,

as turbocharger sizes keep being reduced and exhaust gas temperature increases for efficiency purposes.

Components of the VG mechanism are made of austenitic stainless steel which offers high temperature protection while providing the required mechanical properties to sustain the applied loads. However, the wear resistance is lower than that of other materials. Wear can subsequently increase friction between parts and seize them, causing failures to the turbocharger and the engine.

Cobalt-base superalloys are known as alternative materials that can improve the tribological performance of the contact at high temperatures [7], but these alloys tend to be very expensive [8] and prices seem to be increasing [9]. Further, they have more limited manufacturing routes due to their lower ductility.

Another alternative is coatings or surface treaatments, which can provide more cost-effective solutions to improve a component's lifetime and has been previously shown in other industries i.e. tool industry [10]. Coatings/surface treatments can provide a high-performance composite material, which combines a cost-effective substrate for the application combined with a material that can counter or reduce the effects of any surface degradation processes. However, these technologies face some problems, which are:

- Little knowledge about their behaviour in specific applications.
- Literature and supplier knowledge can guide in the coating/surface treatment selection process, but it is not clear how they would perform in specific applications.
- Coating/surface treatment specifications need to be more refined as different suppliers have different processing methods, which can change the end result properties and, subsequently, their tribological behaviour.
- During the component design stage, coating/surface treatment and substrate materials need to be taken into consideration and tested, making the stage more time consuming.
- Expensive quality control processes
- No industry standards or generalised ones.
- Introduction of a new failure mechanism, which is related to the failure of the layers formed/deposited and delamination.

Currently, CTT uses a nitrocarburizing treatment, which improves wear and friction performance of the stainless steel components used for the VG mechanism, but this treatment suffers from a variety of disadvantages:

- Cost
- Proprietary process
- Supply chain from a logistics perspective as the treatment application is done by a unique supplier at one location in the world. This makes the company dependent on the supplier for specific products with little to no possibility to respond to any issues. In addition, products that are produced on other continents that require this proprietary treatment must travel to this one place and back, slowing the supply chain and increasing production costs.
- Reduction in the corrosion resistance, which limits the technology to lower temperatures
- Future environmental compliance of the coating/surface treatment process
- While friction performance is acceptable, further improvement would be beneficial

Therefore, there is a need to understand the behaviour of the current and different treatments/coatings to improve the performance of high temperature tribological contacts and to be able to design systems that provide the tribological performance required. In the context of this research, this relates in particular to reducing material loss and friction reduction across a range of temperatures.

1.2. Benefits

The outcomes of this project aim to provide a range of different benefits that can be classified by six different topics: wear, friction, dual sourcing, global supplier presence, environmental, and knowledge.

A reduction in wear can provide:

- A better component performance over time as the concepts under study may wear less, maintining the component's original geometry for longer
- Reduction of maintenance costs or occurrences of component replacement
- Longer component lifetimes
- Higher reliability of the product

A reduction in friction can provide:

- Cheaper actuators by reducing friction, since load requirements are reduced
- Faster response

- Further benefits can be related to the improvement of supply chain by the possibility of dual/global sourcing or using more globally present companies. From a dual sourcing perspective, the benefits can be:
- Limited supply chain disruption due to uncontrollable risks, such as natural disasters.
- Flexibility and reliability as the "better supplier" may be given bigger production volumes. Higher performance of a supplier depends on cost, lead times, product quality, global presence and the seller-buyer relationship. However, dual-sourcing may worsen the customer service of the seller or will impact the willingness to improve required services, as improvement entails investment.

Benefits from being supplied by a company with a larger global presence are:

- Helps to reduce cost, as their product may be cheaper due to increased access to materials and an abundant workforce.
- Facilitates expanding to new markets as they adapt easier to the new conditions
- Adapts better to uncontrollable changes, such as political conditions of a country.

Knowledge outcomes:

- Thinking practices of other engineers trying to solve tribological issues
- All cost improvements, as previously mentioned
- Start of new product development projects, not just for the component under study, but for other applications within turbomachinery
- Depending on the desired outcome of any new project, work instructions can provide a reference of techniques that could be used and save time

1.3. Risks

This section states the risks that could have affected both the research being undertaken and Cummins from having a subcontractor, the author. The risks were divided into four categories: technology, research process/methodology, facilities and organisation.

1.3.1. Technology

- **Patents that relate to functional applications of the technology.** This is considered to be a small risk. A patent, which restrains a material that is widely used for other applications, is unlikely to have been successfully filed.
- **Technical Success, within the selection requirements explained in Section 3.1.** As the project was a starting point in understanding the potential technology for the application, there was a high risk that the concepts under study would not be

successfully implemented in the application. To try to mitigate this risk, a wide range of concepts have been looked at in this project.

- **Laboratory performance not matching application performance.** Even though the environment is replicated as closely as possible when doing a laboratory test, the environment to which materials are exposed in a real-life application is more dynamic (non-constant loads and/or varying temperature) and more corrosive (air vs exhaust gas). This could cause changes in real application performance. To ensure the performance of the concept, the next step when doing a product development project should be testing the product capability at a component, full turbocharger, full engine system, and real-life application level.
- **Dealing with different new suppliers.** This includes the need to understand how the suppliers work and how they can be integrated into CTT's supply chain. Also, there was a need to understand the specific supplier's product as it may have some microstructural and chemical differences despite being advertised under the same 'name'. Understanding the supplier and having a good relationship with them can establish grounds to develop projects targeting specific needs within turbomachinery components.
- **Unsuccessful knowledge transfer.** Monthly meetings were organised for groups with relevant interest. The work was presented at internal conferences and to groups within CTT.
- **Base technology knowledge of the author at the beginning of the project.** Priority was given in the first few months to conduct an extensive literature review of tribology, coatings and characterization techniques and to align the author's understanding with the state of the art knowledge of the field. All learnings were regularly presented (monthly) and discussed (weekly) to improve and reflect upon them.

1.3.2. Research process/ methodology

- **Difficulties in obtaining answers from the different environmental tests.** Equipment training included software training. Main equipment training was received within the first year of research. Niche equipment knowledge was acquired as needed.
- **Skills of the person conducting the research.** An interview process was applied, which tested base skills and subject capability to improve. An EngD project always takes into account a learning process of the person carrying out the project.
- **Unsuccessful research process.** The project was reviewed on a monthly basis by the stakeholders, who advised on strategies to keep the research on track.

1.3.3. Facilities

- **Requirement of equipment to carry out the testing.** The tribometer was purchased through a tender process and installed and commissioned during the EngD project. The risks were reduced by buying a standard tribometer capable of the testing conditions required. Risks arose from the installation of the equipment and testing as it was unknown if it was going to perform as expected. In addition, functional issues needed to be addressed remotely as the supplier was based in another continent in a different time zone, causing delays.
- **Training for using different facilities.** Main equipment training was received within the first year of research. Other equipment training was obtained as needed.
- **Time available on equipment.** Most equipment could be booked in advance (2-4 weeks) based on testing plans.

1.3.4. Organization

- **Introduction of new suppliers in the supply chain; this includes lead times, costs, product quality, possible sources and procurement strategy.** This required working directly with the procurement team in CTT and joining meetings with suppliers. This presented a considerable risk as project was concerned with the final stages of the production line. As long as time lines were met, this would not present any issues. In order to pre-empt any problems, lead times plus a buffer were taken into consideration.
- **Project monitoring.** Project development was needed to monitor the progress of the project on a regular basis and to ensure that the project was on track to provide helpful information for future product development projects. Meetings were carried out monthly.
- **Confidentiality breach.** Legally binding contracts were set up between the university and Cummins to keep the work carried out confidential throughout the duration of the EngD.

1.4. Project Definition

As time was the main limitation and the research needed by CCT was broad the aim of the project was selected to focus on two key aspects to drive the innonvation and knowledge necessary to introduct new technologies in CCT's turbomachinery product portfolio: (1) comparing and contrasting a range of surface treatment/coatings to inform and develop a standard material characterisation procedure and (2) designing a selection process for future projects and applications that take engineering and purchasing requirements into consideration.

As the project focused mainly on materials engineering and material characterisation aspects of coating systems and focussed on:

- Surface topography, before and after coating/surface treatment application
- Microstructure and bonding characteristics
- Mechanical properties
- Corrosion and oxidation at room/high temperature
- Tribological performance at different temperatures

The environment that was used to benchmark the different concepts was derived from the VG mechanism. Coatings/surface treatment were applied to a 300 series stainless steel and the performance was tested under laboratory conditions. There are two main reasons why the VG mechanism was chosen:

- The VG mechanism allows study of the behaviour of the technology under a wide range of condition i.e. temperature, sliding distance or speed, and a range of contact stresses.
- In addition, CTT groups developing VG mechanism turbocharger for different application had an interest in the research.

The strategy of Cummins is to reduce the impact on the environment and for their products to add value by giving superior performance. This includes their products to be reliable, durable and dependablewhile reducing their running costs, which includes acquisition and maintenance costs [12]. The author believes that this project is clearly in line with Cummins views which were previously mentioned on the Section 1.2.

As can be seen throughout the whole work, this project was in particular about implementing new technology in the business through:

- Spreading knowledge across different research/technology groups about the technology under study
- Stressing benefits and disadvantages when applying these technologies
- Highlighting opportunities to expand certain concepts under study and to develop projects where the technology can offer a benefit.
- Finding new possibilities to keep or improve the performance of the VG mechanism.
- Understanding of how the different technologies perform in the environments they were exposed to.

As time was the main limitation, the aim of the project was to compare and contrast a range of surface treatment/coatings, develop a standard material characterisation procedure and design

a selection process for future projects and applications that take engineering and purchasing requirements into consideration.

As the project focused mainly on materials engineering, and characterisation aspects, coatings/surface treatment were studied regarding:

- Surface topography, before and after coating/surface treatment application
- Microstructure and bonding characteristics
- Mechanical properties
- Corrosion and oxidation at room/high temperature
- Tribological performance at different temperatures

The environment that was used to benchmark the different concepts is the VG mechanism. Coatings/surface treatment were applied to a 300 series stainless steel and the performance was tested under laboratory conditions. There are two main reasons why the VG mechanism was chosen:

- The VG mechanism allows studying the behaviour of the technology under a wide range of condition i.e. temperature, sliding distance or speed, and a range of contact stresses.
- In addition, CTT groups developing VG mechanisms turbocharger for different application had an interest in the research.

The strategy of Cummins is to reduce the impact on the environment and for their products to add value by providing the required performance and complying with regulations. This includes their products to be reliable, durable and dependable, and reducing their running costs, which includes acquisition and maintenance costs [12]. The author believes that this project is in line with Cummins views which were previously mentioned on the Section 1.2.

As can be seen throughout the whole work, this project was in particular about implementing new technology in the business through:

- Spreading knowledge across different research/technology groups about the technology under study
- Stressing benefits and disadvantages when applying these technologies
- Highlighting opportunities to expand certain concepts under study and to develop projects were the technology can offer a benefit.
- Finding new possibilities to keep or improve the performance of the VG mechanism.
- Understanding of how the different technologies perform in the environments they were exposed to.

1.5. Thesis Structure

The thesis is divided into eight chapters:

- **Chapter 2** contains a literature review divided into two section. The first section covers basic tribology principles and summarises the tribological behaviours of various metallic materials, austenitic stainless steel and Co-based superalloys. The second section covers different coatin systems and technologies, and how these materials may behave in a tribological loading environment.
- **Chapter 3** states the different methods used to select and characterize the different materials for the application under study. This includes details about the equipment used and the way the experiments were carried.
- **Chapter 4** reports and discusses the findings regarding behaviours of the material pairs under laboratory simulated wear and friction conditions at 250°C.
- **Chapter 5** reports and discusses the findings regarding behaviours of the material pairs under laboratory simulated wear and friction conditions at 650°C.
- **Chapter 6** reports and discusses the findings regarding behaviours of the material pairs under laboratory simulated wear and friction conditions at 760°C.
- **Chapter 7** summarises and concludes all findings and relates them back to the initial aims and objectives of the project. This is followed by a range of projects or understanding from different observed problems encountered or could be encountered and further information for understanding purposes.

1.6 Submission Structure

Four submissions were presented with the Innovation report that complement the data and show the behaviours observed and discussed during the tribology chapters.

- **Submission 1** is the paper presented at the 13th International Conference on Turbochargers and Turbocharging. This submission contains more information about how the different materials behave during the different environmental tests, in addition to a brief overview to the material tribological behaviour at the three test temperatures selected.
- **Submission 2** shows all the morphological, microstructural and chemical behaviours observed at the surface and cross-section of the wear scar after the materials were tribologically tested at 250°C. Complements Chapter 4.

- **Submission 3** display the different morphological, microstructural and chemical changes of the surface and the cross-sections of the different material pairs after they were tribologically tested at 650^{o}C. Complements Chapter 5.
- **Submission 4** presents the the topographical, microstructural and chemical changes observed at the surface and the subsurface of the material pairs after being they were tribologically tested at 760^{o}C. Complements Chapter 6.

2. Literature Review

2.1 Introduction

This chapter presents a critical review of the sliding behaviour of coated and uncoated materials at a range of temperatures. This chapter it is divided into the following sections:

- Section 2.2 presents the basic aspects of friction, focusing on dry friction
- Section 2.3 discuss the different wear theories and the main wear mechanisms
- Section 2.4 expands on the behavior of wear debris at the contact and the formation of transfer layers in unlubricated systems at different temperatures
- Section 2.5 examines the performance of different alloys, mainly stainless steels and Co-based superalloys.
- Section 2.6 looks at different surface treatments and coating deposition methods focusing on thermo-chemical processes (TCP) and physical vapour deposition processes (PVD). Each topic will be expanded for the specific surface treatments/coatings examined during this research. After an introduction to the coating/surface treatment material, their tribological performance will be examined.
- Section 2.7 concludes the literature review.

2.2 Friction

Friction is defined as “the resistance to motion that exists when a solid object is moved tangentially with respect to the surface of another that it is in contact with, or when an attempt is made to produce such motion” [13]. Friction is not a material property; but a system response and it is expressed as the forces that oppose the relative tangential displacement.

Friction is mainly divided into dry friction and viscous friction and subsequently divided into sliding and rolling friction. The tribological system under study will predominantly experience dry sliding, therefore a closer look to how dry sliding friction is influenced by wear and corrosión behaviour will be taken [14].

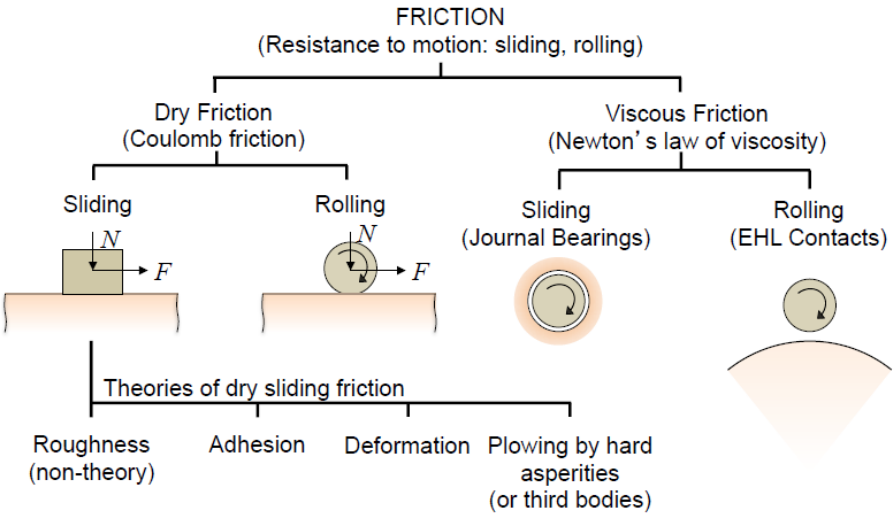

Figure 2.1. Diagram Showing Types of Friction [14].

In a sliding friction system, friction force (F^*) is define as the coefficient of friction (μ) times the normal force (N). In a sliding friction system we can also distinguish between static; which is the frictional force encountered in a stationary system, and kinetic friction; which is the frictional force measured in a system in motion. In a stationary system; static friction is overcome by applying a force greater than the resistance force in the direction of motion. In a system in motion, three scenarios can be observed. If the force applied is lower than the resistance due to friction, the system will stay stationary. If the applied force is equal to the resistance due to friction, the system will move at a constant speed for a system in motion and it will stationary for a stationary system. Finally, if the applied force is greater than the frictional resistance, the system will accelerate; for a static or system in motion.

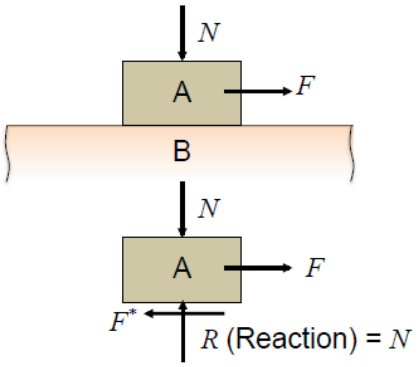

Figure 2.2. Sliding Friction Free Body Diagram [14]

$$F^* = \mu N \tag{1.1}$$

where: F*= friction force, μ= coefficient of friction and N= normal force.

Currently, there are four laws of friction concerned with its magnitude:

- The friction coefficient of a system is dependent on the normal load [15]
- The friction coefficient is independent of the nominal contact area [15]
- The friction coefficient is independent of the sliding velocity [16]
- The friction coefficient is independent on the surface roughness [17, 18]

These rules are sometimes oversimplified and there are many of exceptions to each of these rules [17]. Also, these rules do not tend to consider any wear mechanisms acting on a system and later on by showing people's work it will be shown that the consequences of changing some of these parameters can change the friction magnitude of the system.

2.2.3 Friction Theory

There are four main dry Friction theories, Roughness, Adhesion, Deformation and Ploughing, of how friction araises in a system, but all of them have their controversies. These main theories are developed thinking that friction raises due to the asperities interacting at the micro-/nano-scales [19].

2.2.3.1 Roughness Theory

The roughness theory, developed by Coulomb in 1781, believes that friction raises from asperities interlocking. Even though, he believed that an adhesive component existed, it was not the main cause as an increase of the friction value was not observed as the area of contact increased [16, 20, and 21].

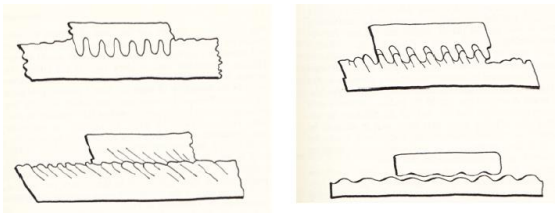

Figure 2.3.Coulomb's Asperity Interlocking Thoughts [16].

Therefore, friction araises from the work done to drag the asperities over the counterface asperities in a system at which rigid solids are mating. If that is the case, the friction coefficient of a system can be obtained by [16, 20, and 21]:

$$\mu = \frac{F}{N} = tan\theta \tag{1.2}$$

where θ= the surface inclination angle

This is true if θ is constant, no energy is lost and if the energy change goes from an initial to a final state continuously. Even though, this theory complies with the laws of friction of the time, it raised a lot of questions, such as what values to use as θ. This theory assumes that the mating materials are rigid [21].

This theory was not criticized until 1804 by John Leslie [e.g. 21]. He agreed with energy being used and recovered when asperities are climbed up and descend, but when adding the relative different positions, the system average will be a horizontal straight line as climbing and descending asperities will cause a variation with an average value of 0. On the other hand he believed that material deformation was produced when the asperity dropped and indent the opposite surface, using work to do [e.g. 20, 21]. He also opposed to adhesion of the surface rising the friction value of the system as a vertical force component (adhesion) does not have a horizontal component (friction), therefore cannot have an effect on it. Though this statement was disproved by Desagulier's lead spheres experiments, taking high shear forces to separate the lead balls [21].

2.2.3.2. Adhesion Theory

The adhesion theory was proposed by a few groups in the middle of the 20th century. This theory suggested that friction rises due to the strong adhesion of asperities in contact and the normal force upheld by the weaker asperities, which may undergo plastic flow [17, 22, 23, and 24]. When the tangential force applied translates relatively to the asperities, the weaker ones will undergo shear [9] as shown in Figure 2.4. This theory describes the coefficient of friction as [14]:

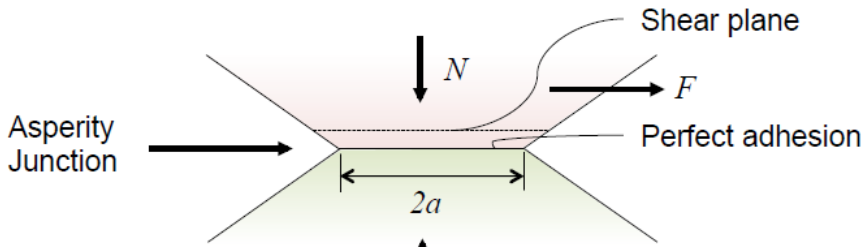

Figure 2.4. Free Body Diagram Representing Perfect Adhesion Between Two Asperities [14].

$$\mu = \frac{F}{N} = \frac{\pi a^2 H}{\pi a^2 \tau_y} = \frac{H}{\tau_y} \tag{1.3}$$

where a= area in contact, H= hardness and τ_y= shear yields strength

For a metallic material,

$$H = 3\sigma_y = 6\tau_y \tag{1.4}$$

where σ_y= tensile yield strength

Therefore,

$$\mu = \frac{\tau_y}{H} = \frac{\tau_y}{3\sigma_y} = \frac{\tau_y}{6\tau_y} = \frac{1}{6} = 0.167 \quad (1.5)$$

These theories strong point was the material deformed by the forces, normal and tangential, induced on the system. The problem was that it gave a universal friction coefficient, which is not true as shown by vacuum studies of metals. Also, shear and plastic deformation were treated separately [17], shear force calculated by a lower-bound analysis and the normal force by an upper bound analysis, which is not valid for systems that work in the material deformation regime for a weak point analysis [25]. Another issue, pointed by Buckley [26], was the existence and easily formed chemisorption and physisorption surface layers, leading to wrong measurements of surface energy.

Despite these shortcomings [17], this theory started to show that friction is related to material deformation and it is still believed that an adhesion component has an effect to the overall static and dynamic coefficient of friction [27]. This adhesion component (μ_a) tends to change from 0 to 0.4 depending on the surface interaction, on the lower end for lubricated systems or highly contaminated surfaces [27].

2.2.3.3. Deformation Theory

While the adhesion theory treated the stresses due to normal and tangential forces separately, the deformation theory treats them as one problem. This theory proposed that friction araises due to plastic deformation of the asperities in contact at the boundary [28, 29]. In this theory, the friction coefficient is calculated by a slip-field problem, in which stresses and forces at the interface are calculated, as illustrated in Figure 2.5 [28].

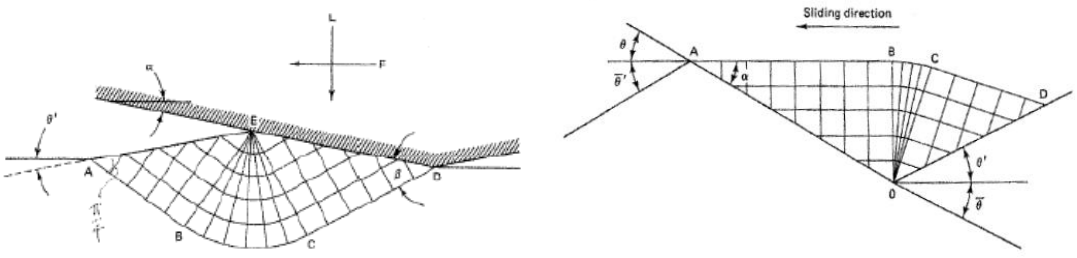

Figure 2.5.Slip-Line Field Representation of Two Asperities in Contact [30].

This theory it is believed to apply in a static system more than one already in motion. The reason for this is believed to be due to reduction of asperity interaction as original asperities deform; therefore, new asperities must be generated for this component to contribute to the system

friction. This deformation component it is said to contribute 0.43 to 0.75 to the overall coefficient of friction [19].

2.2.3.4. Ploughing Theory

Surface ploughing arises from the penetration of an asperity or wear particles penetrating in one or both of the surface in contact. The hard body ploughs on the soft body, permanently displacing it and leaving a groove on its path [31]. This behaviour was first described by Bowden and Tabor [20, 21].

The coefficient of friction during ploughing, depends on the projected area of contact at the plane normal to the sliding direction and the particle's relative hardness to the material surfaces. Calculation of the forces of the system is divided into two upper-bound issues; wedge ploughing is a 2D issue while ploughing by a cone or sphere is a 3D problema as illustrated schematically in Figure 2.6 and 2.7. For the 2D problems, μ is [14]:

$$\mu = tan\theta \qquad (1.6)$$

$$\mu = \frac{2}{\pi} tan\theta \approx tan\theta \qquad (1.7)$$

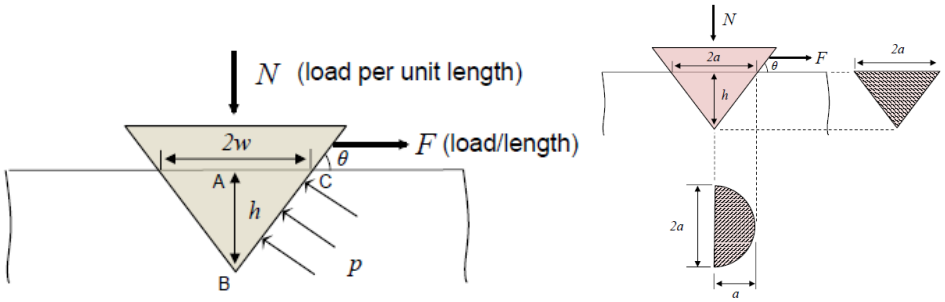

Figure 2.6. Free Body Diagram of a Wedge (left) and Cone (right) Shaped Body Plowing in a Surface [14].

While a 3D problem tends to be more complicated:

$$\mu = \frac{2R^2}{\pi a^2}\left\{\sin^{-1}\left(\frac{a}{R}\right) - \frac{a}{R}\left(1 - \frac{\delta}{R}\right)\right\} \qquad (1.8)$$

where R= radius of the circular body and δ= δ_1+δ_2, where δ_1 and δ_2 are the displacement of both solids due to compression.

If δ is smaller than R, then:

$$\mu \approx \frac{2R^2}{\pi a^2}\left\{\sin^{-1}\left(\frac{a}{R}\right) - \frac{a}{R}\right\} \qquad (1.9)$$

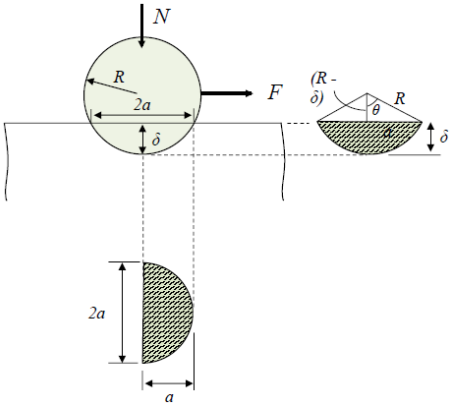

Figure 2.7. Free Body Diagram of a Spherical Body Plowing in a Surface [14].

The ploughing component varies from 0, seen when wear particles are absent or soft surfaces are in contact, to 1.0, when two identical metals are in contact and wear particles are penetrating both surfaces [27].

2.2.3.5. Combination of Friction models

The Bowden and Tabor model of friction brings together adhesion theory and plastic deformation theory, by accounting for the force required to overcome surface adhesion and the force required to move the asperity or particle by pushing the material away from its path. This model represents an idealised situation and does not take into account asperity deformion [13, 14] nor does it explain the friction behaviour under static conditions, or stick and slip due to junction growth, increasing the real contact area [18].

Shu [27] based his studies in metals in tribological contact and suggested that friction is mainly controlled by three components: asperity deformation, adhesion and ploughing. While asperity deformation controls the static friction behaviour or running-in, adhesion and ploughing mechanisms are more prominent friction contributors. This does not mean that friction can increase due to other components present [27].

2.3. Wear

Wear is defined as “the progressive loss of substance from the surface of a body brought about by mechanical action” [32]. The wear process tends to be steady and continuous, making it hard to detect during a casual inspection, but can have high consequences; such as effiviency loss and/or component failure.

Wear resistance is a system property, not a material property. As such, the different material information reported by other researchers may not be the same due to a change in the tribological behaviour

2.3.1. Archard wear theory

Archard's wear theory [33] is a simple model that is used to understand the basis for wear processes. This theory, similar to Bowden and Tabor's theory of friction, says that wear is caused by the formation of wear particles that are created by the asperities or high points that are in contact during the relative motion of both surfaces. The main assumption of this theory is that the number of asperities or major points in contact is limited.

The next assumption is that the number of asperities that are in contact depends on the applied load and the indentation hardness of the material.

$$W = \frac{K_s P}{H} \tag{2.1}$$

where: W= wear volume, K_s=probability of an encounter leading to the generation of a wear particle, P=applied load, H= indentation hardness of the softer material.

After simplification,

$$W = K_1 P_s \tag{2.2}$$

Where K_1 is known as surface condition the K factor or wear coefficient.

From this theory, the laws of sliding wear were developed and, as with the sliding friction laws, they should be used as a guideline [33]:

-Wear volume is directly proportional to the applied normal load

-Wear volume is directly proportional to the sliding distance

-Wear volume is inversely proportional to the hardness (with exceptions)

Therefore,

$$V = k\frac{NS}{H} \tag{2.3}$$

where: V=Wear volume, N= Normal load, S= Sliding distance, H= Hardness and k=wear coefficient.

As explained in the discussions above, friction and wear are related and this theory/equation does not capture this relationship. Although the equation is not based on rigorous testing, it gives a useful engineering approximation, due to the neglect of other material or environment properties, such as brittleness. It ignores material deformation and some assumptions are arbitrary, such as no changes in wear as the surface changes [33]. This approximation tends to

be more precise if applied to metals, even though as the metallic system becomes more complicated, for example: for metals with more than one phase present, the precision can be reduced drastically. For ceramic and polymer materials it is les precise because other parameters tend to be more important for these materials, such as toughness and elastic/viscoelastic behaviour, respectively.

2.3.2. Abrasive wear

Abrasive wear occurs when a solid is loaded against another solid, countersurface (two-body) or particles (third-body) from the environment or from one of the surfaces in the system. One condition is the harder material must be at least 1.3 times harder than the softer for abrasive wear to occur [20, 34]. Researchers have developed a wide range of ways to classify the different abrasive wear mechanisms depending on other factors affecting the system such as stresses [35], but the most widely used are to differentiate between two and three body abrasive modes.

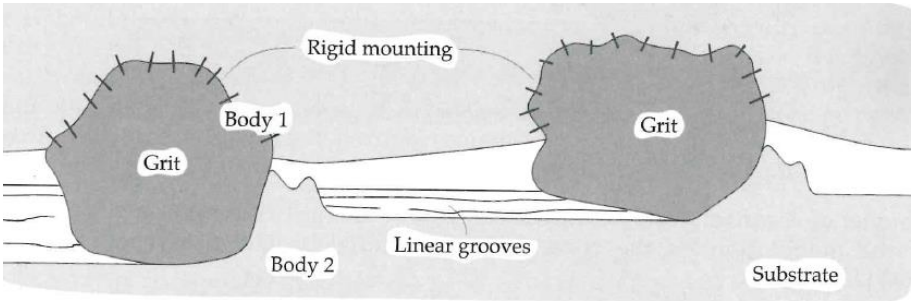

Figure 2.8. Representation of a Contact under two Body Abrasion [36].

Two-body abrasive wear occurs, as mentioned above, when two surfaces come into contact. In this situation, the soft surface gets abraded by the hard surface. For this mode, different wear mechanisms are involved [37]:

-Cutting involves the removal of soft material by a hard body. The damage caused on the surface is in the shape of deep grooves and elongated strips of material can be seen as debris. Cutting is illustrated in Figure 2.9.

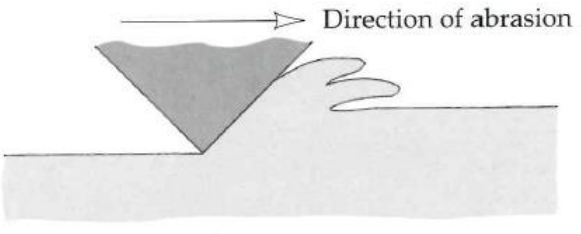

Figure 2.9. Representation of the Cutting Mechanism [36].

-Ploughing produces deep grooves due to the penetration of asperities on the counter-surface, as shown in Figure 2.10.

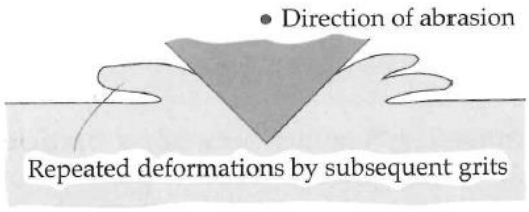

Figure 2.10. Representation of Ploughing Mechanism [36].

-Wedge-forming is caused by a build up of material ahead of the asperity, causing flaked shape debris, and is considered a less detrimental form of abrasion wear.

-Fracture abrasion wear is caused by brittle fracture at one of the solids in contact and is shown in Figure 2.11. There are three different ways in which this brittle fracture can happen: localized cracks that cause localized fragmentation, accumulation of cracks in an area that causes high volumes of material being released and deep median cracking.

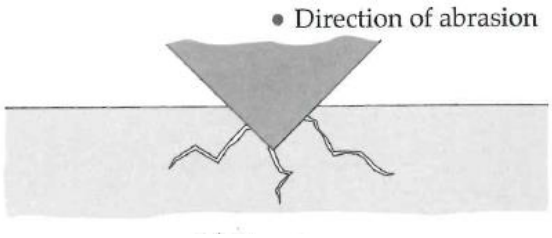

Figure 2.11. Representation of the Fracture Mechanism [36].

-The asperity deformation mechanism of abrasion relies on the plastic deformation of asperities when they collide against each other. As the asperities become work hardened due to continuous deformation, they also increase their brittleness and they break off [27].

2.3.2.1. Third-body abrasion

Third-body abrasion wear (Figure 2.12) is caused by loose particles entrained within the interface experiencing relative motion, which come from the wear process or particles from the environment. This wear mode tends to show slower wear rates, normally one or two orders of magnitude slower than two-body abrasion [35, 38, 39], as the debris will spend some time rolling and abrading the surfaces.

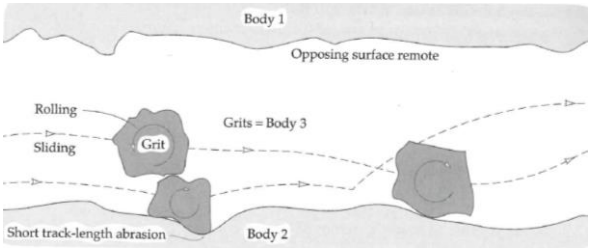

Figure 2.12. Representation of a System under the Effect of Third-Body Particles [36].

These wear particles, normally are in an oxide or work hardened state, can help the system reduce overall wear by acting as solid lubricants [40], but they can also be detrimental by acting as abrasive particles. This difference in behaviour depends on the system characteristics, such as contact pressure, sliding speed, temperature, etc., and the particle morphology, size and mechanical properties. These particles created during the wear process can be classified into two categories [41]:

- **Passive debris** or debris is withdrawn from the contact, it does not have any positive or negative impact on the system except the wear volume lost due to the particle formation.
- **Active debris** or retained debris can have a positive or negative effect on the system. Jiang proposed four mechanisms in which these particles could behave at the contact interface [36, 42, 43]:
    - Rotating mechanism is caused by the rotation of an entrapped particle around its own centre.
    - Skidding mechanism occurs when the particles fixed in one of the surfaces slide across the opposite surface.
    - Rolling mechanism occurs when particles are free to rotate at the surface interface of the contact.
    - Rolling restriction mechanism occurs when the particles rolling at the contact are strongly adherent, restricting their rolling and increasing the force required for motion.

Production or removal of the particles can occur harmoniously keeping an equilibrium. When a given volume of particles is reached, they will bear the load and therefore, they will affect the wear and friction of the system. The volume required will be dependent on the surface roughness and particle size [44]. Rice [45] adds that the effect on the system tribological performance will also depend on their mechanical properties. On the contrary, Suh [46, 47] has shown that the lack of volume of these particle layers can have a positive effect on the

performance of the tribological perspective, from a friction reduction perspective, by 'undulating' the surface topography of the material.

The agglomeration of particles can form compacted layers, which can serve as a system protection [48]. In a high temperature environment. a 'compacted layer' composed of oxidation products from the surfaces and or third body particles is sintered as a transfer layer.

2.3.3. Adhesive wear

Adhesive wear (Figure 2.13) is considered one of the most detrimental wear mechanisms that a system can experience as it causes high wear rates. Surface adherence comes from the attractive forces between both surface atoms. As a result, one of the materials' properties to consider is its chemical affinity and/or material electropositivity to the counterface, as reported by Subramanium [49-51] using aluminium-silicon alloys worn by different materials.

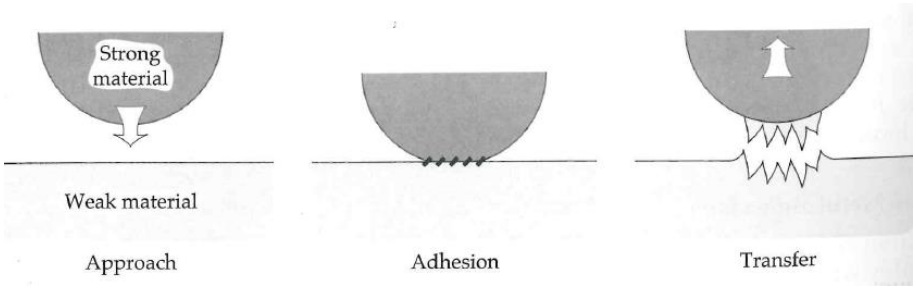

Figure 2.13. Metal Transfer when both Surfaces Adhere [16].

Adhesive wear occurs when material is pulled off one surface due to strong adhesive forces between the atoms that come into contact, causing bonds to break not at the surface-surface interface, but within the substrate material [17]. Subsequently, adhesive wear can lead to debris formation or transfer of material back to the original substrate. This typically this would equate to material from the softer surface being transferred to the harder material surface. Adhesive wear is more likely to observed for smoother surfaces [17], as a smoother surface tends to show a higher real area of contact i.e. the area of asperities in contact is higher.

The main condition in order for the material being pulled from one surface is that the shear strength of the joint junction is higher than the shear strength of the bulk, or subsurface in this study of coatings, of the material with lower shear strength. As this is not normally the case, the production of a fragment by adhesion is rare [17] as it requires local regions to have lower strength or regions with lower strength formed due to the material continuously plastically deforming by creating or increasing the size of defects, such as voids. Others, such as Green and

Tabor [52], showed that sometimes the junction stops being parallel to the sliding direction, which can give raise to the formation of a particle.

Bowden and Tabor [53] stated adhesion happens at the asperity tips and due to the tangential motion, the softer asperity is pulled from the substrate. This hypothesis was later criticized by Shu, Saka, Jahanmir [54] and others for the following reasons:

-Hard surface wear cannot be explained

-Surface roughness cannot be explained

-Loose particles cannot be explained

-Metallurgical and microstructural material parameters are not taken into account

-Cannot relate wear and friction behaviour changes

-Work required to generate wear particles will be between two to three orders of magnitude smaller than the external work done

-Interface between adhered surfaces is unlikely to be stronger than the bulk of the material due to vacancies and impurities.

Researchers like Shu [27] and Jahamir [54] believe that if that is the case, adhesion mechanism does not influence the overall wear volume, except when large flash temperatures are experienced in the system. This point will be further discussed in Section 2.3.5.

2.3.4. Corrosive wear

Corrosive wear (Figure 2.14) occurs when the surfaces in contact interact chemically with the chemical species in the environment and tends to be divided into two steps [17]. The first step is the surface reaction with the environment, which can result in the formation of a protective layer or the continuous corrosion of the material due to the formation of a non-protective layer or if the protective layer is porous, brittle or spalls off. The second step is the removal of the protective layer formed due to the sliding motion of the surfaces in contact.

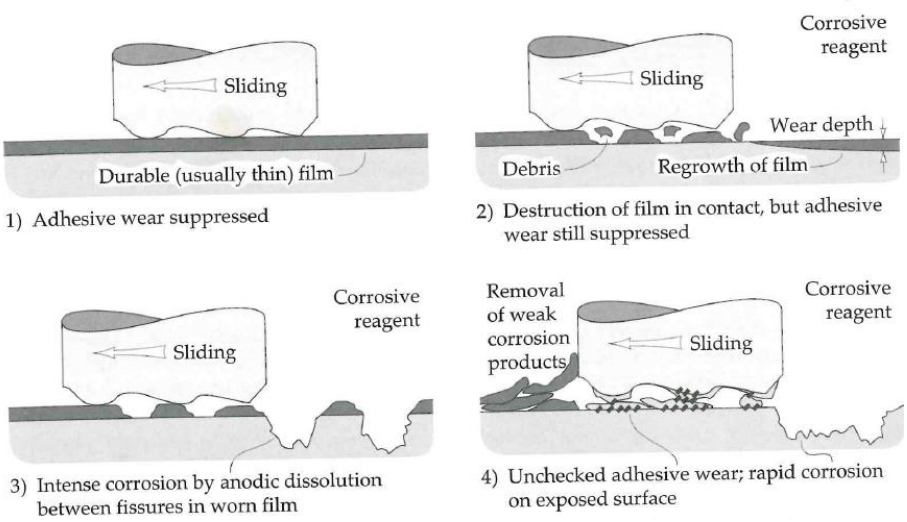

Figure 2.14. Effects of Corrosive Reagent in a Tribology System [36].

In an environment in which oxygen is present in an unlubricated system, metallic surfaces will undergo a type of corrosive wear known as oxidative wear. This type of corrosive wear is characterized by the formation/removal of an oxygen-based compound layer by the mechanical action of the sliding motion in the system [17].

Quinn developed a model [40] that relates the wear rate to the formation/removal of the oxide layer. In his theory, he assumes that the oxide layer formed requires to be a critical thickness before it can no longer sustain the tangential load [55].

Quinn's model should be able to predict the contribution of oxidative wear to the total wear of the surfaces if the the static oxidation behaviour of the materials and the critical thickness of the oxide layer are known, which can be measured experimentally.

As mentioned, wear rates using this theory are related to static oxidation, while wear rates for materials mainly undergoing this wear mechanism are experimentally far greater. Firstly, the model does not consider the temperature difference caused by friction, also known as the flash temperature. As Archard [56] showed in his studies, flash temperatures at the surface due to load or speed can have a significant impact on the wear behaviour due to material changes. Secondly, while the energy required for oxidation reactions remains the same in a tribological system in which surfaces undergo oxidation, the Arrhenius constant does not, due to constant changes in the surface condition, such as an increase of dislocation density due to work hardening, which can affect the oxidation behaviour [57]. Finally, as this theory is based on static oxidation, it does not take into account crack formation in the oxide layers and oxide transfer to the counter-surface; and therefore, it does not take into account the formation of transfer/glazed layers during the wear process or the presistant removal and re-formation of

the oxide film due to mechanical and tribocheical effects, which will further explained in Section 2.4 [55].

2.3.5. Delamination Wear Theory

In 1972, the delamination theory (Figure 2.15) was proposed by Suh [58] in order to explain how metals and other solids wea. This theory was later supported by other researchers and it answers many of questions unanswered by other theories.

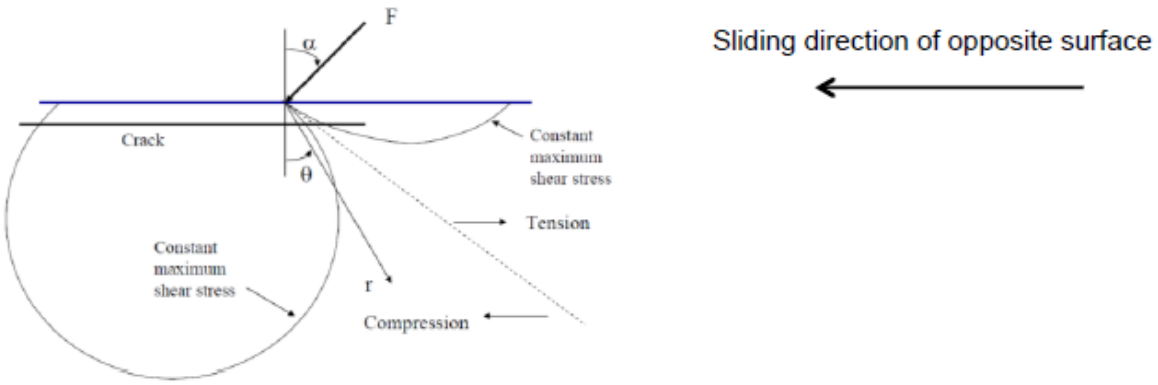

Figure 2.15. Delamination Theory Diagram [14].

This theory states that asperities of the surface are deformed and fractured, due to continuous loading, producing wear particles. Because the wear rate of harder asperities is slower, they apply a traction force on the smooth parts of the surface, which will cause an increase in the amount of plastic deformation per loading cycle. Due to this cyclic deformation of the material subsurface, cracks nucleate and grow as the material continuously deforms. This process continues until the cracks propagate to the surface and produce a sheet-shaped wear particle.

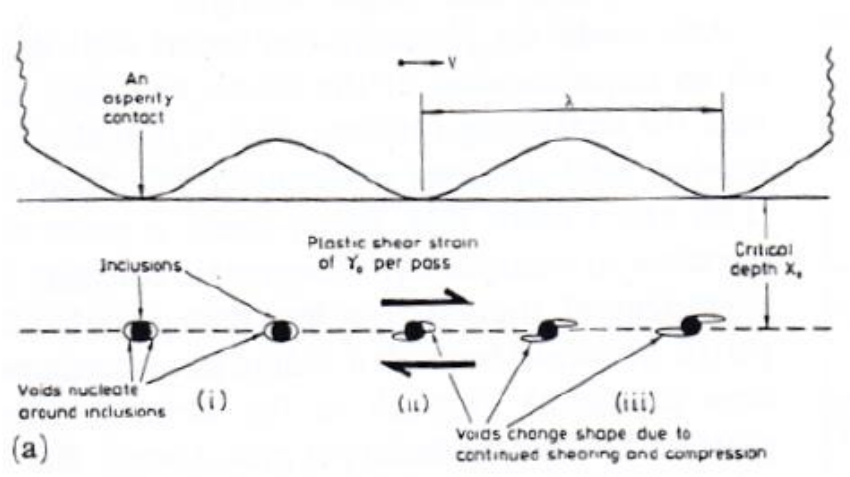

Figure 2.16. Diagram of the Material Delamination Process [58].

There are several reasons, some of which are illustrated in Figure 2.16, as to why cracks are generated at the subsurface, which are [27]:

-The surface is under a triaxial compressive load

-The hardening process due to plastic deformation is lower at areas near the surface due to dislocation annihilation. Subsurface hardening due to dislocation pile-up can lead to the nucleation of voids, which may coalesce due to void growth or shear action.

-The maximum shear stress present due to a Hertzian contact is higher at a distance below the surface, which suggest that the material will yield first at the subsurface.

-The tangential load or friction force, produces tensile stresses in the material behind the contact.

- The presence of inherit defects/ secondary particles at the higher shear/tensile stress area.

Delamination theory does not reject the behaviours explained by previous theories. In a tribological system different wear mechanisms act to certain degrees on the contact depending on the material pair and the conditions experienced, meaning that a wear mechanism may be prominent or absent depending on the conditions.

2.4. Wear at High Temperatures

While the mechanisms explained above will still be acting in a high temperature environment (≥200°C), their contribution to the overall wear will differ from the one seen at a lower temperature. The key considerations as the temperature increases are the changes in mechanical properties and the other changes due to the interactions with the environment e.i. oxidation.

Materials used at high temperatures are often linked to very aggressive environments. One method of reducing the wear in a high temperature tribosystem is to take advantage of the oxidation behaviour of the material because the oxide debris can act as a solid-lubricant [42]. Furthermore, in combination with the high temperature and contact stresses, a compacted layer can be formed as shown in Figure 2.17 [59]. This compacted layer can reduce the overall wear in the tribosystem; however, the formation of a compacted layer is hard to predict for a material combination because the mechanism of formation needs to be understood, which relies upon the environment characteristics such as temperature, contact pressure, oxygen partial pressure, sliding speed, etc.

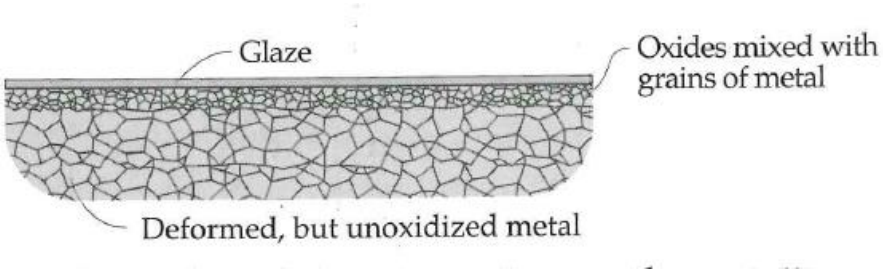

Figure 2.17. Glazed layer structure in a metallic surface [36].

There is a minimum temperature, known as the critical temperature, for the formation of a stable glazed layer. This critical temperature depends on the material under evaluation and other system parameters, such as load [48], speed or frictional heating [60]. When the temperature is lower than the critical temperature, the formed layers are brittle and cannot form a coherent layer and, as the temperature increases, the density of the layer is greater and the sintering of the layer is easier, offering higher protection due to its faster formation and higher durability. In addition, the type of oxide/oxides formed have an effect on the critical temperature. Scott, Glascott and Woods saw the formation of glazed layers at temperatures in between 200°C-300°C under fretting conditions for iron-based alloys. In their study, they attributed the difference in critical temperature for glazed layer formation to the ductility of oxides formed [61].

Burkinshaw and Blacker [62] from CTT reported on wear performance of wastegate materials at different temperatures and developed a test procedure for assessment. In their work, two different Cobalt-superalloys had the best performance at temperatures greater than 850°C. At 600°C, a material pair comprising of a Nickel superalloy against a sintered stainless steel performed better from a wear perspective, showing that different material pairs perform differently when subject to specific system conditions, in this case temperature due to the formation of the compacted/transfer layers.

Wood [63, 64] has studied the tribology behaviour of dissimilar metals in a fretting type of wear at a temperature range between 21 °C and 750°C, in which he combined Iron, Nickel and Cobalt alloys. He showed in a system for which most of the third body particles will be retained, such as fretting conditions, alloy combination has a significant impact on the wear rate due to the different characterisitics of the compacted layers formed by the different oxidation behaviours. During his study, the higher wear regime seen at intermediate temperatures was attributed to delamination of the material, as plate like debris was observed, demonstrating how the nature of the oxide affects the stress at the subsurface.

As the particles formed are based on the contacting materials to, the alloy combinations will influence theparticles and hence will dictate the properties of these layers. Pauschitz [65] mentions that the properties of these layers are dependent on the conditions of the tribosystem, including the mating materials and the wearing materials, and identify four different scenarios. These scenarios are the (1) formation or (2) not of a transfer layer mainly composed of one of the materials in contact with very low oxygen content, (3) a mechanically mixed layer composed of original and oxidized material, and (4) a composite or compacted layer mostly composed of oxidized particles.

Scott, Lin and Wood also proposed three mechanisms for the debris generation during the formation of glazed layers during a study of fretting wear of iron-based alloys at temperatures between 200°C and 600°C [66]. Theses mechanisms are:

-The oxidation-scrape-reoxidation mechanism in which the oxide layer formed is continuously removed by the mechanical action acting on the surface forming third body particles which can remain or be removed from the system. This mechanism is dependent on the bulk temperature of the material in contact and the flash temperature at the asperities.

-The total oxidation mechanism relies on the development of a coherent stable oxide layer which is not removed by the mechanical action. This layer will continue growing and providing wear protection.

-The metal debris mechanism which involves the formation of metal debris. The metal debris is broken down until it spontaneously oxidises.

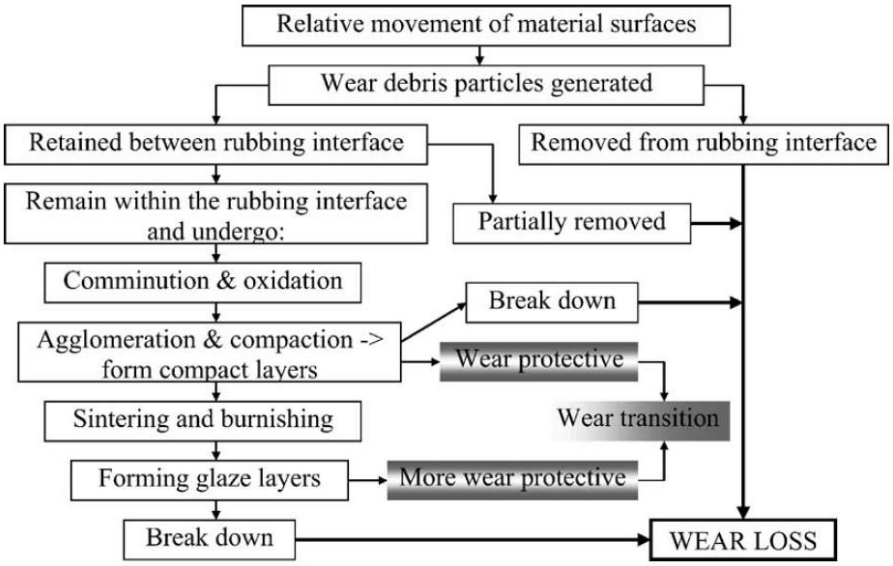

Figure 2.18 Dry Sliding Wear Schematic of Metals [49].

During the study of Nimonic 80A by Jiang [41], he developed a model for the formation of compact and glazed layers by the sintering of third body particles. This model assumes the following [41, 68]:

- Wear rates after compact layer formation are negligible.
- All particles formed during the wear process are retained in the system and compacted.
- In his case, he assumed that most of the oxide formed was Nickel oxide.

It was reported that this model is reasonable in comparison to the wear rates obtained during pin-on-disk testing conducted on the material pair; however, the calculated values tend to show lower wear rates than the values obtained during testing as shown in Figure 2.19.

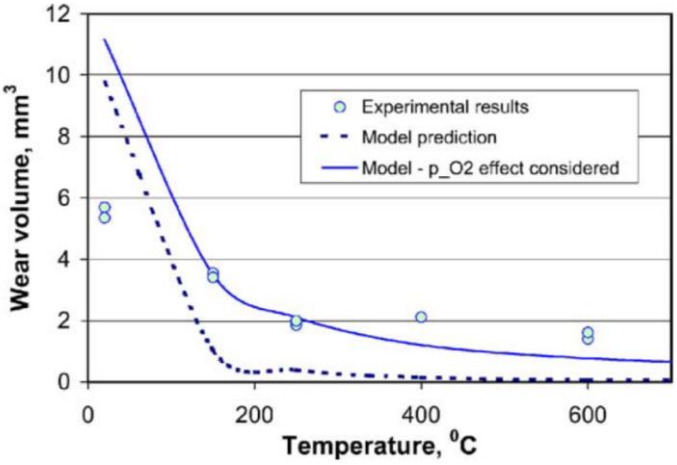

Figure 2.19. Comparison of Predicted and Test Results [41].

The previously presented literature suggests that the properties offered by the compacted layers are related to their physical properties and condition [67], such as thickness, particle size and defect density, and not their chemistries; however, the chemistry of the particles present in the wear debris and their condition may dictate their formation and nature of the compacted layers. The following sections discuss the wear behaviour of steels and cobalt superalloys and will show further how the mechanical properties of the alloys and the formation of these compacted layers improve the wear and/or friction behaviour of material pairs.

2.5. Tribology of Metals

2.5.1. Austenitic Stainless Steel

Austenitic stainless steels are a group of steels heavily used by industry due to:

- The retention of their mechanical properties at higher temperatures, which is mainly dependent on the Nickel content and other alloying elements due to solid solution strengthening. Ni content also aids stabilizing the autenite phase.
- The higher oxidation and corrosion resistance, which is mainly dependent on the Cr content in the alloy as Cr is used to form a regenerative passive layer that prevents further chemical reaction between the bulk and the environment at which is subjected.
- They are considered to be a cost-effective alloy, as the main component is iron (tends to be low cost) and fulfill requirements in a wide range of conditions.

The disadvantage of these alloys is that they tend to be considered to have a lower wear resistance, gving the tendency of the tribological systems composed of these alloys to suffer from scoring, galling and seizing [69].

These alloys are face-centre-cubic (f.c.c.) with the possibility of being metastable, which is normally found on the alloys with low stacking fault energy (SFE) [70]. The SFE of the alloy depends on:

- Temperature, with the SFE increasing as temperature increases [71].
- Alloy composition, with Ni, Cu, Al and C increasing the SFE and Cr, Si decreasing it with increasing concentration. Mn reduces the SFE below 13wt% Mn and while contents above raises it, and N effects on the SFE are very dependent on base material and strain rate [70]. Just note that depending on the original composition of the alloy, the solute element added can have completely the opposite effect [72]. This makes it hard to establish universal composition equations for the purpose of calculating stacking fault energy.

These alloys can easily undergo a martensitic transformation, which is caused by the displacement of atomic planes during plastic deformation. This martensitic phase was found to have a number of forms - a b.c.t. (α') at high strains; hexagonal close-packed (h.c.p.) or ε-martensitic, shown to be maximum at low strains, and transforms to α'-martensite as strains increase; and a combination of both [73, 74], which is dependent on both the work-hardening conditions and the alloy elements of the steel [75,76]. This martensitic transformation is favoured by lower SFE alloys, while higher SFE alloys will deformed by twinning, or dislocation glide[twinning and martensite in 304 austenitic stainless steel]. The different deformation mechanisms, work-hardening, twinning and dislocation gliding, are very important from a tribological perspective as the mechanical properties and the fracture behaviour of the area near the contact will be continuously changing during the wear process and will affect the friction behaviour as the zone affected by the load will cause continuous changes in crystal structure and the formation of defects, such as pores and shear bands.

2.5.1.1. Tribology of Steels

After Suh [58] highlighted the problems of the adhesion theory and proposed the delamination wear theory, more researchers studied how these microstructural changes at subsurface could affect the wear and friction behaviour [77, 78]. Rigney and Glaeser suggested that highly deformed surfaces produced plate-like debris due to the conversion of the sub-surface to a cell-like structure as a consequence of the increase in dislocation density, which depends on applied stress, temperature and stacking fault energy of the alloy [78]. The amount of delaminating material is dependent on the ''cell'' size, which decreases as the material hardness increases [79].

Korshunov and Mints [80] studied various metastable and stable austenitic stainless steels against a 4Cr13 steel disk on a disk-type friction testing machine at various speed (0.75, 1.5, 4.5 and 7.5 m/s) and pressures (1, 2, 5, 10 kg/cm^2). They showed that metastable austenitic steels give higher wear resistance than stable ones, which they attributed this to the ease of formation of the martensitic phase at the contact area. Similar results were seen by Dumbleton and Douthett [81] when adding different contents of Si and Ni to a base AISI 301 stainless steel alloy tested against a 440C stainless steel using a 6.1lb load at 1500 and 2500 rev/min. They reported that as the steel work-hardening rate increased, the running-in period is reduced due to the faster formation of the martensitic phases.

On the contrary, other researchers found completely opposite behaviours. Hsu [69] tested 304, a low SFE alloy; Nitronic 60 (a higher alloyed austenitic stainless steel), with slightly higher SFE

than the 304; and 316, with the highest SFE, against a 440C stainless steel on a block-on-ring configuration using three 40min loading cycles; 64N, 133N and 200N, with a speed of 30rev/min in an argon and air atmosphere. From his experiments, he saw an increase in wear for the lower SFE alloys, from which Nitronic 60 showed lower wear rates in comparison to the 304 stainless steel, attributed to the stability of the austenite phase. A lower CoF for the lower SFE alloys was attributed to a larger particle formation for the 316 causing long term friction variations. Although Nitronic 60 and 304 showed a similar average friction, 304 exhibited larger-amplitude changes due to the larger gradient of mechanical properties between the steel bulk material and the martensitically-transformed areas. This last behaviour is the cause of galling and not the wear rate due to the following reasons:

- The harder areas will be more likely to fracture.
- The harder areas and particles are more likely to damage the opposing surface.
- The harder areas will increase the volume of material plastically deformed. This behavior was seen by Bressanelli and Moskowitz [82] during tensile testing of metastable stainless steels.

Similar behaviours were seen by Shende [83] in his study of 304, 305, 310, 316 and 332 stainless steels self-mated in an argon atmosphere. Singer [84] in his studies of ion implanted steels, such as 304 stainless, found a reduction in wear and friction as the load capacity of the surface of the material is increased, reducing the work-hardening rate. This behaviour reduces the (1) size of and (2) delays the formation of the plate-like particles due to changing the fracture behaviour from a ductile fracture (large particles) to a brittle fracture (finer particles).

Few researchers have looked at the behaviour of steels at higher temperatures and even fewer on the behaviour of austenitic stainless steels. Stott and Jordan [85] looked at the friction and wear transitions of carbon steel against high-speed steel and high-chrome steel due to load, (10N, 15N and 20N) and temperature (500^{o}C, 550^{o}C and 600^{o}C). They reported that lower CoF and wear for the high-chrome steel was achieved due to the formation of glazed layers, while higher wear rates were seen on materials with unformed or unstable glazed layers due to increased particle formation and poor particle retention due to shallow grooves.

Hirsch [86] looked at the tribology performance in fretting conditions of AISI 301 stainless steel/ AISI 52100 steel at different temperatures (20^{o}C, 250^{o}C, 400^{o}C and 500^{o}C). Hirsch reported an improvement of wear performance at 250^{o}C from 20^{o}C due to glazed layer formation, but wear increased at the highest temperature due to reduction in the fatigue resistance at higher temperatures. On the other hand, Hirsch also observed a reduction in the stabilized CoF as the

temperature increased due to a change in composition of the oxide and a decrease of particles in the contact.

Smith [87] studied the performance of 316 stainless steel against itself steel between 20-500^{o}C in a reciprocating motion test in air. From a wear perspective, Smith saw a decrease in wear up to 300^{o}C, due to the formation of α-Fe_2O_3. Also, he noted semi-circular patterned areas of oxides at the subsurface of the steel, which seemed to correlate with the stress fields calculated by Dautzenberg and Zaat [88]. At 300^{o}C, the formation of a compacted layer was observed, which subsequently breaks and rebuilds. Above 300^{o}C, the wear is reduced further by containing the wear debris due to the formation of deep grooves. Similar behaviours were seen by Skinner and Newman [89].

Roy [90] looked at the behaviour of 253MA austenitic stainless steel against 100Cr6 in a pin-on-disk configuration at ambient temperature, 473K, 673K, 873K and 1073K in an air environment. For ambient temperature and 473K, the material underwent delamination wear, causing higher wear rates and higher CoFs. When the temperature reached 673K, mechanically mixed layers were formed. In addition, at this temperature both materials exhibited similar mechanical properties and the CoF achieved its lowest value with very low wear. At 873K, the material from the 100Cr6 transferred to the 253MA and oxidized, giving a small wear rate but with increased friction from the previous temperature due to the compacted layer formed not being very adherent. Finally, 1073k showed a lower wear rate and friction than the previous temperature due to the formation of a stable compacted layer.

2.5.2. Cobalt based Superalloys

Cobalt superalloys are heavily used in high temperature applications, where other alloys cannot be used due to:

- Their high temperature mechanical properties, provided by solid solution strengthening and the precipitation of a carbide and/or an intermetallic phase.
- Their high corrosion resistance due to the addition of Cr.

The main disadvantage of these alloys is their cost that continuous to increase due to the use of cobalt in the energy sector for batteries [91] and also the challenge of processing the material to the desired component shape due to the presence of the hard precipitated phases.

Pure cobalt and its alloys can undergo an allotropic transformation from f.c.c. to h.c.p., or *vice versa*, due to temperature or plastic deformation. The temperature or strain level of these transformation will depend on the alloying elements present. f.c.c. is stabilized by Ni, Fe, C, Mn

and Ti, and h.c.p. is stabilized by Cr, Mo, W and Si. Nickel seems to have the highest influence on stability, and alloys with high Ni contents require greater amounts of h.c.p. stabilizers elements if that is the preferable phase [92]. The h.c.p. phase may be preferable as h.c.p. crystal structures provides a more limited amount of slip planes, therefore offering a higher hardness alloy.

As previously mentioned, precipitation hardening of cobalt superalloys is key for their high mechanical properties at higher temperatures, but it is also seen that thse particles can increase the performance of the alloy from an abrasive resistance perspective. This section provides a review of the performance of a carbide precipitated alloy, Stellite 6®, and an intermetallic precipitated alloy, Triballoy® T-400, as these alloys were used in the present study.

2.5.2.1. Stellite 6®

Stellite 6® is a hypo-eutectic cobalt superalloy that has been mainly used for wear-resistant applications, such as cutting tools, or where temperatures and corrosion restrict the use of most other materials. Stellite® 6 is characterized by a cobalt-chrome rich matrix and Cr_7C_3 eutectic precipitates [93], with hardness and modulus values of 24.3 and 346.7 GPa, respectively [94].

2.5.2.1.1. Tribology of Stellite 6®

Rose [42] examined the performance of Stellite 6® against MA956, Nimonic 80A and itself under reciprocating motion conditions from 25°C to 750°C and a range of loads from 7N to 25N. Rose showed how at low temperatures these material pairs tend to show a low wear due to their mechanical properties and to the formation of fine particles that reduce the metal-metal contact time. As temperature increased, an increase in wear was caused due to the loss of mechanical properties resulting from change in wear mechanism (delamination of material). After that transition, wear of the material became more stable again, followed by a second transition to abrasive wear until stable compacted layers are formed, which resulted in a high reduction in wear. In addition, this stability seem to be very dependent on the strength of the alloys at the testing temperature, supporting the importance of the mechanical behaviour in dictating the wear response of this alloy.

Inma [60] looked at Nimonic 80A against Stellite 6® at different temperatures, from room temperature to 750°C, at a speed range of 0.314m/s to 0.905m/s. At low temperaturas, both speeds caused a similar behaviour in which particle debris kept surfaces separated, resulting in low wear and low friction. At the mid temperature range, low speeds caused the formation of compacted patches, while at higher speeds, the system exhibited delamination, giving high wear and high friction. At low speeds and from 510°C up to 750°C, particle agglomeration formed a

compacted layer that reduced friction and wear of the system. On the other hand, at higher speeds the compacted layer did not form. Inma believed that was due to the behaviour of Nimonic 80ª as when the same conditions were applied against a Nickel 200 a glazed layer composed mainly of NiO was formed.

2.5.2.2. Tribaloy® T400

Tribaloy® T400 is considered a Co-based wear and corrosion resistance superalloy containing intermetallic Laves phases. These Laves phases with a hardness of 21.81GPa and an elastic moduli of 397.5GPa, improve its high temperature mechanical properties and offer high wear resistance properties [95]. This phase is a hypereutectic phase, mainly Co_3Mo_2Si or CoMoSi, surrounded by a eutectic phase matrix, which can have an f.c.c. or h.c.p. structure depending on the manufacturing conditions which influence the allotropy of Co as previously mentioned [95].

2.5.2.2.1. Tribology of Tribaloy® T400

Renz [96] studied the performance of this alloy for a valve application, running against a CrMo steel at 40, 400 and 600ºC. At low temperatures, Tribaloy® T400 material was transferred to the steel pin, protecting it from the wear process. When the system was at 400ºC, an increase in wear was seen and was attributed to the loss of mechanical properties of the alloy. Finally, at 600ºC, the wear decreased due to the formation of a compacted layer. At all temperatures, wear behaviour and friction behaviour did not show a one-to-one correlation, as when friction decreased, a decrease in wear was not observed.

Nsoesie [97] also examined the wear behaviour of Tribaloy® T400 from 250ºC up to 450ºC and against two other cobalt alloys; T400C and T-401. Nsoesie saw the best wear performance given by the hardest material. As the temperature increased to 250ºC, an increase for all materials increased material lost due to material softening. At the highest tested temperature of 450ºC, the three alloys benefitted from the formation of compacted layers, reducing wear.

On the other hand, Liu [elevated temperature wear behavious of a Co-Mo-Si ternary metal silicide alloys] studied the behaviour of Triballoy against an austenitic stainless steel at 400, 500 and 600ºC at a range of loads. During his studies, he showed the increase of wear rate with load and a decrease with temperature for the triballoy, while the autenitic stainless steel increased wear as load and temperature increase. No compacted layers were observed at any of the testing temeratures.

2.6. Surface Engineering

Tribological mechanisms and others, such as corrosion and fatigue, can lead to equipment failure. These phenomena happen at the boundary between the environment and the bulk of the component, altering the surface. Therefore, the best way to improve the material behaviour against these mechanisms is to change the surface properties.

Surface engineering is a "the design of a substrate-surface(coating) system to give a combination of properties that neither componentis capable of providing alone [98]. The reason surface engineering is earning a higher importance is because of the possibility of more cost-effective solutions, a wider range of solutions from an array of coating/surface treatment processes. Using surface engineering reduces demands for niche bulk materials while enhancing the performance of the component.

Although coatings/surface treatment can provide a variety of advantages, industry is still sceptical of coating/surface treatment solutions for their components due to:

- Uncertainty generated by the little understanding of coating technologies and their implementation in a real-life application, with some exceptions in other industries like aerospace and tool industries, which have been using coatings for longer periods of time.
- Testing in simulated conditions which tend to accelerate the testing process, causing uncertainty in the long-term performance of the technology.
- Expensive quality control measures needed in markets that are under heavy regulations, becoming a high financial risk in the short term.
- No standards that help customers select the appropriate technology required for their application. In the context of tribology, the information provided about the technology may not apply to the system performance improvement, which can mislead and require extra time to probe the technology efficacy for the application.
- Material recycling can be an issue as it may require removal of the coating from the substrate.
- Introduction to a new failure mechanism in the system, coating delamination. If delamination occurs, the substrate may not longer perform in the same manner as the coated system. In a tribological contact, this type of failure can drastically increase component degradation.

- Although suppliers provide information of how their technologies behave in different environments, the information provided might not apply to the system under improvement.

As shown above, the application of coating solutions to improve component performance has advantages and disadvantages, and from an engineering perspective there is a need to understand the behaviour of the technologies under the conditions in which they are used in service. This understanding must be gained in the most cost-and tim-effective way to entice companies to use coatings for their components.

2.6.1. Tribology of Coatings

From a tribological perspective at the microscale, mechanisms previously observed are present in coated materials, such as asperity behaviour due to stress and strains, crack nucleation, crack propagation, and particle formation. These microscale behaviours produce the behaviours seen at the macroscale, which describe the tribological behaviour of the system. From a coating context, Holmberg and Matthews set out four different macroscale processes for coating systems and these will be discussed [99]. A deeper look will be taken to the use of hard coatings as a way of reducing the impact of the tribological contact on the system, although soft coatings can also achieve improvements by taking advantage of different mechanisms [99].

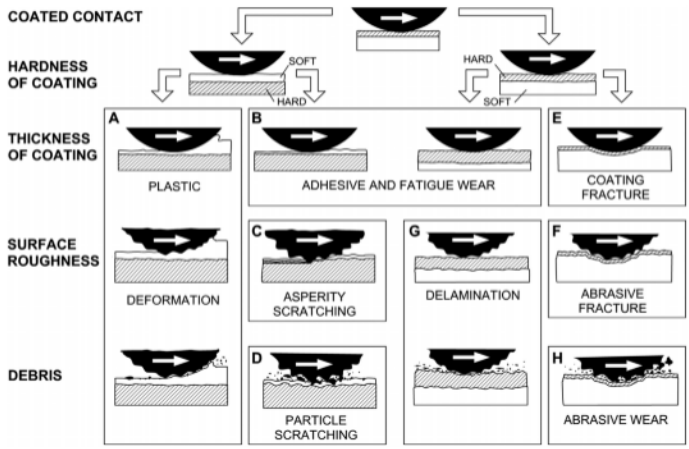

Figure 2.20. Coating macromechanical mechanisms for coating systems [99].

The first macroscale mechanism described by Holmberg and Matthews arises from the relationship between the hardness of the substrate and the coating applied. The application of hard coatings helps reduce the contact area of the system and reduces the ploughing of particles and asperities, aiding in reducing both wear and friction. The reduction of friction is not as high as expected for a soft film because hard coatings have higher shear strength, which has been

considered a higher importance effect for the friction reduction by researchers like Shepard and Suh [100] and, Bull and Rickerby [101].

The second macroscale mechanism is related to the coating thickness. Two scenarios are possible depending on the ability of the coating to support the load of the system. If the coating is very thin, there is the possibility of the substrate supporting the load. This behaviour can cause the coating to break off or crack due to the continuous deflection of the substrate, as seen by Leroy and Villechaise [102]. On the contrary, when the hard coating applied is thick and stiff enough, the effect of the load on the substrate can be reduced or neglected (stress shielding), preventing or reducing the rate at which the coating will fail and resulting in a more favourable situation.

The third macroscale mechanism results from the roughness of the surfaces in contact, and four situations can develop due to the effect of the previous macromechanism. On one hand, rough surfaces of a thick coating can have a beneficial impact on the friction behaviour of the system as it can reduce the points in contact These points can be maintained if the materials are hard and tough enough to allow the asperities to carry the higher loads, as reported by Sainsot [103]. On the other hand, a rough surface can increase the CoF of the system due to asperity break off and/or interlocking. From a thin coating perspective, substrate deflection can increase the number of asperities in contact and therefore reduce contact stresses at the asperity tips by distributing the load among more asperities. However, as these deflect, the substrate is loaded and failure can occur causing coating delamination.

The final macroscale mechanism described relates to the behaviour of the particles in the contact. Five different scenarios can occur depending on the roughness of the surface and the particle shape. The first behaviour considers the particles “hiding” in the valleys, having no effect on the friction and wear behaviour. As roughness can be reduced with time due to the wear process, these hidden particles can begin to increase the wear rate and friction as they will not be able to “hide”. This behaviour is shown by Shu and Saka in their work with “undulating” surfaces [34, 35]. In order for the particles to be contained in the valleys, they are required to have a critial size, which is a function of the surface roughness. Before the critical size is reached, particles are crushed if they have lower hardness than the surfaces in contact. If these particles have higher hardness than the surfaces, the particles act as abrasives, ploughing and scratching the surfaces. Also, if particles can act as load carriers and rounded enough, and the surfaces are smooth, they can act as rollers, helping reduce the CoF of the system [104].

2.6.2. Thermochemical Processes

Thermochemical processes involve the saturation of the substrate material with a desired element by their mutual reaction through the use of heat and a chemically active medium, typically a powder pack (solid), paste (solid with binder), bath (liquid) and/or gas. Saturation of the base material by diffusion is very dependent on the process temperature, time, element concentration in the medium, and the base chemistry of the substrate as it will dictate any further reactions. There are a wide variety of elements used in processes, which includes carbon, nitrogen, chromium, titanium, silicon, sulphur, niobium, vanadium, aluminium and zinc [105]. Some considerations in using these processes are [106]:

- Temperature cycling can cause distortion or introduction of residual stresses in component
- Deterioration of surface finish of the component
- Components are often left in an annealed condition and possibly undergone grain growth
- Can result in dimensional changes to the component.

During this work, three pack cementation processes, (aluminising, chromizing and boronizing), two nitrocarburizing treatments applied by a salt bath process, and a nitriding process via a gas were studied.

2.6.2.1. Pack cementation

A pack cementation process consists of the immersion of the components in a sealed or semi-sealed retort with a powder mixture that contains the surface treatment element source, a halide salt activator and an inert filler. Subsequently, the retort is introduced into a furnace since the process relies in the formation of halides of the surface treatment element, which are absorbed then decompose at the surface and diffuse into the substrate [107].

2.6.2.1.1. Aluminising

As the name suggests, Aluminising uses aluminium or an aluminium alloy to form a layer of mainly aluminides, and in the case of steels iron aluminides. The process is carried at temperatures between 700-1100^{o}C for hours [108]. These types of surface treatment tend to be used to improve the hot-corrosion resistance of components [109]. As iron aluminides are formed during this process, the end result will differ due to possible thermodynamic and kinetic factors depending on the process parameters and/or base material chemistry and the phase diagram shown in Figure 2.21 can be used to gain insight into the posible phases that can form.

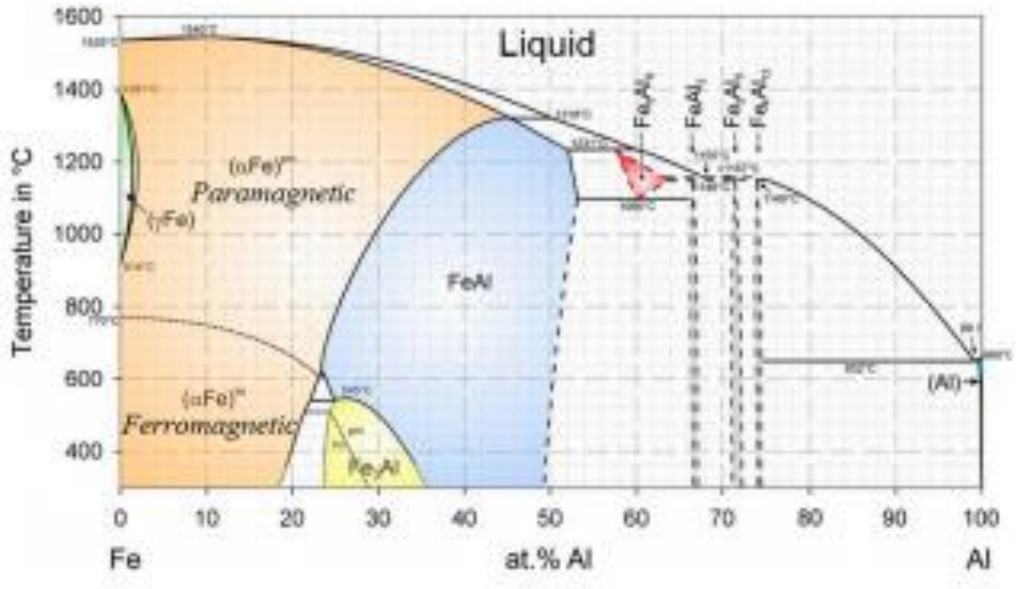

Figure 2.21. Fe-Al Phase diagram [110].

From a mechanical perspective, these intermetallics are considered to have low ductility and low fracture toughness [111], with higher Al contents lowering the ductility of the iron aluminide. Some researchers have found a beneficial effect by the addition of Cr, as it can improve the ductility of these materials [112]. As temperature increases, the Young's modulus drops in a linear fashion [113]. From a hot-corrosion perspective, the higher the Al content the higher the resistance to these environments [110].

A few researchers have looked at the tribological performance of intermetallic materials. Sharma [114] studied the Fe_3Al-ordered intemetallic at room temperature using a tungsten ball at three different frequencies. The studies showed that load and speed increase the wear rate of the material, with microcutting and microploughing wear mechanisms, in addition to detachment of surface material as the load increases. A similar tribological behaviour was seen by Yang [115] while looking at the tribological behaviour of an FeAl intermetallic against a bearing steel at different sliding speeds.

Zhang [116] studied the difference in performance of hot-dip aluminized and uncoated H13 at room temperature and 600°C. Even though the steel performance was better at room temperature, the aluminized layer appeared to perform better at 600°C due to the aparent formation a solid-lubricant Fe_2O_3 surface oxide film. This beneficial effect was also observed by Kato [117] as he added Fe_2O_3 particle that compacted into a tribolayer. Ahmadi [118] saw a similar behaviour in his studies, in which the steel performed worst at high temperatures

compared to the aluminized layers and was attributed to the higher capability of the layers formed to maintain the tribolayers formed during the wear process.

2.6.2.1.2. Boronizing

Boronizing is a process in which boron is introduced into the substrate of interest and forms a range of boride compounds (Figure 2.22) that change the microstructure, chemistry and mechanical properties of the surface. Boronizing tends to be done at temperatures between 850-950^{o}C resulting in the formation of an iron boride layer that aids steel alloys by improving their wear resistance and their corrosion resistance [119].

As mentioned previously, substrate chemistry plays an important role. From a boronizing perspective, the elements that have an impact in the end are Fe, Cr, Ni, Mo, V, W, C and Si [119]. In a simpler system, such a low carbon steel, boronizing, as explained by Carbucicchio [120], forms a hard jagged boride layer composed of the Fe_2B phase. In comparison, as more elements are present the process becomes more complicated, such as in the case of a stainless steel. For a stainless Steel, the boride layer tends to be composed of a FeB/Fe_2B layer. The Cr present can easily diffuse in the boride layers, forming compounds such as (Fe,Cr)B and $(Fe,Cr)_2B$, and at the grain boundaries forming chromium carbides, such as Cr_3C_2 and Cr_7C_3. Ni tends to form a Ni-rich layer in the form of Ni_3B below the formed layers due to the lower diffusion of the Ni during the process [121].

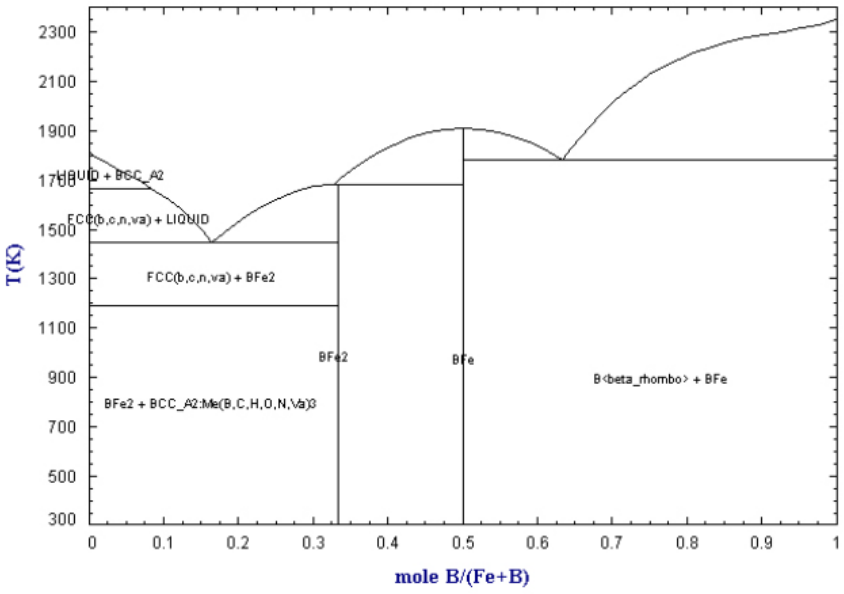

Figure 2.22. Fe-B Phase Diagram [122].

The FeB phase is not a desirable layer as it has poor adherence to the Fe_2B layer and tends to have high residual tensile stresses. A post treatment can be applied at 1000°C in an inert atmosphere in order to remove FeB and form a thicker Fe_2B layer [121].

Tabur [123] in his studies of boronized AISI 8620 steel showed how temperature and time of the process affects its wear performance. The longer the processing time, the higher the wear resistance of the simples. This behaviour is attributed to longer times making the grooves at the FeB layer finer and increasing the layer thickness, but as the temperature of the treatment increases a reduction of wear resistance was shown and is attributed to an increase in size of the grooves and their depth. Also, as load increased, the wear rate was found to increase as the wear scars get wider and deeper, increasing abrasive wear. Some of these behaviours were seen by other researchers - Wang [124] and Jain [125].

Motallebzadeh [126] studied the performance of two different boronized steels at room temperature and 500°C and found that wear increases at higher temperatures. This was attributed to cracking and spalling, believed to result from removal of water in the ceramic layer, based on the observation of arc-shaped cracks, and from thermal stresses, where the crack pattern was seen to be more branched. A similar behaviour was seen by Cimenoglu [127] while studying the behaviour of the single-phase and dual-phase layers, although the cracking was just attributed to thermal stresses. Previously to these studies, Taktak [128] examined two bearing steels. with and without the boronizing treatment, up to temperatures of 600°C. Taktak saw the same trend of wear increase as temperature increased even though glazed layers were formed on the surface. The wear mechanisms were suggested to be delamination changing to oxidative above 300°C. In general, the boronizing steels performed better than the untreated steels.

2.6.2.1.3. Chromizing

Chromizing is a thermochemical process which relies on the introduction of chromium into the desired substrate, which can be steel, nickel and cobalt alloys, and is carried out at temperatures between 700-1100°C [129]. Chromizing tends to be applied to improve service life of components, to increase service temperature, to prevent adhesion of molten metals and salts, to improve tribological performance of components and/or reduce the tolerances caused by other layers formed, such as overlay layers [130].

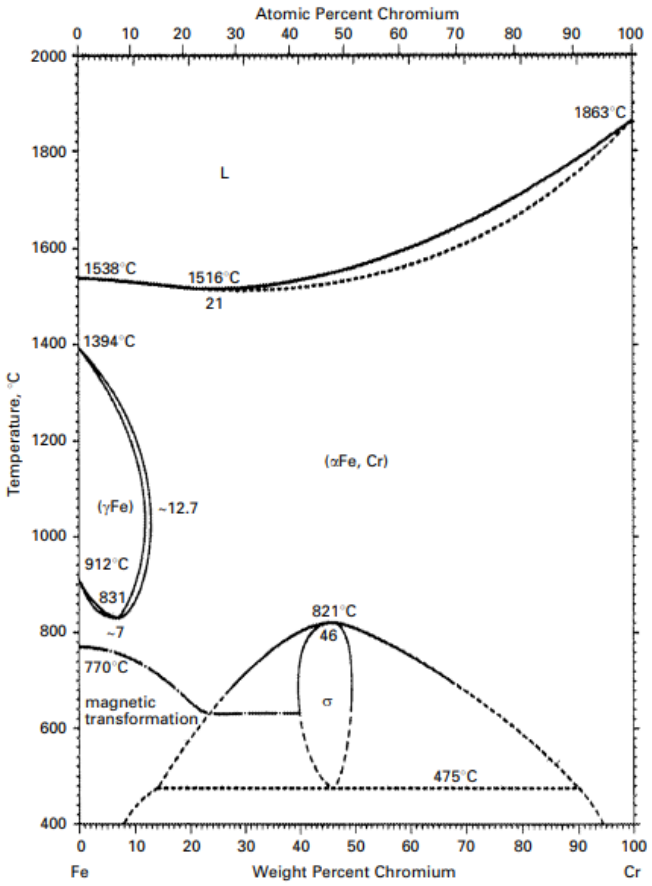

Figure 2.23. Fe-Cr Phase diagram [130].

The end result depends on the treatment temperature and time, as well as on the carbon and chromium concentration of the substrate. For a simple binary system, the end result can be visualized using the binary Fe-Cr equilibrium diagram shown in Figure 2.23. For a basic system, the steel will be retaining its austenite phase (at low temperatures) up to an intake of 12-13%wt of Cr. When this limit is exceeded, the system will transform to a ferritic phase when cooling down. Lastly, the two areas to note are the fully tetragonal area and the ferrite and tetragonal areas, which requires the layers formed to be held at temperature for a long time for these phases to form [130].

Carbon, as mentioned previously, can have an impact on the end result as carbon has a high affinity with chromium and will form chromium carbide compounds [130]. Other important elements that can have an effect are sulphur and phosphorous, which can have a detrimental effect on the chromium compounds, austenite stabilizers such as nickel and manganese tend to produce lower thickness layers formed, and finally ferrite stabilizers such as chromium and silicon tend to give higher thickness layers [130].

The end result is an outer layer with higher chromium content that improves the strength in addition to introducing high compressive stresses in the layers, which tend to be balanced by tensile residual stresses present at the area close to the interface between the substrate and the layers. Finally, depending on the carbon content, formation of an outer carbide layer (high and medium carbon contents) and/or the formation of carbide precipitates in and below the layers formed at the grain boundaries [130].

From a tribological perspective, chromizing uses hardening by formation of carbide/nitride particles or layers via single [131 and 132] or duplex treatments [133 and 134]. Hakami [134] studied a chromized AISI 1045 steel and two plasma nitride versions of the chromized steel. The wear and friction were lower than for just the chromized sample due to the formation of a continuous layer of carbides and nitrides. Lee [132] compared two steels and their chromized versions. The chromized steels formed a layer composed of nitrides and carbides and exhibited a higher wear resistance.

Taktak [133] compared two chromized steels at room temperature and 500^{o}C against the same steels with an additional nitriding treatment. During this study, it was shown that the chromized steel fail due to delamination, while applying the nitriding treatment and forming the nitride layer caused the the wear mode to transition to an abrasive wear mode, lowering the wear rate and reducing steady-state CoF. Elevated temperature reduced both the wear rate and the CoF of all the treatments due to the tribolayers formed.

2.6.2.1.4. Nitriding and Nitrocarburizing

Nitriding and nitrocarburizing are two of the oldest and most popular diffusion processes used to increase the hardness of the surface of a material. These treatments can be carried at temperatures between 420 and 630^{o}C [135]. As shown in Figure 2.24, at lower concentrations nitrogen will be in solid solution forming the austenite phase if it was not present before the treatment. As the amount of nitrogen increases and exceeds the maximum solubility limit, nitrides will start individually to grow and form a continuous nitride layer (Fe_4N) as shown in Figure 2.24. As the concentration increases even further, $Fe_2N_{(1-x)}$ forms, where x ranges between 0 and 0.5. The sequence described is a very general overview of the changes made to the surface and subsurface, as the initial composition of the substrate material can significantly affect the final microstructure, and consequently, properties. Other variations include the formation of a Fe_2N layer or nitride precipitates in the presence of nitride formers such as Cr, Mn, Ti, V and Al [136]. All these phases can be obtained as main phases if the process is adjusted, giving Nitriding a very wide range of end results that can be tailored to different applications.

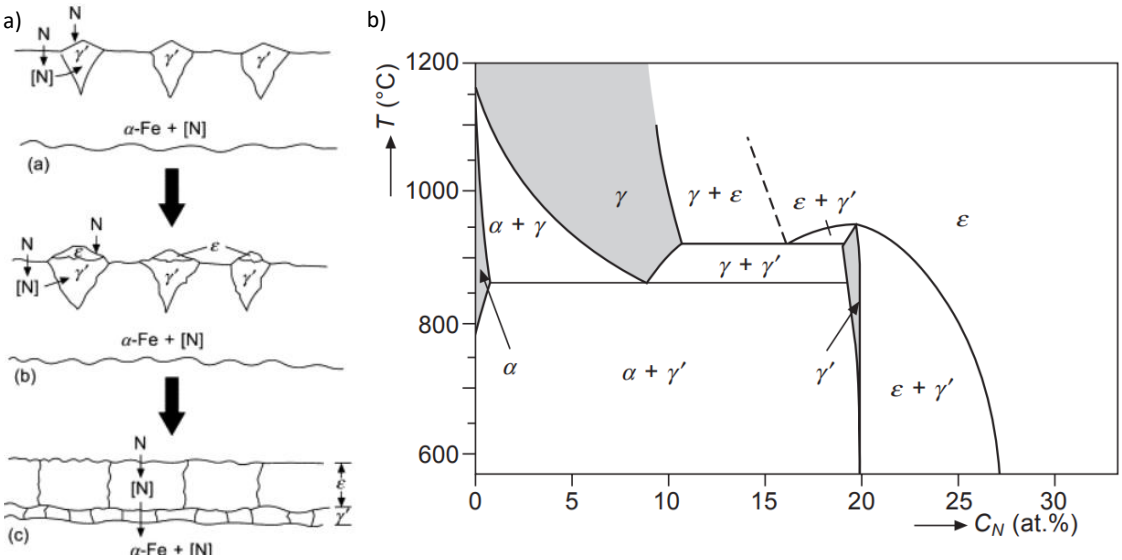

Figure 2.24. Growth of Fe-base nitrides during a Nitriding process (a) [135], and Fe-N Phase Diagram (b) [137].

For an austenitic stainless steels, the transition in mechanical properties between the bulk material and the nitride layer, which ranges hardness between 800HV and 1200HV, is very sharp in comparison to other steels which exhibit a smoother transition. In addition, when nitriding is applied at temperatures higher than 450°C, Cr tends to form CrN precipitates, which will have an impact on the oxidation and corrosion behaviour. Gas or plasma nitriding carried out at temperatures lower than 450°C can be further case-hardened without reducing the corrosion properties of the base material. In these conditions, the outer layer formed is supersaturated austenite (hardness between 1200-1700HV) with the drawback of requiring longer processing times [135].

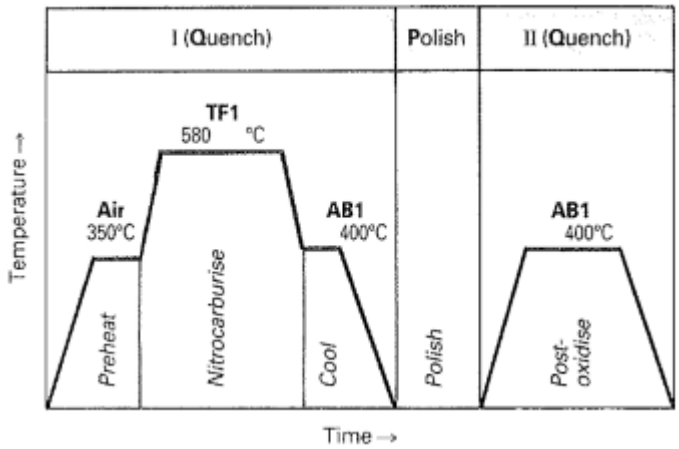

Figure 2.25.Schematic representation of a QPQ nitrocarburizing treatment [138].

The main advantage of nitrocarburizing over nitriding is the reduction of processing time, as the addition of carbon aids the formation of the nitrides, specifically Fe_2N_3 phase [135]. When doing

these treatments, sometimes they are followed by an extra two steps, polishing of the surface and a post-oxidation step, known as QPQ process (Figure 2.25) [138]. The addition of a Fe-base oxide layer aids corrosion resistance and fills any pores close to the surface with oxides [139].

From a tribological perspective, the behaviour of these treatments is very dependent on the final composition. Studies have shown that nitriding and nitrocarburing can improve the wear performance in comparison to a steels [140 and 141]. For example, Heydarzadeh [142] looked the difference in behaviour of different compound layers, and Quiang [143] looked at the difference in behaviour of QPQ treatment and demonstrated how different processing parameters can significantly affect the wear and friction performance of these treatments. Heydarzadeh showed in his studies of an AISI 52100 steel that the layer with higher amount of Fe_2N_3 had the highest hardness and wear resistance, and lowest CoF. He also pointed out that the running-in behaviour of these materials show a high CoF due to the higher average surface roughness generated as a consequence of the treatment. Qiang's ring-on-block tests against an AISI 52100 steel showed that in unlubricated conditions, a QPQ process improves the wear performance but increases wear in comparison to a Fe_2N_3 layer, attributed to the hexagonal lamellae crystal structure of this phase. Creating an oxide layer without the polishing step provides a decrease in the wear resistance and slightly lower CoF than a QPQ process.

At higher temperatures, the literature concerning the tribological behaviour of these treatments is very limited. Emami [144] showed that the nitrided steel performed better than the untreated steel at all temperatures in terms of wear and friction attributed to the development of compacted layers, with higher oxygen contents in the layers at higher temperatures. Pellizzari [145] looked at the behaviour of nitriding and other hard coatings for an aluminium extrusion application. From his experiments, in which the plate was at 350^{o}C and the block at 250^{o}C, the wear improvement was not as significant for the nitrided steel in comparison to the other hard coatings as it was found that the nitrided steel undergoes material delamination accompanied with by a large and unstable CoF.

2.6.3. PVD

Physical Vapour Deposition (PVD) is the process of applying thin films and is done at reduced pressures, 10^{-2} to 10^{-5} Torr. The process takes advantage of the different physical phenomena that take place after the material that is to form the coating is atomised or vaporised, which are [105]:

- High energy is applied or bombarded to the "target" material causing it to vaporized or atomize.

- The atoms are then transported to the surface of the substrate and can react with the atmosphere at which they are subjected i.e oxygen, nitrogen or a carbon-based gas like methane. In order to prevent reactions argon tends to be the prefer gas.
- The final step is the build up of the coating at the surface of the substrate material. During this stage reaction between the vaporized material and the atmosphere can still ocurr.

Depending on the PVD technique (thermal evaporation, cathodic-arc depostion and sputtering) and the specific conditions, some of the steps shown above may not occur. Also, a plasma flux may be used in order to direct the ionized atoms onto the substrate and can be used in different atmospheres in order to achieve different chemistries and microstructures.

As with the other treatments, the PVD process shows advantages and disadvantages [106] over that need to be considered before the decision to use it as a coating process for the desired component. These relate to the process itself, the deposition materials and the component requirements.

Advantages:

- Wide range of coating material possibilities, which includes the deposition of pure materials or compounds and inorganic and organic materials
- More environmentally-friendly than other deposition techniques such as electroplating
- Substrate is not required to be in a high temperature environment, giving the possibility to coat a much wider range of substrates than other techniques
- As the precursor materials are not toxic, pyrophoric or corrosive, makes material handling easier
- Can improve adhesion between coating and substrate by pre-cleaning of the surface using ion bombardment when compared to other processes which rely on a mechanical bond
- No post-processing, such as polishing and machining, as the coating replicates the original surface
- Specific process parameters, such as deposition rate, can be highly controlled.

Disadvantages:

- Line-of-sight process, which makes it difficult to coat intricate components
- More expensive than other processes, such as some thermochemical processes
- Requires highly skilled operators

- Equipment requires a high degree of cleanliness or one kit per coating to avoid cross contamination
- Substrate requires a high degree of cleanliness in order to achieve the superior coating adhesion
- Surface texture of the substrate material can impact the success of the coating process
- Different sources used for the PVD process can give different coating structures and properties.

From a PVD perspective, magnetron sputtering and arc-evaporation are the most widely used techniques to apply nitride base coatings, with each one having advantages and disadvantages for consideration as shown in Table 2.1 [146].

Table 2.1. Advantages and Disadvantages of PVD deposition by Magnetron sputtering and Arc evaporation.

Advantages	
Magnetron sputtering	Arc Evaporation
• Smoother surface due to the formation of smaller particles during the deposition process • Ease scaling up the process • Good thickness control • Good uniformity • Higher control over layer structure and properties • Lower deposition temperatures allowing a wider substrate range, more concerning with polymer substrate materials • Wider range of deposition materials	• Higher ion to neutral ratio providing better adhere and more densify layers • Higher deposition rates
Disadvantages	
Magnetron sputtering	Arc Evaporation
• Lower density • Lower adhesion • Target poisoning	• Defects formed when use low melting point materials • Defects can lead to higher roughness surfaces

2.6.3.1. AlTiN

TiN was heavily researched at the 70-80s, but this coating could not be used for tool applications with temperatures higher than 600°C due to its oxidation behaviour and loss of mechanical properties. A way of increasing its temperature stability, the addition of Al to TiN to form a $Ti_XAl_{1-x}N$, was developed. It was found that a maximum of x=0.6 was required to keep the layer as a single phase by arc evaporation (146) and x=0.4 by a dual-magnetron sputtering process [147]. This $Ti_{1-X}Al_XN$ improved the oxidation resistance due to the formation of an Al_2O_3 -TiO_2 dual oxide layer [148], in comparison to TiN just forming a TiO_2 which is unstable at higher temperatures. In addition, the retention and/or increase of mechanical properties at high temperatures (600-1000°C) was observed and attributed to a split into cubic AlN and cubic TiN, hindering the motion of the boundaries between each phase due to a development of elastic strain fields [149].

From a tribological perspective, Rodriguez [150] looked at a series of nitride-based coatings, which include AlTiN, in room temperature environments against a half-hardened 100Cr6 steel. Rodriguez found that the least hard coating used (CrN) in comparison to the AlTiN was better from a wear perspective. Aihua [151] also studied a range of nitride-based coatings, which included TiN, TiAlN, AlTiN (higher Al content) and AlCrN, at room temperature against a silicon carbide ball using a ball-on-disc configuration. Ahia [151] showed that the lower Al content coatings showed both better friction and wear behaviour. In the case of AlTiN, its poor performance was attributed mainly to brittle fracture, while the poor performance of AlCrN was attributed to a higher number of particles from the silicon carbide ball, since the ball of this contact showed the higher wear. This behaviour of the AlTiN described by Aihua [151] was previously described by Hsieh [152]. Hsieh showed that the Ti-based thin films containing Al tested at room temperature against Al_2O_3 balls have the worst wear performance. This was attributed to the oxide formation, being TiO_2 for the Ti-based films in comparison to Al_2O_3 formed for the coatings that contained aluminium, which exhibited the brittle fracture mechanism noted previously. On the contrary, on tool studies of these coatings, higher Al content AlTiN yielded better wear performance up to Al contents of 0.66 at% [149] attributed to the decomposition of the single phase AlTiN into c-AlN and higher Ti content c-TiAlN. The detrimental effect of >0.66 Al content is due to the formation of h-AlN in a c-AlTiN matrix during deposition, which has a large volume mismatch [153]. Similar detrimental mechanisms for the tribological performance of the coating was highlighted by Chen [148], while the magnetron sputtered coating suffered from precipitation of h-AlN when the same at% was tried to achieved. causing a reduction in the tool life

Even though tool testing highlights mechanisms that occur at higher temperature due to the heating of the tool, these mechanisms can change when reciprocating or rotational motion tests are carried at high temperatures. Liu [154] studied the performance of AlTiN at temperatures ranging from room temperature up to 700°C against a silicon carbide ball. Liu showed that from room temperature to 400°C, the wear rate increased and this was attributed to a mild abrasive wear. At higher temperatures, wear was not measurable due to the formation of a tribolayer from debris material from the silicon carbide and the coating itself. On the other hand, the friction behaviour was dependent on the stability and amount of TiO_2, as Liu showed that as temperature increased up to 500°C, the CoF decreased, while it increased again higher temperature. Dejun [155] looked at higher temperatures than Liu; from 700-900°C against a Si_3N_4 ball. Results showed a decrease in the CoF as temperature increased due to the oxidation of the coating. From a wear perspective, it increased as temperature increased due to a change in wear mechanisms from a mainly abrasive and oxidative wear to an adhesive and fatigue type of wear. Similar results to Dejun were obtained by Nohava [156] who examined the performance of a range of nitride-based coatings, including AlTiN, at room temperature, 600°C and 800°C. Novaha [156] showed an increase in wear as temperature increased, being very high at 800°C due to coating failure attributed to oxidation of the substrate causing cracks from the top layer to inside the substrate.

2.6.3.2. CrN

After the development of AlTiN to improve the performance of the TiN for higher temperatures, a second generation of nitride base coatings was developed, CrN-based systems, to improve the efficiency of these hard coatings in high temperature environments. In comparison to TiN, the CrN-base systems are known for the better performance in corrosion/oxidative environment, due to their chemical inertness, low internal stresses, high hardness, thermal stability and wear performance [157 and 158]. Mayrhofer [158] adds that the end result after deposition, in terms of microstructure and internal stresses, not only on the mechanical properties of the coating, but also on its thermal stability. The thermal stability is dependent on the transformation of c-CrN to h-Cr_2N [159], which as previously pointed out, it is dependent on the coating characteristics given by the application process. At 900°C the h-Cr_2N is further decompose into Cr and N. It has been show that this phase transformation can change the oxidation behaviour of the coating [159, 160 and 161].

As with TiN, to further increase the stability of CrN for higher operation temperatures, Al additions in CrN were carried in order to “improve” the thermal stability at more demanding temperature environments. The addition of Al into the system increases the temperature at

which the single phase coating starts to undergo phase transformation. As with AlTiN, the amount of Al has an effect on the phase of the AlCrN coating. When the aluminium content is lower than 60-80 at%, the coating will have an f.c.c. structure; while above, it will be hexagonal [162 and 163]. Also, AlCrN undergoes a phase transition at high temperatures due to the precipitation of h-Al. Lin showed that there is a phase precipitating at 900°C; h-AlN, for a $Cr_{0.77}Al_{0.23}N$ and as Al content, the h-AlN phase precipitation can increase up to 1000°C for a $Cr_{0.4}Al_{0.6}N$. for $Cr_{0.77}Al_{0.23}N$ and with increasing Al content, the temperatura at which h-AlN phase precipitates can increase up to 1000°C for a $Cr_{0.4}Al_{0.6}N$. The precipitation causes a Cr enrichment in the parent phase resulting in a further phase transformaion to Cr_2N [164]. Yttrium is added to nitride base PVD coatings, such as AlCrN and CrN, in order to improve their thermal stability, improve mechanical properties and oidation resistance [165]. From a thermal stability perspective, yttrium hinders grain boundry diffusion preventing the coating elements, oxygen from the environment and susbtrate elements [166, 167, 168], as Mirkka [169] shown the presence of Fe and Cr along the column boundries of a TiAlCrN coating.

From a mechanical properties standpoint, the behaviour of these coatings is different depending on the ratio of the elements contained in it and the processing method and its parameters; and these variations have been reported in the literature. Normally, CrN coatings are reported to have hardness values, ranging between 15-25 GPa [170, 171, 172, 173 and 174]. Hones [170] explains that the variation comes from the ratio between the CrN and Cr_2N phases- the higher the Cr_2N content, a higher the hardness for the coatings with the same amount of internal tensile stresses. Also, Hones [170] saw a reduction in hardness due to an increase in grain size, which is in accordanc with the Hall-Petch relationship [174]; however, Sundgren [175] stated that the influence of the grain size on the hardness of single-phase refractory materials is not significant. Adding Al into the CrN system tends to increase the hardness of the coating, which varies between 10-36GPa [164, 171, 172, 173, 176 and 177]. This can be attributed to the hardening effect produced by the introduction of a solute element, which distorts the crystal lattice and increases slip resistance [179], a decrease in grain size which increase the lattice friction and/or the increase in residual stresses in the coating. All these papers report different trends in the mechanical behaviour of this coating system. Some authors showed an increase in hardness as the at% Al increased [164], probably because the Al content to produce a coating composed of hexagonal and cubic phases was not reached. Others have seen a decrease in hardness when the at% Al is very high [171,173 and 177]. In some cases, it was attributed to an increase in grain size [166], but most attributed this to the existence of both cubic and hexagonal phases.

As temperature increases, for the CrN coating system, there is a drop in mechanical properties up to 800°C [164,171 and 172] due to a decrease of the internal stresses, defect density, and an increase in grain size. Reiter [171], showed an increase in mechanical properties after the 800°C, which he attributed to the precipitation of the h-Cr_2N phase. Increasing the at% Al has been shown to increase the thermal stability of the mechanical properties of the Cr-N system [164, 171 and 176]. The higher stability of the system at higher Al content is attributed to the stability at higher temperatures of h-Al [154]. William [176] noted a high increase in hardness at 725°C for an $Al_{0.68}Cr_{0.32}N$ coating, attributed to the formation of the previously mentioned h.c.p. phase, but a decrease after higher temperature annealing, attributed to a larger grain size, and the distribution and the higher volume fraction of this h.c.p. phase.

From a tribological perspective, these coatings can demonstrate different behaviours in the same system depending on the counter-face and coating characteristics. Su [180] have shown an increase in wear resistance of CrN, in Su's study against two bearing steels. He also reported that coating thickness affects the wear resistance of the coatings, comparing CrN and Cr(N,C) coatings in his study [181]. In this paper, he attributed this to the combined behaviour of coating layer and the substrate, which will depend on test load. For his system, a 7µm CrN layer was the optimum. Others, like Warcholinski [182], looked at the tribological behaviour of different phases present in CrN layers and CrN multilayers. From a single layer perspective, a CrN layer showed lower CoFs and higher wear resistance than the harder h-Cr_2N, which was associated to its lower shear strength. A further room temperature study was done by Lin [183] who looked at the behaviour of different thickness CrN deposited by modulated pulsed power magnetron sputtering, from 5-55µm, applied on a range of substrate against AISI 440C steel. During this study, Lin concluded that the best tribological performance was given by the hardest substrate and thicker coating as this system provided a higher load carrying capacity. The wear mechanisms ranged from minor cracking for the hardest substrate with a 55µm thick coating to heavy delamination of the coating for the softest substrate. The last observation was an increase of wear rate as load increased which was attributed to higher flash temperatures on the surface and an increase in the ploughing force.

Sanchez [177] and Ding [173] studied the performance of different at% Al in the Cr-N system on the wear and the friction behaviour against a 6 mm diameter 100Cr6 ball and 9.5mm diameter Al_2O_3. respectively. In addition, Sanchez [177] did the test using a 5N load at 10cm/s, while Ding [173] used a 10N load at 20cm/s. Sanchez looked at the behaviour of coatings with at% Al of 0.5-0.7 and showed that both friction and wear were the lowest when the at% Al content provided the highest hardness. He attributed this wear behaviour to the difference in wear mechanisms,

being mainly abrasive at the lower at% Al to an adhesive type of wear for the higher at%Al, while the friction behaviour was attributed to rougher surfaces giving higher friction coefficients. Ding, from a wear perspective, showed a similar trend for coatings with at% Al between 0-0.5, but the harder coatings provided higher friction coefficients attributed to an increase in coating roughness at% Al increased. From a wear perspective, Bobzin [184], showed a similar behaviour by comparing CrN to $Cr_{0.77}Al_{0.23}N$ mated against Si_3N_4 and Al_2O_3. Bobzin also identified the wear modes to be adhesive transitioning to abrasive when particles are pulled into the contact and attributed the better wear resistance of the $Cr_{0.77}Al_{0.23}N$ to the better abrasive resistance resulting from a higher hardness. On the other hand, Aihua [150] and Mo [185] showed in their experiments that more basic coatings, such as TiN and CrN, perform better than AlCrN. During Aihua's experiments, AlCrN wore more of the SiC counterface, causing a higher debris accumulation and a higher wear of the system. Mo [185] attributed the difference in tribological behaviour to their difference in oxidation behaviour due to the heating caused during the test, as their relative hardness did not aid to predict their tribological performance. i.e CrN best performing, while AlTiN worst performing from a wear perspecive.

From a high temperature perspective, the behaviour of the coating was attributed to transfer layers formed on the coating surfaces. Zhang [186] looked at the behaviour of CrN up to 500°C against a WC ball with a range of loads. During his studies, he observed that at temperatures up to 315°C, the CrN layer suffers ostly from abrasive wear. At higher temperatures, the wear mechanisms shifts to a mild oxidative wear due to the formation of an oxide layer, but as the load of the test increases, it transitions to severe wear mode as the oxide ayer breaks and the unprotected coating surface adheres to the counterpart. Additionally, this translated to an increase in friction. If these layers were not broken down, Zhang showed that wear and friction decreased for the system studied. Similarly, Polcar [187] and Sue [188], observed these friction and wear trends when testing these coatings against a 100Cr6 and a Si_3N_4 balls and Inconel 718 disc up to 500°C and 600°C, respectively. The wearing of the 100Cr6 steel and the Inconel 718 disc formed transfer layers that protected the CrN layer, causing a reduction in wear and lowering the friction CoF. In addition, Polcar looked at the differences between CrN and Cr/CrN multilayers [189] at temperatures between 600-800°C. From a wear perspective, the multilayered coating outperformed the single layer in their system, even though wear was found to be negligible for both. Polcar also claimed that the CoFs of the different coatings were very similar and proposed this was due to the formation of dense tribolayers composed of chromium-based oxides.

Gangatharan [190] studied the behaviour of AlCrN (pin) at temperatures up to 400°C against EN31 steel discs on a pin-on-disk configuration. During his studies, both wear and CoFs increased as temperature increased due to the wear of the steel disc counterpart, even though the coating performed better than Ti-6Al-4V. A similar behaviour was seen by Polcar [191], who carried out tests up to 600°C against Al_2O_3 and 440C balls. Polcar saw the formation of tribolayers at 500°C, followed by the coating failing at 600°C due to the formation of large coating particles that increased both the CoF and wear rate. Nohava [156] also saw similar results for the coating behaviour at room temperature and 600°C, but found that at 800°C, the wear rate of the system increased due to coating failure. Finally, Pulugurtha [192] looked at the difference in the tribological behaviour between CrN and CrAlN against a WC pin of 6mm at room temperature and Al_2O_3 ball at 700°C. In addition, both CrN and CrAlN were deposited with Ar/N_2 flow rates of 43-43, 60-40 and 70-90 sccm at 1.5 mTorr chamber pressure. During his studies, AlCrN showed higher CoFs and higher wear rates for the higher at% Al contents at both temperatures attributed to the lower hardness of the coating obtained at higher Al content. Pulugurtha suggested the difference in behaviour with other previous authors studies is due to the purity of the films, with others having oxygen in the Cr-N.

2.7. Conclusion

In conclusion, this literature review presented basic friction and wear mechanisms that could be observed for the systems under study. As the basic friction and wear mechanisms explained were developed by the study of metallic materials, further information about the behaviour of coating systems was also reviewed. After the tribological summary, an overview of the different materials and the different coating/surface treatment processes applied during the project was undertaken, including the different behaviours observed by a range of researchers using various testing conditions.

The trend, for both coated and uncoated system, shown by literature was the improvement of wear and friction performance as temperature increased attributed to the formation of compacted layers. This reduction of friction and wear caused by these layers were generally related to the reduction of particles in the system, since as particles are compacted, the formation of these layers create surfaces with higher load carrying capacity, mostly mention on the studies of the metallic pairs.

The reduction in the performance of the coated and uncoated systems was generally found to be caused by the loss of mechanical properties of the material under contact, as well as layer

failure. As the temperature increased, the performance degradation was also attributed to the absence of the compacted layers or to their low durability.

The formation of compacted layers was said to be dependent on all the system conditions, including the material pair under study, but at the same time, it is still not well understood due to the complexity and inter-relationships of a rango of mechanisms. From a wear performance, it was mentioned that protection was obtained when a high density, high adherence layer is formed with the ability to reform fast if broken. Similar requirements were assumed from a friction perspective, but no explanations were found for the varying friction behaviours observed in different systems with slightly different ''durable'' compacted layers. Friction is a sum of all the different acting mechanism and its complexity is a function of time, temperature load, frequency, environment, and both large and small changes in alloy/layer composition.

As observed during the literature, coatings/surface treatment showed a wide of different wear and friction behaviour and enlighted me that all paths can give a solution to the "problem" under study. However, as enlighting as it was to read the literature, the data obtained was not used in order to select the concepts that will be used for the study for the following reasons:

- Most cases in the literature do not replicate the contact under study. Also, most cases in the literature and most prominent observed on the coating/layer treatment literature than the literature related to the behaviour of the bulk metals, are interested in the behaviour of one of the sides in the contact; while neglecting the behaviour of the other material. For this study is both important to replicate the contact and the behaviour of parts of the system.
- In order to understand how the material could behave during the application from a tribological perspective, a series of "snaptshopts" were taken at different temperatures. For some materials selected, that information was not available.
- The selection of the different materials under study is restricted not only by the environment in which they are introduce in, but also in what is commercially available, the capabilities of the suppliers to fullfill demand, component geometry and costs.

Taking into consideration the experience and at the same time inexpirience in the topics touched during this EngD and all the things learn during the literature search, a wide range of materials with a wide range of behaviours, from a tribological, mechanical and chemical interactions with the environment, were selected in order to understand for current and future reasearch

3. Methodology

3.1 Selection Process

Coating technology opens a wider pool of possibilities for the application under study, but it can be detrimental as finding solutions for the different challenges are time critical in industrial situations. Therefore, a cost-effective process that aids the selection process needs to be developed. Matthews, Holmberg and Franklin [193] introduced a 9-stage process which progressively eliminates the materials under study; in contrast, previous methodologies such as that in James [194] dictate that if something works it is used, eliminating the opportunity to explore other possible candidates that may outperform it. In addition, the Matthews, Holmberg and Franklin methodology takes into consideration the contact type/condition and not the wear mechanism, unlike the traditional selection tools such as those developed by Smart [195]. This 9 stage selection process is comprised of the following stages [193]:

1. Application and Design, which involves assessing the need to develop a general specification of the required solution.
2. Component Specification, which defines the environmental and service conditions, and the constraints to which the components will be subjected.
3. Functional tribology requirements, which involves the statement of the limitations, such as noise and vibrations, and the requirements from a friction and wear perspective.
4. Functional coating/surface treatment requirements, which is a coating/surface treatment specification for the application.
5. Non-functional requirements, which include parameters of the coating/surface treatment and the process that are necessary but do not have an effect on the tribological properties.
6. Economic and procurement requirements, which are related to the economic, legal and procurement factors.

The following three steps relate the steps 4, 5 and 6 and use the different requirement types as filtering options.

7. Coating/surface treatment process characteristics
8. Coating/surface treatment material characteristics
9. Specific layer material and process characteristics

As proposed by Matthews, Holmberg and Franklin, the methodology needs to take into account:

- The conditions to which the components are subjected

- Constraints due to the material application
- Limitations added by the 'rules'. These rules are based on different tribological contact conditions.

Based on this process presented by Matthews, Holmberg and Frankling, a methodology was developed for the current studyusing the engineering and purchasing requirements given in Table 3.3.1. For each application, these requirements were evaluated and scored using a Cause and Effect (C&E) matrix following the filtering process shown in Figure 3.1.

Engineering requirements	**Purchasing requirements**
Adhesion between coating and substrate	Intellectual property
Corrosion resistance	Environmental compliance
Thermal shock	Cost
Thermal capability	Dual source/global availability
Surface treatment uniformity	Bringing capability to manufacture in-house
Surface finish requirements	-
Component dimensional changes	-
Tribological characteristics	-

Table 3.1. Elements taken into consideration during the selection process.

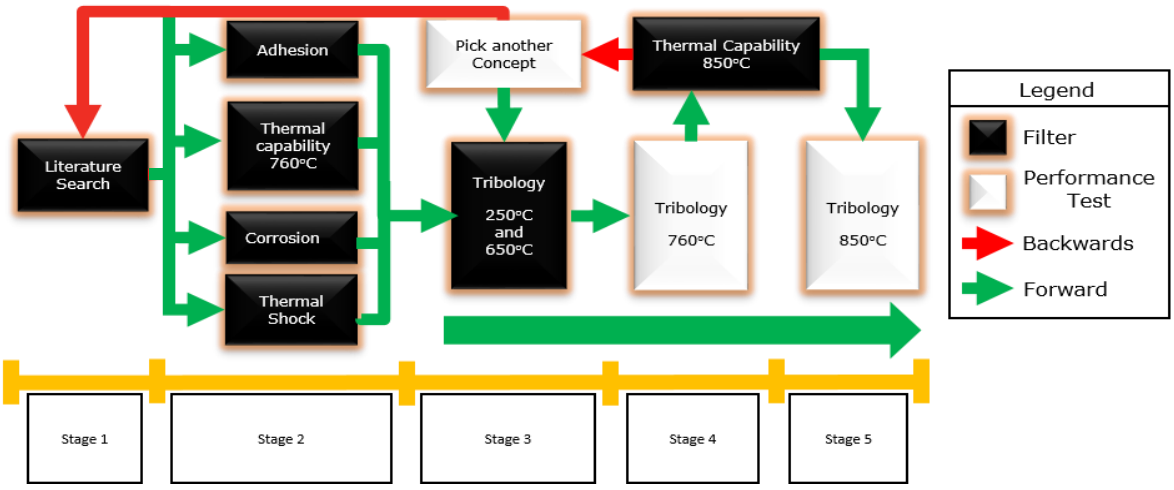

Figure 3.1.Filtering process diagram.

Initially, at Stage 1 information regarding the purchasing and engineering requirements of the different coatings/surface treatments were obtained, including some knowledge of their tribological characteristics. Then, based on the information gathered, a set of coatings and surface treatment were selected and samples were purchased. During Stage 2, this set was

filtered down based on other coating/surface treatment characteristics, such as adhesion, thermal capability, corrosion and thermal shock. At Stage 3, the 250^{o}C and 650^{o}C tribology testing was used to further filter the concepts prior to the testing at the final temperature. Between Stages 4 and 5, a new thermal capability test was added to address the future requirement of 850^{o}C, followed by the 850^{o}C temperature tribology test for future applications (note that this temperature test was not carried during this project due to time restrictions caused by the different challenges faced). Although the cycle finishes at Stage 5, if an appropriate solution is not found, or more time is available, the previously rejected samples may be reconsidered or the cycle may need to restart from Stage 1.

In order to rank the different coating/surface treated materials, a Cause and Effect Matrix (C&E) was developed. In this matrix, each of the requirements proposed in Table 3.2 are assigned an importance rating from 1-10, according to a set of rules as shown in Table 3.2. Each coating/surface treatment concept is assessed for these criteria and scored accordingly.

Requirement (importance rating)	Test	Score	Criteria
Life of Coating (10)	Adhesion Test	9	H1
		3	H2
		1	H3, H4
		0	H5, H6
Corrosion Resistance (7)	Environmental testing: Corrosion	9	Reduced pitting with no oxides on the Surface
		3	Similar pitting and small amounts of oxides formed
		1	High amounts of iron oxide with none or small pitting
		0	Excessive pitting and high amounts of oxide formation
Thermal Shock Test (5)	Environmental testing: Thermal Shock	9	High resistance to temperature change. No coating delamination and no discolouration
		3	Very minute (Slight?) amount of visible cracking, flaking of the surface treatment or discolouration
		1	High (Severe?) damage to the surface treatment i.e. flaking, cracking or delamination
		0	No resistance at all
Thermal Capability (9)	Environmental testing: Oxidation/Thermal Stability	9	Stable oxide layer generated at temperatura
		3	Stable but partial oxide layer formed at temperature or unstable, but full oxide layer formed at temperatura
		1	Unstable partial oxide layer formed at temperature. Or substrate oxidation observed
		0	No oxide layer formed at temperatura
Surface Treatment Uniformity (8)	A combination of surface roughness, thickness variation, coating coverage, substrate close surface properties (case depth and phase changes) and porosity	9	Low thickness variation, low variance of surface roughness between samples, full coverage of the surface and no porosity
		3	Intermediate thickness variation, medium surface roughness variance between samples, full surface coverage with few missing spots of coverage and low porosity
		1	High thickness variation, good surface finish with occasional coverage miss and some porosity
		0	Very high thickness variation, high surface roughness variance between samples. Poor coating coverage
Base Material Surface Finish Requirement (7)	Experiences earned with suppliers through meetings or after coating samples or parts	9	No change to current surface finish specifications. Rough machined and cast surfaces are aceptable
		3	Surface finish specification ≥ 1.6 µm ≤ 4.0 µm
		1	Surface finish specification < 1.6 µm
		0	Polished surface specification
Changes to Final Component Dimensions (4)	Experience earned during literature search as some coating/treatments grow and other subsurface properties are changed	9	Change in component dimensions ≤ 5 µm
		3	Change in component dimensions ≤ 25 µm
		1	Change in component dimensions ≤ 100 µm
		0	Change in component dimensions ≥ 101 µm
Tribological Characteristics (10)	Environmental testing: Tribology test	9	Better wear and friction behaviour tan nitrocarburizing 1 at all temperaturas
		3	Coefficient of friction and wear resistance at all temperatures equivalent to nitrocarburizing 1
		1	Coefficient of friction and wear resistance at all temperatures 30% worse than nitrocarburizing 1
		0	Coefficient of friction and wear resistance at all temperatures 50% worse than nitrocarburizing 1
Proprietary Technology (7)	To ensure that no patents are infringed that may hinder our ability to apply surface treatment/coating concepts to the shroud and nozzle ring. Consider opportunities for securing patents on a selected treatment option.	9	Non-proprietary
		3	Non-proprietary technology, but using proprietary variations
		1	Proprietary technology
		0	Proprietary technology to a CTT competitor
Sensitivity of Process to Component Geometry (9)	Ability of the process to be used with different component geometries	9	Uniform surface treatment deposited irrespective of component geometry
		3	Surface treatment process limited by angles and certain geometries
		1	Limited areas of components can be surface treated
		0	Surface treatment cannot be applied to components
Cost (8)	Per unit price from supplier	9	Lower Price than nitrocarburizing 1
		3	Nitrocarburing 1 price
		1	Higher price than nitrocarburizing 1
		0	
Environmental Compliance of Process and Components (10)	Evaluate concept to ensure it meets global environmental legislation	9	Complies with current and future environmental legislation
		3	Risk of being non-compliant in the long term (< 5 years)
		1	Risk of being non-compliant in the short term (< 2 years)
		0	No compliance with current environmental legislation
Dual Source and Global Availability (9)	This includes a number of considerations such as whether the surface treatment is proprietary, who are suppliers, their geographical location, are they TS16949 certified, company size and global reach	9	Global and multi-company sources
		3	Multiple local suppliers around the world or one global supplier
		1	Single, local source
		0	No source
Risk of Supplier Design Control (7)	Financial stability, willing to collaborate for their own development (ex: coating improvement) and leap times/deliver in time.	9	Process outcomes and details shared with CTT to create work instruction for surface treatment process
		3	Process outcomes shared with CTT and designs remain CTT owned
		1	Minimal data shared with CTT. Supplier design ownership
		0	Total supplier control
Integration of Manufacturing Technology into Cummins Facility (2)	Add technology into production line	9	Process conducted in a small, well contained unit
		3	Process conducted in a large, self-contained unit with safety implications for surroundings áreas
		1	Process requires separate manufacturing line
		0	Not possible to integrate process

Table 3.2. Criteria used to rank the different concepts in the C&E matrix.

3.2 Starting Materials

Several coatings and surface treatments were evaluated and compared against some uncoated materials; these are listed in Table 3.3. Note that all coating/surface treatment materials were applied to 304L and 321 stainless steel.

Uncoated Materials	Diffusion Treatments	PVD	CVD
304L Stainless Steel	Boronizing	CrN	Al_2O_3
321 Stainless Steel	Chromizing	AlTiN	-
Nitronic 60	Aluminising	AlCrN	-
Tribaloy 400	Nitriding	-	-
Stellite 6	Nitrocarburizing 1	-	-
-	Nitrocarburizing 2	-	-

Table 3.3. Materials studied during the EngD.

The chemistry of the different uncoated materials is shown in Table 3.4.

Material	Fe	Co	Cr	Ni	Mo	Si	Mn	W	Ti	Nb	V	C	Ph	S	N
304L SS [196]	Bal.	-	18.0-20.0	8.0-10.5	-	0.75	2.0	-	-	-	-	0.03	0.045	0.03	0.1
321 SS [197]	Bal.	-	17.0-19.0	9.0-12.0	-	0.75	2.0	-	5*(C+N)-0.7	-	-	0.08	0.045	0.03	0.1
Nitronic 60 [198]	Bal.	-	20.5-23.5	11.5-13.5	1.5-3	1	4-6	-	-	0.-0.3	0.1-0.3	0.06	-	0.03	0.2-0.4
Tribaloy T400 [199]	Neg.	Bal.	8.5	Neg.	28.5	2.6	-	-	-	-	-	≤0.1	-	-	-
Stellite 6 [200]	Neg.	Bal.	28	Neg.	Neg.	Neg.	-	4.5	-	-	-	1.2	-	-	-

Table 3.4. Chemical composition of the uncoated materials in wt%

3.3 Analytical techniques

In this section a summary of the different techniques used along the Project in order to characterized the coating/layer chemistry, structure, mechanical properties and their performance under different conditions.

3.3.1 Light Optical Microscopy

Optical Microscopes are used for metallurgical analysis work. The working principle is light reflection of the light incident on the surface of the sample, unlike microscopes used for biological purposes, which rely on the transmitted light through the sample [201]. The light is generated using a type of bulb/lamp; tungsten-halogen lamps are the most popular [201]. The light then passes through a condenser that focuses it onto the desired point [202]. A series of diaphragms (both aperture and luminous field types) are used to minimize internal glare and

reflection and to alter the amount and the angle of the light going into the objective lenses [202]. The light is then shone on the surface of the sample and the reflected light is collected by the objective lenses, passes through the tube lens into the observation tubes and/or towards a mounting digital/video camera [202].

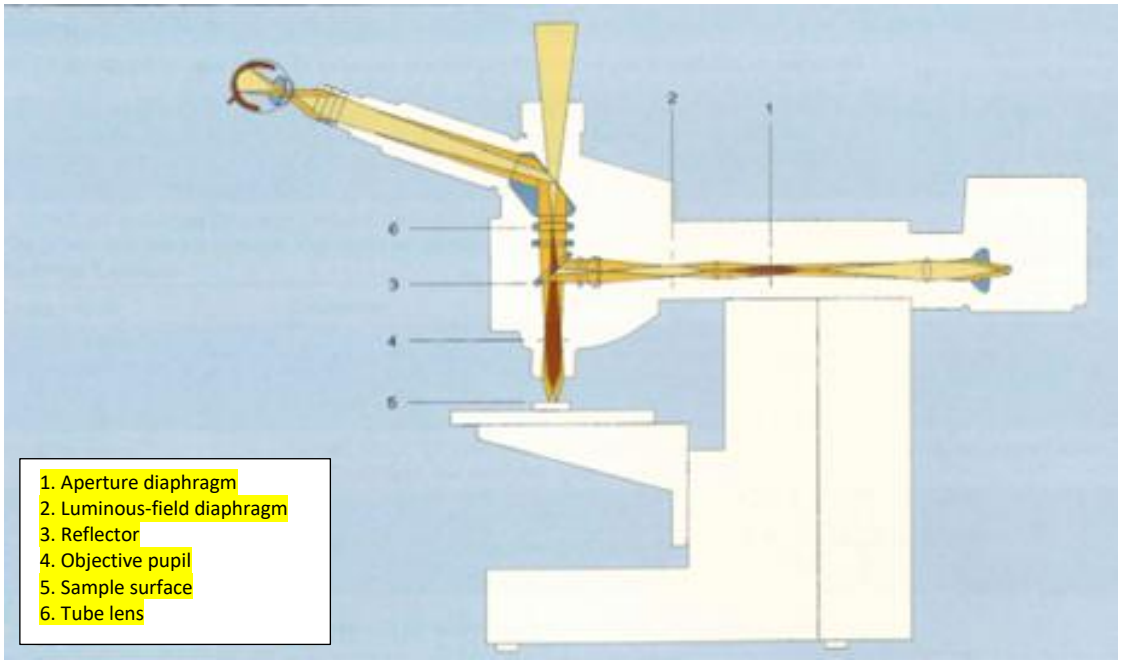

Figure 3.2. Schematic representation of a metallurgical optical microscope [202].

In combination with OmniMet™ Modular Digital Imaging System software, optical microscopy was used to look at the different coating/surface treatments, measure their different thicknesses and to measure the micro hardness indents to obtain hardness measurements.

3.3.2 White Light Interferometry

The working principle of white light interferometry is to split a beam of white light into two equal beams, one 'reference' beam that goes to a mirror, and another that goes to the sample surface [203]. When the beams are reflected, they recombine at the beam splitter and are superposed, constructively or destructively, producing interference fringes [203]. For each point measured in the 2D plane at every height, the interference fringe pattern is recorded and the coherence

between wave fields is measured [203]. This is finally represented by the statistical parameters that represent the area measured.

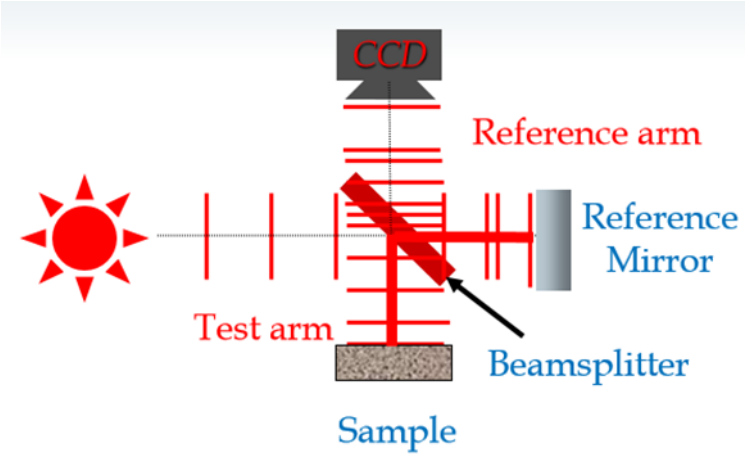

Figure 3.3.Ray Diagram of Michelson Interferometer. Beam originates at Sun symbol [204].

A Bruker Contour GT White Light Interferometry was used to obtain 2D and 3D surface parameters before and after coating/surface treatment was applied on the stainless steels in order to investigate whether any changes are produced after the application of different treatments/coatings. Topography measurements were carried out using a white light source in Vertical Scanning Interferometry mode (VSI), and using a magnification lens of x5. Data was analysed using Bruker Vision64® Operations and Analysis Software.

3.3.3 Focus-Variation Microscopy

A white beam is generated from a source and is projected on the desired area of the sample. The light is reflected to the optics and conducted to a photoelectric detector by a beam splitter [205]. The small focal depth allows the system to search for the focussed areas and reconstruct a 3D image from which topographical parameters that represent the surface can be attained [205].

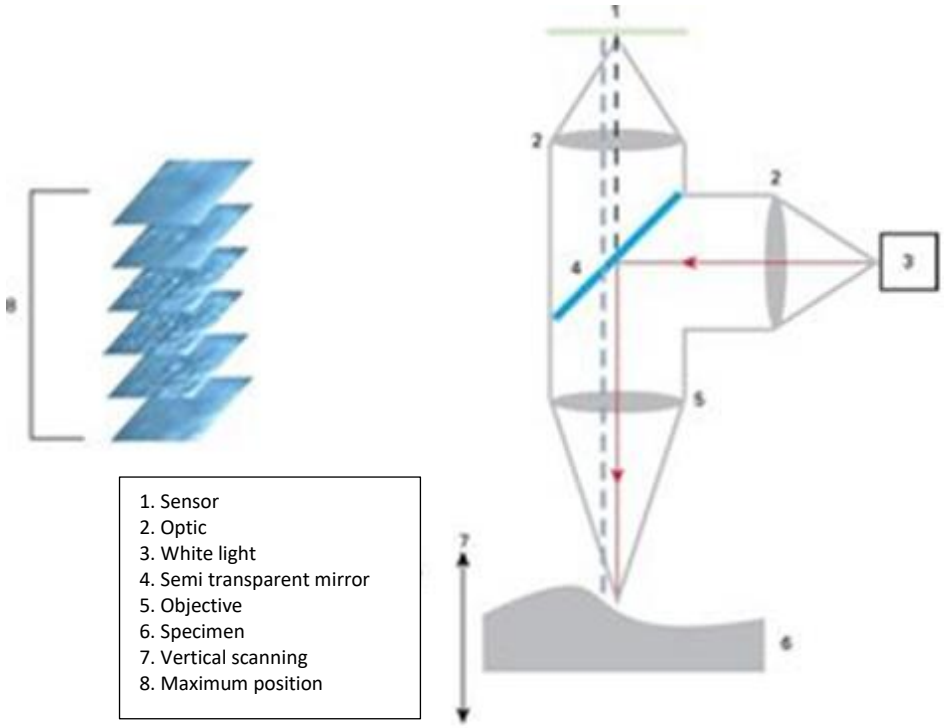

Figure 3.4.Schematic representation of a white light path in a focus variation microscope [206].

Surface Topography was obtained using an AliconaTM InfiniteFocus® microscope. The confocal microscope was used to measure topography before and after coating/surface treatment application, as well as wear scars.

Topography measurements were carried out on three plates and pins at a magnification, lateral and vertical resolution of x20, 1.25µm, and 1.00µm, respectively. 3D surface topography measurements were performed using a 4mm x 4mm square and a cut-off wavelength of 800µm. Measurements comply with ISO25178/12781-1. Surface topography characteristics were defined using S_a (Area arithmetical mean height), S_z (Area maximum height) and S_q (Area root mean square height) parameters using the IF-MeasureSuite Software.

Wear scar measurements were carried out on all the tested plates and pins using magnification lens of x5. Wear measurements were carried in two different ways:

- Subtracting the wear scar from an interpolation of the original surface, using MATLAB software.
- Obtaining perpendicular and transversal surface profiles of the wear scars. In addition, these profiles were used to obtain a 2D recreation of the pin cross-section to obtain the wear depth by recreating the original pin surface and comparing it agaisnt the obtained profile.

3.3.4 Scanning Electron Microscopy (SEM)

The electron beam is generated at a cathode subjected to a voltage from 0-30kV, which can vary the intensity of the beam as desired [207]. Other important parameters that can be controlled are the beam current and aperture, which will dictate the amount of electrons reaching the sample surface of interest [207]. When electrons reach the surface, they physically interact with it by a series of inelastic scattering events, used for imaging, and elastic scattering events, that produce X-rays, Auger electrons and photons used for chemical analysis [207]. An elastic event occurs when the electrical field of an atom deviates the path of electrons in the beam, subsequently producing back scattered (BSE) and secondary electrons (SE) [207]. SEs are produced by the inelastic scattering of weakly bound valence electrons (for ionic and covalent bonded materials) or electrons in the conduction band (for metallic bonded materials); while BSEs are the electrons that, during the scattering events, completely reverse their path and exit in the same direction in which they entered the surface [207]. These two types of scattered electrons are used for different purposes; the SE are used to provide topographical information due to contrast between surface features, while BSE can offer a visual representation of chemical differences within the same samples, such as different phases, due to the different contrast generated by compounds with different atomic numbers [207].

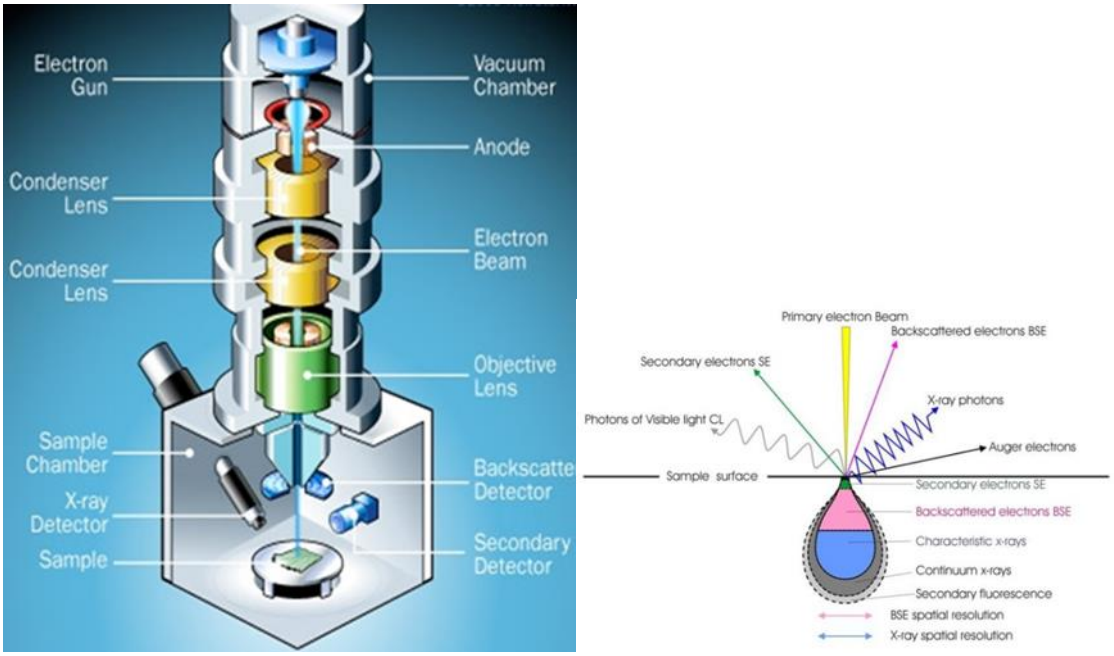

Figure 3.5.Left: Schematic representation of an SEM [208]. Right: Schematic representation of the different radiation and the possible volume of interaction of the electron beam with the sample [209].

An SEM was used to characterize the wear scar, using a ZEISS ∑igma, FEI Scios, FEI Versa and Jeol 7800, to obtain high magnification images of the materials before and after testing. Additional

techniques including EDX and EBSD were used to further characterize the materials before and after testing and will be described later in this section.

3.3.5 Dual Beam SEM

FEI Scios and FEI Versa were used to analyse cross sections and Transmission Electron Microscope (TEM) samples of the areas of interest within the wear scars. Dual Beam platforms combine SEM and Focus Ion Beam (FIB) functionalities. Ions are extracted from a liquid metal, normally Ga [211], using a strong electric field and, similarly to an SEM, by controlling the voltage and the apertures of the system the ion density reaching the surface can be controlled in order to use the ion beam for imaging purposes, sample cleaning or etching, sputtering, chemical analysis or micromachining [210].

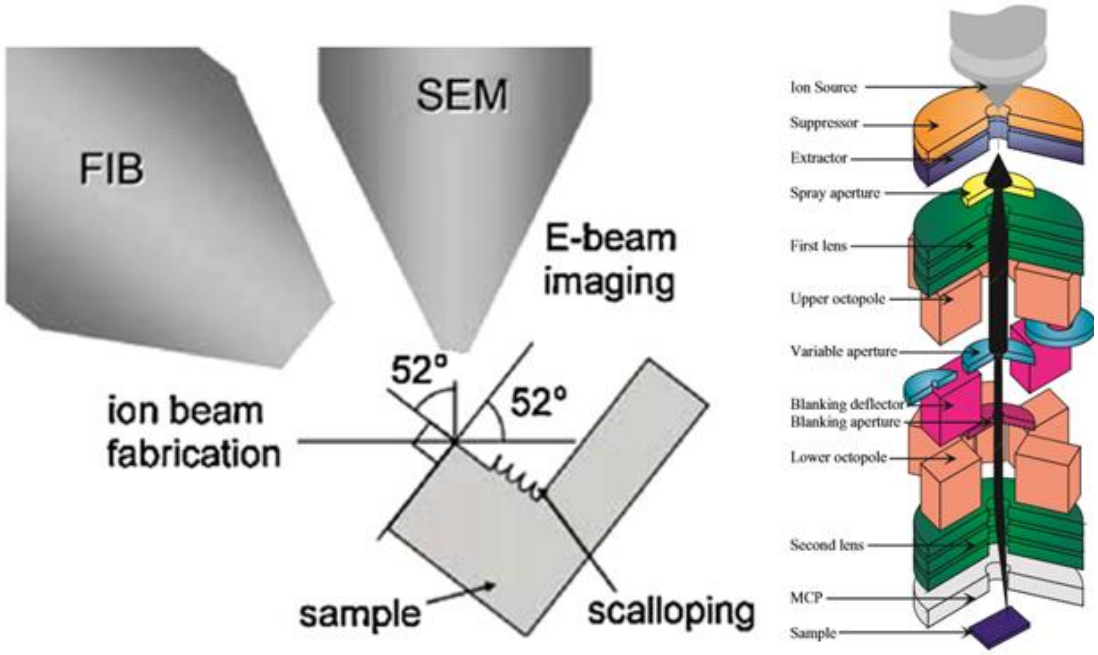

Figure 3.6.Left: Schematic representation of the SEM, FIB and sample [212]. Right: Schematic representation of an ion beam [211].

FIB was used to do cross-sections of the co-superalloys wear scars and to prepare Transmission Electron Microscope samples.

3.3.6 Transmission Electron Microscopy (TEM)

Electrons are generated from a cathode, and are then accelerated and focused into a uniform beam using a magnetic lens known as a condenser lens [213]. Next, a condenser aperture is used to remove electrons that deviate from the optical axis. The beam then goes through the sample and is diffracted; this diffracted beam is subsequently focused to form an image [213]. Finally, it is magnified by the projector lenses [213].

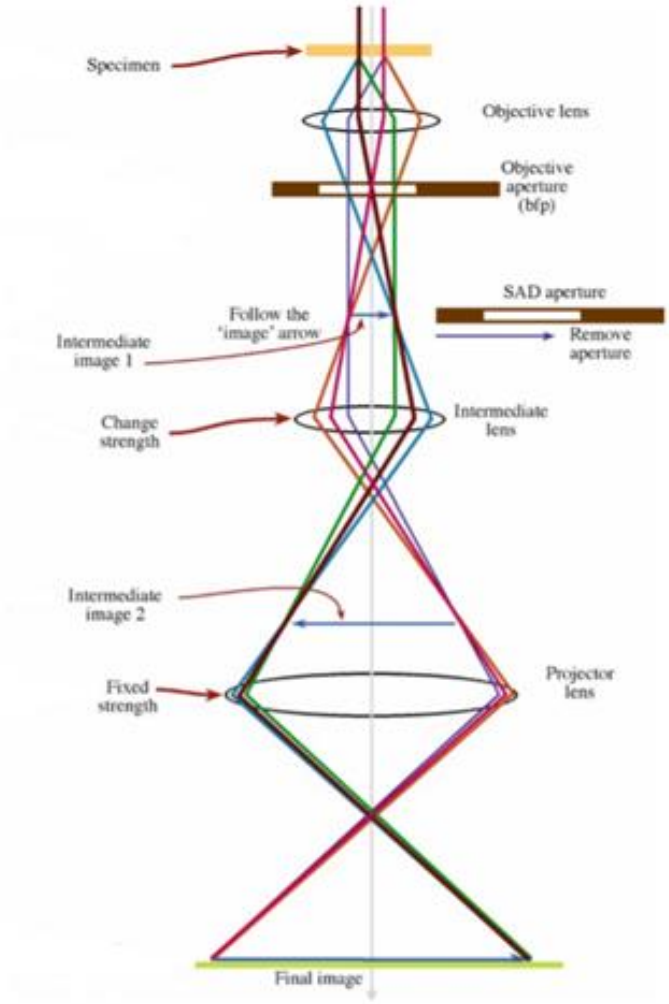

Figure 3.7.TEM schematic representation of the beam path before reaching the detector [213].

TEM was used to look at the layers of the material close to the surface, in order to understand the performance of some of the materials. The TEM used during this work it is a FEI.

3.3.7 Scanning Transmission Electron Microscopy (STEM)

STEM is a mode in which the beam is used to scan an area of the sample and can be used both for imaging and to map the chemical composition of the area of interest [213]. The TEM probe is used to scan the desired area and it is control by the 'double deflection scan coils' that can be found between the Diaphragm and the 3rd condenser lens [213].

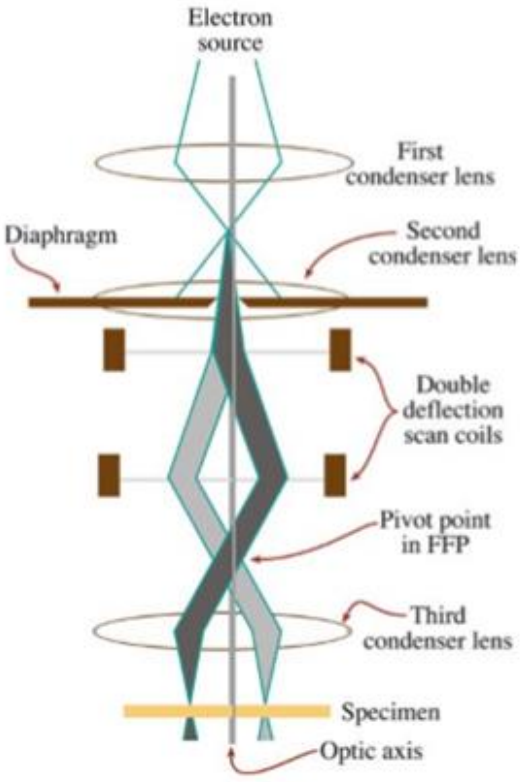

Figure 3.8.Schematic representation of the electron beam in STEM mode [213].

STEM mode was used to study how the material changes near the surface of the wear scar and obtain chemical information of the area. Information was obtained in the formed of elemental distribution maps and lines to understand the composition of the layers and the material below and to characterise the chemistry of the PVD concepts.

3.3.8 Energy-Dispersive X-Ray (EDX)

The operating principle the EDX technique is the formation of X-rays from the interaction of the electron beam with the sample [207]. Atoms have unique number of electrons in specific position/shells that jump to a higher energy shell, when it absorbs the energy from the SEM electron beam, creating an X-ray. The X-ray energy is measured by a detector [207]. The energy lost during the process is taken into account, then the measured energies are correlated with the known energies of the X-rays formed in specific electron shells of an element [207]. Finally, the number of specific energies is counted and shown in the EDX spectrum related to the abundance of the element using propietry software.

EDX was used extensively during this research in order to understand the possible chemistry and chemical changes of the different materials before and after most of the environmental tests.

When using the EDX detector on the SEM, measurements were carried at two different electron beam voltages:

- 5kV was used to map where lighter elements like carbon, boron or nitrogen were distributed, but it was not used to quantify
- 20kV was used to map and quantify the heavier elements. The quantification process required to set the sample to the "calibrated" working distance and voltage. In addition, current was set to get a high number of photon counts for statistical significant.

3.3.9 Electron Backscatter Diffraction (EBSD)

EBSD was used to obtain the phases and their distribution of some of the diffusion treatments. These are determined by the collection of EBSD patterns, also known as Kikuchi patterns. If the backscattered electrons satisfy Bragg conditions, please refer to section 3.3.10, for diffraction, then the electrons are diffracted into two cones that represent each plane normal to the diffraction plane. Two features that are important for crystallographers are the points of intersection, or zone axes, and the angles between the zone axes and the Kikuchi bands, which are inherent to a specific crystal structure. The diffracted inelastic electrons are collected on a thin fluorescent screen, from which the Kikuchi patterns are imaged using an optical fibre or a lens situated behind the screen. The image is then transmitted to a charged couple device or a complementary metal-oxide semiconductor solid state imager [207]. Propietry software is used to index the patterns and identify phases

EBSD was used to characterise the phases present in some of the diffusion treatments, mainly Boronizing, Aluminising and Chromizing, due to limitations found on other surface treatments, Nitriding and Nitrocarburizing. such as grain size and internal stresses. Phase distribution maps and coating/layer growth direction were used to understand whether the layer was grown on the surface or a case hardened layer was created below the original surface of the steel.

3.3.10 X-Ray Diffraction (XRD)

XRD relies on the generation of high energy electromagnetic waves using a target material (Cu is the most commonly used) that is bombarded by X-rays, which then are diffracted from the irradiated volume of the sample [214]. The diffraction of the X-ray beam results in a constructive interference event at each lattice plane and direction that satisfies Bragg's law, given by Equation 1. Bragg's law states that if an X-ray with a specific wavelength (λ) hits a crystal with interatomic spacing (d), the X-ray will have enough intensity to be detected at a specific angle (θ) [215]. Bragg's law is met for different crystal symmetries at different θ (incident angle of the X-rays), forming the diffraction information specific to the material [214].

$$n\lambda = 2d_{hkl}\sin(\theta)$$

Equation 3.1. Bragg's Law [209].

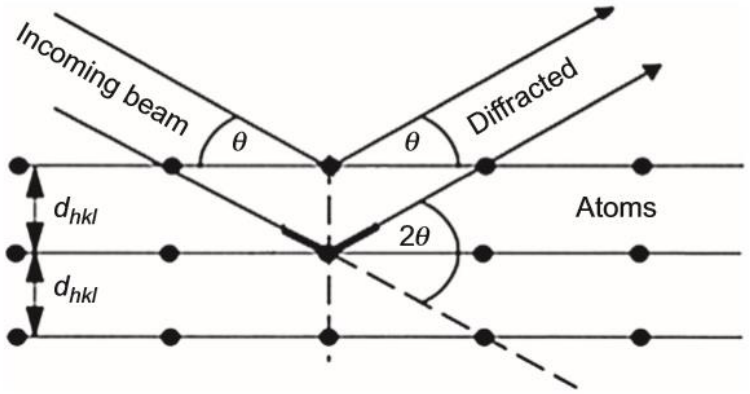

Figure 3.9.Schematic representation of an X-ray diffracting from a crystal under Bragg's Law conditions [214].

The data is represented by a spectrum with different peaks, each representing a different d-spacing and therefore all the different reflections can be observed and represented by the intensity of the peaks at θ.

XRD experiments were carried with a PaNalytical X'Pert Pro with a cobalt target due to reduce the fluorescence caused by Fe when using a copper target. The technique was used to identify the different phases in each material before any test was performed.

3.3.11 Raman Spectroscopy

When the laser interacts with the surface, photons are scattered due to the induction of a dipole moment caused by the polarization of the molecule. >99% of these photons are elastically scattered (Rayleigh scattered) and <1% are inelastically scattered (Raman scattered) [216]. The frequency shifts of the inelastically scattered photons are recorded into the spectrum. And the intensity and shape of each spectral band can be used to determine the quantity and the distribution of each phase present [217].

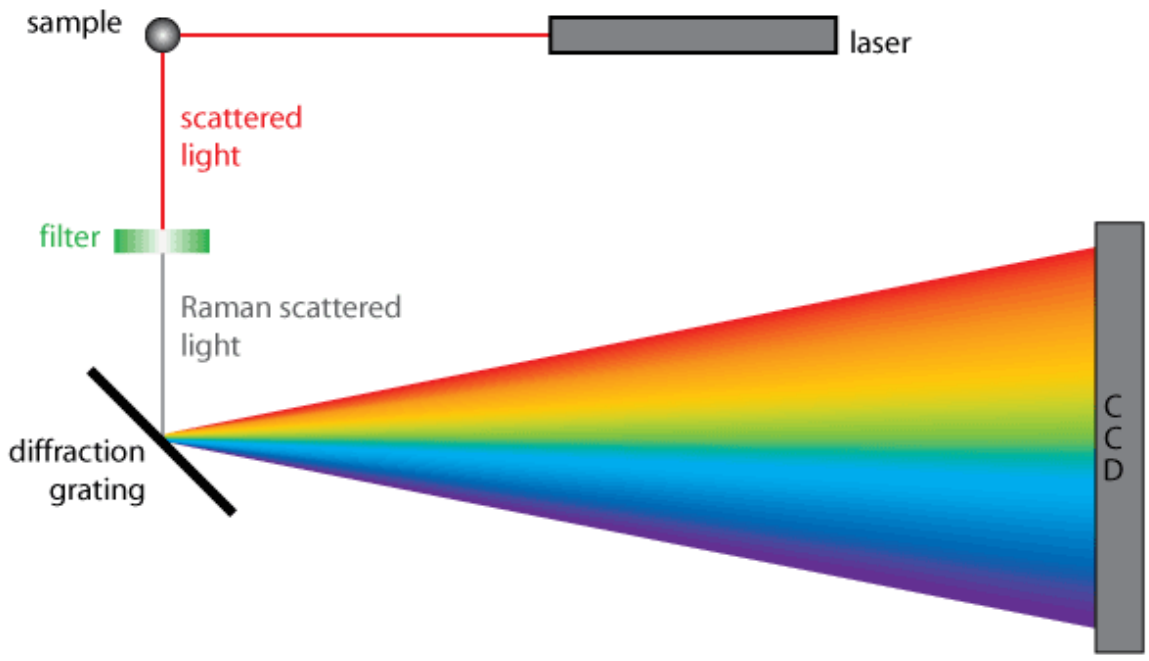

Figure 3.10.Schematic representation of the operation of a Raman spectrometer [218].

Raman Spectroscopy was used to identify the oxides present on the surface of the wear scars by radiating using monochromatic laser with a wavelength of 633nm. Measurements were carried through the length of the wear scar.

3.4 Indentation techniques

3.4.1 Rockwell C

VDI 3198 standard testing [219] was used to understand the adhesion performance of the coating/layer system to the substrate and the brittleness of the coating/layer system. Note that standard does not specify minimum or maximum coating/layer system thickness requirements for application, in addition other researchers have used this standards to characterize bonding characteristics of diffusion treaatments [220] The test uses a Rockwell C tester and a diamond conical indenter to make an indent using 150kg force. After the test was performed, samples were observed under an optical microscope and the failure mechanism of the coatings/layer system was ranked according to the standard. Depending on how the failure occurred, a score between H1 to H6 was given to each coated concept. H1 to H4 was a regarded as a pass, while H5 to H6 was a failure. A Wilson® Rockwell 574R was used to carry out this standard.

3.4.2 Microindentation hardness testing

Hardness is a measure of the resistance of a material to permanent deformation under a locally applied load [202]. There are a variety of methods at different scales with which hardness measurements can be obtained, from Mohr hardness testing based on scratching the material

to Vickers, Knoop or Berkovich where indenters are used to create micrometre size indents [202]. During Vickers microhardness testing, a diamond pyramidal indenter is forced into the sample of interest with loads lower than 1kg giving the opportunity to evaluated localized areas of interest [197]. When the indentation is made the hardness is calculated by [202]:

$$HV_L = \frac{1854.4 * L}{d^2}$$

Equation 3.2. Microhardness for a Vickers indenter.

Where "L" refers to the load used during testing and "d" is the length of the diagonals of the indent.

Microhardness testing was carried out using a Wilson VH1102 Vickers Hardness Tester in order to obtain hardness values of the coatings/surface treatments and uncoated materials from a metallurgical cross-section using a 0.025kgf-microhardness tester, except for any PVD concepts due to indents being to large and indenting both coating and substrate simultaneously. The data was then analysed using a Nikon Eclipse LV150N upright microscope in conjunction with OmniMet™ Modular Digital Imaging System software by measuring the diagonals of the indents.

3.4.3. Nanoindentation

Nanoindentation relies on the application of a load increasing from zero to a desired value and from that desired maximum back to zero [221]. Simiarly, the test can be done by chosing a depth instead of the load. Different material behaviours can be observed in different portions of the load displacement curve [221]:

1. Elastic-plastic loading
2. Elastic unloading

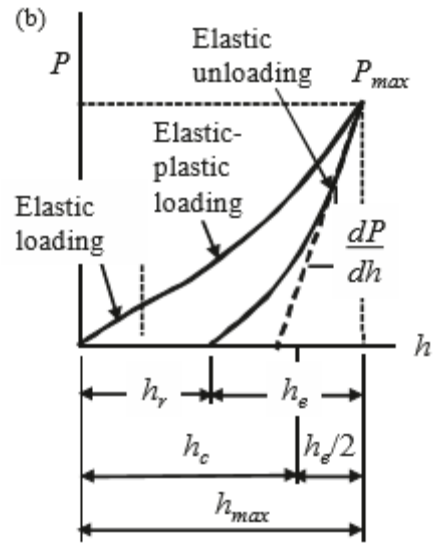

Figure 3.11. **Loading-unloading curve obtainable information [221].**

Berkovich indenters are commonly used because they provide a more controlled indentation test than other indenters [221]. For this type of indenter, the hardness and elastic modulus, determined from the unloading curve, are obtained by the following formulae [221]:

$$H = \frac{P}{24.5h_c^2}$$

Equation 3.3. Nanohardness for a Berkovich indenter.

Where "H" is the hardness, "P" is the load applied during testing and "h_c" is the penetration depth.

$$E^* = \frac{\sqrt{\pi} * dP}{2\sqrt{A} * dh}$$

Equation 3.4. Elastic Moduli for a Berkovich indenter.

"E*" is the elastic modulus and A=$24.5h_c^2$.

Mechanical properties of all samples were acquired from metallographically prepared cross-sections of the samples using a NanoTest Xtreme nanoindenter with a Berkovich style diamond indenter. A depth control experiment was used in which the indenter reached a maximum depth of 250nm. The loading and unloading rates were 0.5mN/s and 0.5mN/s respectively, with a dwell time at maximum load of 5s and an indent separation of 7µm. For the coated/surface treated samples, indents along the coating/surface treated layer thickness were made. For bulk materials, 100 indents were made. The data was analysed using the NanoTest Vantage software. Finally, AlTiN mechanical properties were obtained from literature [222] as surface indentation

was not relaible due to topography causing a high variation on the measurements and not reliable on the cross-section as the coating height level was below the substrate and mount level causing the indentation area to reach the substrate or the mount material.

3.5 Environmental testing

3.5.1 Thermal Shock testing

Thermal Shock testing was performed in order to understand the stability of the coatings/layer system during cooling cycles. A K-type thermocouple was welded onto a sample of size 2mm x 2mm x 2mm which was placed in a 760^{o}C pre-heated muffle furnace. When the sample reached 760^{o}C, it was removed from the muffle furnace and left to air cool. This procedure was repeated 8 times per sample. Samples were inspected by optical microscopy for signs of cracking on the coating material or the layer system after surface treatment.

3.5.2 Oxidation test

Oxidation tests were carried out in order to understand the long-term stability of the materials at high temperature. Oxidation/thermal stability testing was performed in a muffle furnace at 760^{o}C for 250h with test samples of dimensions 35.6mm x 25.4mm x 10mm. Oxidation behaviour was measured by reviewing the thickness of the oxide layer, the depth of the internal oxidation and oxide layer spallation, together with microstructural and chemical changes.

3.5.3 Corrosion test

Corrosion tests were used to replicate the conditions to which the components are subjected when the turbocharger is not running during service. NaCl was used to replicate the humidity encountered ~~in~~ close to sea environments, and H_2SO_4 replicates H_2SO_4 droplets that can form on the components when the turbocharger is stopped. Note that H2SO4 is formed from the reaction of SO3 and water vapour as temperature drop during cooling. For the corrosion test, a solution composed of 2L of water, 100g of NaCl and sufficient H_2SO_4 to achieve a pH value of 5 was used. A volume of 45ml was applied to the samples presented in Table 2. The samples, with dimensions 35.6mm x 25.4mm x 10mm, were subsequently placed in a sealed container for 24h. All samples were cleaned and a new solution was applied in 24h cycles up to 250h. The corrosion performance was determined by reviewing the surface/coating damage, surface compounds formed and the ability of the coating/layer system to prevent damage to the underlying substrate.

3.5.4 Tribology testing

The evaluation of the tribological performance of the sample was conducted using a Rtec multifunction pin-on-reciprocating-plate tribometer. For this work, a variable geometry mechanism was modelled, with the pin representing the shroud as it is always in contact and the plate representing the nozzle. The material pairs that underwent the test, and the contact conditions which were designed to replicate the conditions experienced by the components in operation, are both shown in Table 3.5. Three repeats of each material pair at each temperature was done.

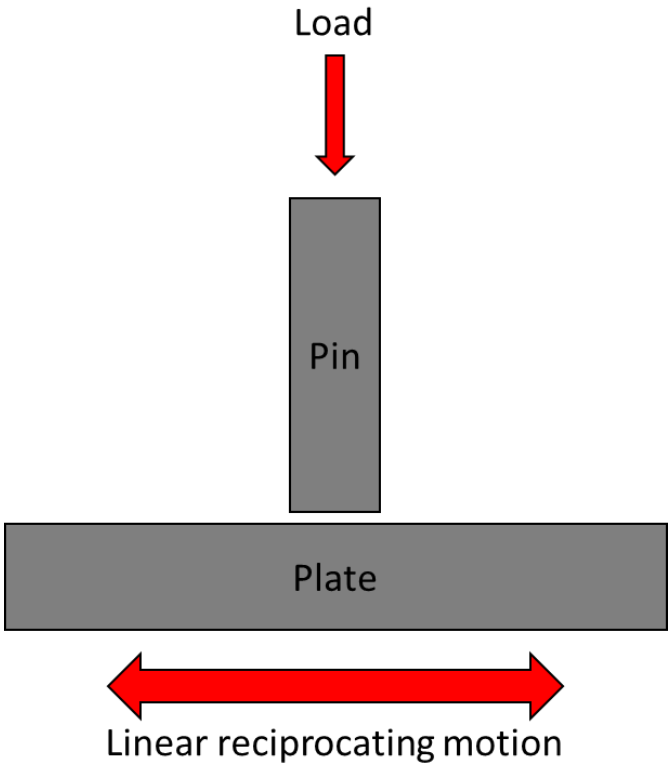

Figure 12. Schematic representation of a linear reciprocating motion pin-on-plate test.

Plate/Pin
304L stainless steel/321 Stainless Steel
Nitronic 60/ 321 Stainless Steel
Chromizing/Chromizing
Aluminising/Aluminising
Nitrocarburizing 1/ Nitrocarburizing 1
Nitrocarburizing 2/ Nitrocarburizing 2
AlTiN/AlTiN
CrN/CrN
Tribaloy 400/Stellite 6
Stellite 6/Tribaloy 400

Table 3.2. Material combinations that underwent tribology testing

As observed from Table 3.3, there are a lot of "like-on-like" material pairs often not considered a good approach to tackle tribological issues due to the chemical affinity for each other, particularly stronger for metallic materials [17]. The different reasons of putting "like-on-like" materials were:

- Amount of commercially available coatings/surface treatments with the capacity to cope with product demand requirements from the sponsor company.
- As previously mentioned, chemical affinity can have a detrimental effect on the pair performance, but it is not known how much more or less that effect it is in comparison to other behaviours that could be present on the contact, such as abrasion due to mechanical properties difference between the dissimilar materials in contact. In addition, this effect is reduced at higher temperatures due to the formation of oxide films.

The geometry of the pin and the maximum contact stress during the test were calculated by conducting a Hertzian analysis using Equations 3.5-3.7 [223], when a load of 4N is applied in the test:

$$\frac{1}{E^*} = \frac{1-\upsilon_1^2}{E_1} + \frac{1-\upsilon_2^2}{E_2}$$

Equation 3.5. Rule of mixtures.

Where E is refered to the elastic modulus and υ is refered to the poisson's ratio of the materials in contact.

$$a_c = \left[\frac{3PR}{4E_c}\right]^{1/3}$$

Equation 3.6. Radius on contact calculation.

Where a_c is the radius on contact, P is the load and R is the radius of curvature.

$$p_o = \frac{3}{2}\frac{P}{\pi a_c^2}$$

Equation 3.7. Maximum pressure at the contact.

Where p_o is the maximum pressure at the contact.

Maximum Contact Pressure	90MPa
Stroke Length	5mm
Frequency	6Hz
Operating Temperatures	250°C, 650°C and 760°C
Atmosphere	Air
Test Duration	2h
Repeats	3

Table 3.3. Tribological test parameters

Pin and plate samples were cleaned before testing by submerging them in a beaker with acetone in an ultrasonic bath for 10 minutes. Data was collected using a National Instruments R data acquisition (DAQ) card and analysed using Rtec labview, Focus-Variation Microscopy and MATLAB.

Due to software issues when recording the Fx data, end result was filtered using a band with filter to remove the low frequency ''noise'' caused. Nitrocarburizing 1 data obtained from sponsor's company tribometer was used to compare against data obtained in university to make sure data did not misguided the analysis.

4. Tribology test at 250°C

4.1 Summary of pre-testing before tribology test

Following the selection process described at the methodology chapter, before the tribology test, the different coating materials and surface treated stainless steels were investigated in order to provide compare and contrast them in the different engineering and purchasing requirements as shown in the C&E matrix (table 4.1). For further information refer to Submission 2.

Rating of Importance to Customer (low 1- high 10)	10	7	5	9	8	7	7	10	7	9	10	8	9	7	2	
Inputs	Life of Coating	Corrosion Resistance	Thermal Shock Resistance	Thermal Capability	Surface treatment uniformity	Base Material Surface Finish Requirement	Changes to Final Component Dimensions	Tribological Characteristics	Proprietary Technology	Sensitivity of Process to Component Geometry	Environmental Compliance Risk of Process and Components	Cost	Dual Source and Global Availability	Risk of Supplier Design Control	Intregation of Manufacturing Technology into Cummins Facility	Total
Boronizing	3	1	9	1	1	9	1	-	9	9	9	9	9	3	1	579
Chromizing	3	3	9	9	9	9	9	-	9	9	9	9	9	3	1	785
Aluminizing	3	3	9	3	9	9	1	-	9	9	9	9	9	3	1	675
Nitriding	1	1	9	1	1	9	9	-	9	9	9	9	9	9	3	661
Nitrocarburizing 1	3	1	9	1	9	9	9	-	1	9	1	3	1	3	0	441
Nitrocarburizing 2	3	1	9	1	9	9	9	-	1	9	3	3	1	3	0	461
AlTiN	3	3	9	3	3	3	9	-	9	3	9	3	9	9	9	597
AlCrN	0	1	0	1	9	3	9	-	9	3	9	3	9	9	9	538
CrN	3	3	9	3	3	3	9	-	9	3	9	3	9	9	9	597
Total	220	119	360	207	424	441	455	0	455	567	670	408	585	357	66	

Figure 4.1. C&E matrix used along the EngD showing the scores given to each material for each engineering and purchasing perspective and their scores at the end of this temperature test.

From the total score obtained, the best to worst materials were:

Position	Material
1	Chromizing
2	Aluminising
3	Nitriding
4	AlTiN
5	CrN
6	Boronizing
7	AlCrN
8	Nitrocarburizing 2
9	Nitrocarburizing 1

Table 4.1.List of best to worst performing materials after the end of Stage 2 of the selection process.

From all the treatments/coating material, AlCrN, boronizing and nitriding did not go foward to tribology test. AlCrN did not go forward as the first supplier did not achieved full surface covarage, while the second supplier was not able to apply a coating with enough adhesion to the surface as it was peeling off without just by touching it with the fingers. Boronizing was removed from the selection process, as even though it was relatively good from a purchasing perspective, its engineering performance was poor and therefore obtaining a low score on the

C&E matrix. Finally, nitriding was eliminated due to its poor performance from an engineering perspective, even though was one of the best from a purchasing perspective and was selected as the 3rd best material.

4.2 Tribology test

Before starting with this section, please note that surface and cross-sections morphology and chemistry can be observed at Submission 2.

4.2.1 Results

4.2.1.1 Friction

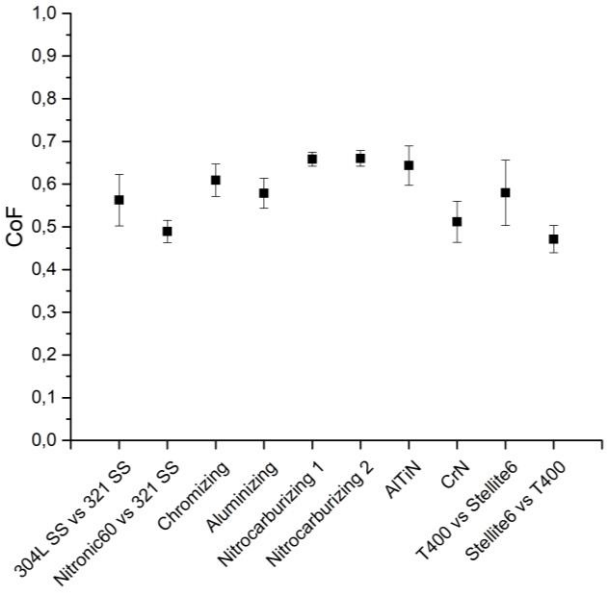

Figure 4.2. Average steady-state CoF of the different material pairs when tested at 250ºC.

Figure 4.2 shows the steady-state CoF of all the material pairs at 250°C. The general trend was that CoF of the material pairs decreased as the temperature increased, with some exceptions to the trend.

At 250°C, the CoF all materials pairs fall in the range of 0.47 - 0.67. The base stainless steel pair (304L plate against 321 pin) had a CoF of 0.57. The Nitronic 60 vs 321 stainless steel material pair had a lower CoF than the base material pair, sitting at 0.49. In terms of the coatings and surface treated stainless steels, chromizing, gave a CoF of 0.62, which is slightly higher than the base material pair. In between the base material and chromizing, aluminisng showed a CoF 0.59. Nitrocarburizing 1, Nitrocarburzing 2 and AlTiN coated pairs showed the highest CoF at this temperature with 0.67, 0.67 and 0.65, respectively. The CrN pair showed lower CoF than the base material with a magnitude of 0.5. Finally, the Co-superalloys CoFs showed a difference in behaviour dependent on the position at which T400 and Stellite 6 were. When T400 was the

plate, the CoF reached an average value of 0.6, while T400 as the pin showed the lowest CoF value of all the tested pairs, sitting on 0.47.

4.2.1.2 Wear behaviour

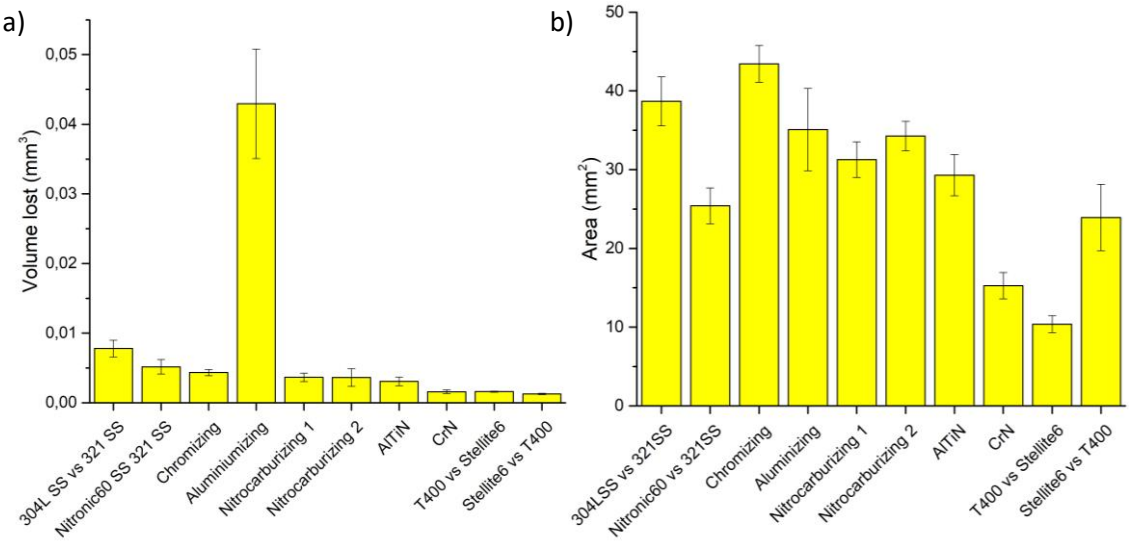

Figure 4.3. Plate worn volume (a) and plate affected area (b) for the different material pairs after testing at 250°C.

Figure 4.3 shows the wear volume and the area affected during the wear process of the plate samples at 250°C. From a wear volume perspective, aluminized stainless steel plate showed the highest wear. The 304L plate showed four times less wear than the aluminized plate. Following the 304L plate, the Nitronic 60 plate displayed half thewear of the base 304L. This is followed closely by the chromized steel plate and subsequently both nitrocarburized steel plates and AlTiN coated steel. The CrN coated and the T400 plate show half of the wear of the previous material plate. The least wear volume measured was the Stellite 6 plate.

From a wear scar perspective, the chromized plate showed the highest area affected by the degradation process. The chromized plate is closely followed by the 304L and the aluminized plate. A 25% reduction in the area affected by the wear process was observed for the nitrocarburizing 1, nitrocarburizing 2 and AlTiN plate. The Nitronic 60 and Stellite 6 plates displayed nearly 50% reduction in the area affected during the test. Finally, the CrN and T400 plate showed a 75% and 80% reduction of the worn area in comparison to the chromized plate.

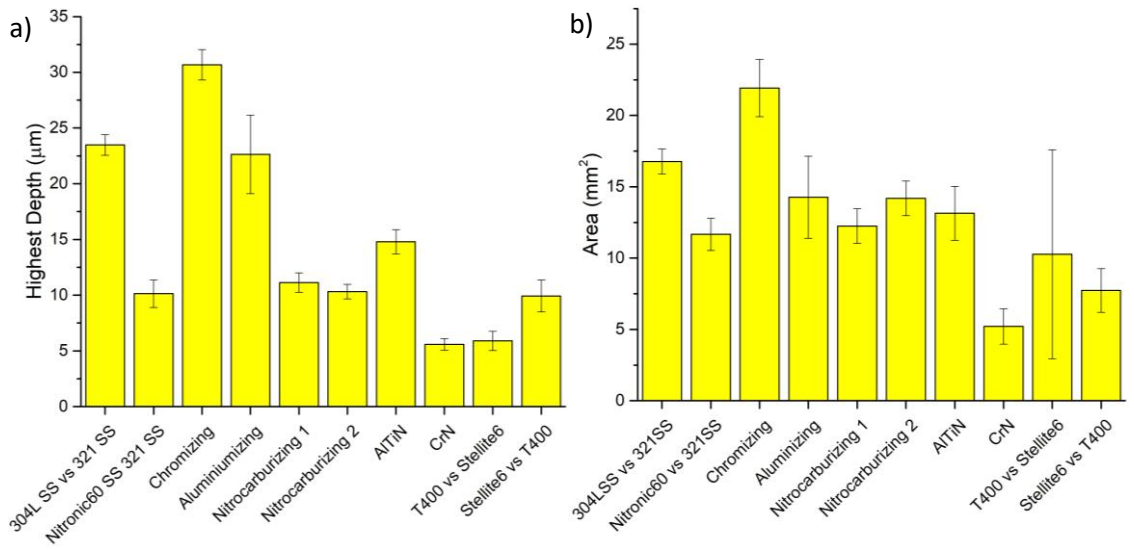

Figure 4.4. Pin affected area (a) and pin wear depth (b) for the different material pairs after testing at 250°C.

Figure 4.4 displays the pin area affected by the wear process and the highest depth achieved on the pin after the test duration. From a pin area perspective, the values for most pairs were in similar proportions as the ones displayed by the plate materials, with one exception. The Stellite 6 plate showed an increase in area in comparison to its counterplate with a high variation between the different test samples.

4.2.2 Discussion

Considering all the data showed during the previous sections and Submission 2, the materials will be rank on how they perform during the tribology test. In order to understand the reasons of how the wear and friction performance differs in between material pairs, the 304L vs 321 stainless steel pair was used as a base line. As from a friction perspective, pairs behaviour was discussed previously, only wear data will be discussed in depth below.

4.2.2.1 Tribological behaviour

As previously described, the 304L vs 321 stainless steel pair tribological behaviour was dependent on the creation of large particle due to the work-hardening [69] for the plate causing heavy abrasion of pin and plate surfaces. While for the pin, the key behaviours were the formation of the oxides within the material, creating a hard phase [87]. The lower work-hardening capability due to lower SFE keeping the surface 321 surface from delaminating [69].

The reduction of friction and wear of the Nitronic 60 vs 321 stainless steel is due to the higher hardness and the slightly higher SFE of the Nitronic 60 [69]. The delamination of smaller particles, with less severe delamination wear aided in not increasing the damage and reducing,

in the long term, the number of particles of the system reducing both abrasive wear and the energy contribution of the ploughing component.

For the chromized pair, an increase in friction, a decrease in plate wear and an increase in wear of the pin were observed. First, the reason why the worn area of the plate was larger than with the previous pairs was due to the pin's poorer performance, as shown by both higher worn area and highest depth. In comparison to the previous 321 stainless steel pin, the chromized pin did not offer as much protection due to not forming internal oxide regions. As there is a higher number of particles, the CoF slightly increased. The slower wear rate of the plate in comparison to the damaged suffered by the pin (up to the point that the chemical treated layer was removed in the centre area) was because of the pin being all the time in contact, accelerating both the delamination and abrasion effects.

The aluminized pair showed a similar CoF than the base material. The pin area and depth, and plate area were similar while the plate showed a much higher worn volume. The friction behaviour was dependent on the ploughing of the surfaces and the particles in the contact. As it was observed that the wear was heavily localized in the middle of the wear scar, this suggests that a catastrophic event happened during the running-in. This event was related to the protuberances on the pin, which increased the localised stress on the surface, and the brittleness [111] of the top layer of the layered system. After the running-in, the hard particles in the contact were kept in the same area, localising the wear process and causing the higher worn volume of the plate.

Both nitrocarburizing treatments, had a very similar values of CoF and wear. In comparison to the steel, these two treatments showed a wear improvement and a slightly higher CoF. The wear improvement was attributed to the existence of both the oxide layer followed by a hardened case. The slightly increase in the CoF was attributed to the ploughing of the oxide entrapped particles on the case-hardened layer.

AlTiN showed similar average CoF and similar wear data values as the nitrocarburizing treatments. From a friction perspective, the AlTiN middle surfaces were behaving like the standard base material, but particle ploughing is higher as the AlTiN particles are harder than the work-hardened steel particles. This adds an extra contribution to the overall friction. From a wear perspective, even though the steel surface were not protected, it is believed that the coating failed at the beginning of the test as CoF barely changes over time [224]. The coating around the steel uncovered areas function as a load carried, reducing the work-hardening of the steel and preventing big particle delamination. Also, the AlTiN layer will aid the abrasive action

of the uncovered regions due to the difference in mechanical properties between the stainless steel and coating material.

CrN showed a slightly lower CoF than the base stainless steel material pair. Additionally, to one of the lowest plate wear volume and area, and pin wear scar area and depth. The reason of the lower average CoF of the CrN in comparison to AlTiN was a lower contribution of particle ploughing, as the CrN coating is not removed during the test duration. From a wear perspective, the better performance over the stainless steel pair was the hardness of the coating, while the better performance over AlTiN was attributed to less/smaller defects and the higher toughness of the material.

The T400 plate and the Stellite 6 pin, showed similar friction, plate wear volume and area, and pin highest depth as the CrN pair, but the pin area showed a higher magnitude and spread. The reason for the observed difference in pin area was due to the particle accumulation area in the three tests, and this behaviour prevented a clear observation of the real wear depth, which is a few microns lower as the transfer layers were observed to be a few microns thick. The better wear performance over the stainless steel pairs is attributed to the hard particles within the alloys, reducing the abrasive wear; while the better performance over the hard materials, such as the PVD coatings, was attributed to the toughness offered by the Co matrix.

The final pair, Stellite 6 plate vs T400 pin, showed different behaviours than the previous Co-superalloy pair. This pair showed a better performance than the stainless steels pairs from all categories. In comparison to the previous pair, this pair showed a lower CoF, and slightly lower wear plate volume and wear area, and pin affected area, but the pin showed a higher worn depth. The reduction in the CoF in comparison to the previous pair was caused by the lower number of particles kept in the contact. From a wear perspective, the worst performance of the T400 [95] pin material in comparison to the Stellite 6 pin was due to the harder particles of the Stellite 6 [94], which probably suffered most of the wear in this material pair.

4.3 Conclusion

Overall, the different material pairs were classified in Table 4.2 as best being on top of the list as:

Position	Friction	Wear
1	Stellite 6 vs T400	T400 vs Stellite 6
2	Nitronic 60 vs 321 stainless steel	CrN
3	CrN	Stellite 6 vs T400
4	T400 vs Stellite 6	Nitrocarburizing 1
5	Aluminising	Nitrocarburizing 2
6	304L vs 321 stainless steel	AlTiN
7	Chromizing	Nitronic 60 vs 321 stainless steel
8	Nitrocarburizing 1	Chromizing
9	Nitrocarburizing 2	304L vs 321 stainless steel
10	AlTiN	Aluminising

Table 4.2. List of best to worst performing materials from a friction and wear perspective.

The list was taking into consideration the numerical measurements, but also the stability of the material pair and the mechanisms acting in the contact.

In summary, hardness was one of they key parameters to improve wear and friction as it reduces the abrasive element contribution for both friction and wear. Hardness also helped to reduce the effect of other detrimental mechanisms, such as delamination. Toughness was also important as it reduced brittle fracture of the material; as an example, Aluminising and AlTiN were not tough enough. It is also worth considering that brittleness may be also be introduced by defects within the material that act as crack nucleation sites. While transfer layers helped from a wear perspective, their failure and the particle retention was detrimental for the CoF magnitude and stability. Finally, surfaces showed slight oxidation, but it did not play an important role towards the performance of the alloys at this temperature, except for the 321 stainless steel pin which formed hard surfaces due to material internal oxidation.

5. Tribology test at 650°C

Before starting with this section, please note that surface and cross-sections morphology and chemistry can be observed at Submission 3.

5.1 Results

5.1.1 Friction behaviour

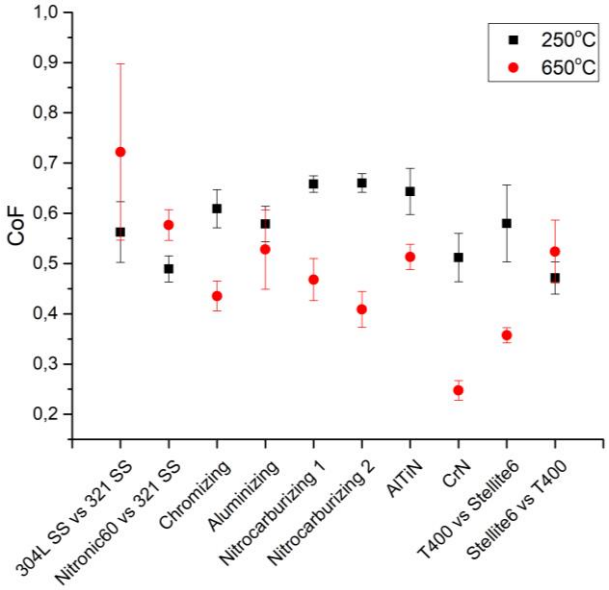

Figure 5.1. Average steady-state CoF of the different material pairs when tested at 250°C and 650°C.

After increasing the testing temperature to 650°C, the base stainless steel material showed an increase in average CoF to a value of 0.73 over the value at 250°C. Although it underwent a lesser increase, the Nitronic 60 showed a CoF value of 0.59. Unlike the other material pairs, the chromizing treated pair showed a decrease in CoF to 0.43. Aluminising showed similar CoF values of 0.59 at 250°C and 650°C, as did AlTiN. The nitrocarburizing treatments also showed a decrease in CoF with average values of 0.49 for Nitrocarburizing 1 and 0.44 for Nitrocarburizing 2. The final coating pair, CrN, showed the lowest CoF values of all the concepts at this temperature, reaching a value of 0.27. Finally, as previously, the position at which each Co-superalloy in the contact had an influence on its friction behaviour. When T400 was the plate, the average CoF value reached was 0.37, while the pair with T400 as the pin showed an increase in CoF relative to 250°C, up to 0.53.

5.1.2 Wear behaviour

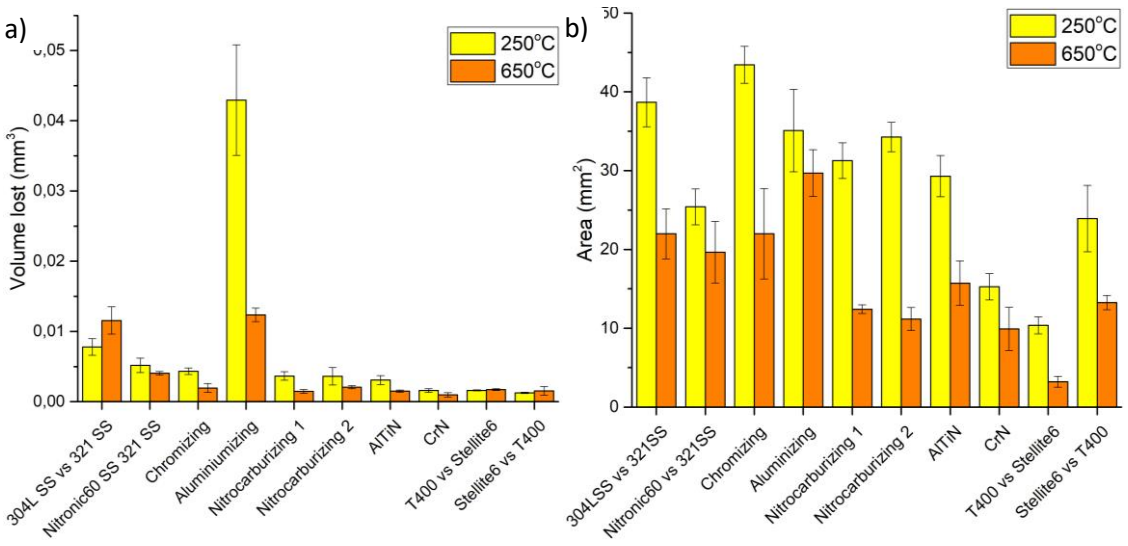

Figure 5.2. Plate worn volume (a) and plate affected area (b) for the different material pairs after testing at 250°C and 650°C.

As the testing temperature increased to 650°C, the general trend is a decrease in the measured loss of plate material. Exceptions were the 304L plate, where the loss volume increased by a factor of 1.5, and the T400 and the Stellite 6 plates, which showed similar values at both temperatures. The largest reduction in wear volume was experienced by the aluminized plate, which lost four times less volume than at 250°C, reaching a similar value as the 304L plate. Nitronic 60 exhibited a slight decrease in the material lost. Finally, the chromized, Nitrocarburizing 1, Nitrocarburizing 2, AlTiN and CrN plates lost half as much material at 650°C as was lost at 250°C.

Comparing the different plate materials with each other, the 304L stainless steel plate showed similar worn volumes to the aluminized plate. These were followed by the Nitronic 60 plate where a third of material was lost, closely followed by the chromized and the Nitrocarburing 2 plate that were reduced by half. The least volume of material lost was observed at the CrN plate, followed closely by Nitrocarburizing 1, AlTiN and the Co-based superalloys plates.

A similar trend was observed when comparing the worn areas. Aluminising had the biggest wear scar out of the different materials. The three stainless steel material pairs followed showing similar scar area values, unlike at 250°C where there was a wide variation. The next smallest scar area was for AlTiN, along with the Stellite 6 plate against the T400 pin. Nitrocarburizing 1, Nitrocarburizing 2 and CrN showed half of the worn area in comparison to the stainless steel pairs. Finally, the T400 plate vs Stellite 6 pin showed the smallest worn area out of all the material pairs; that area is a factor of 3 lower than the previous three pairs.

Comparing the worn areas from different plates at 650°C, the aluminized plate showed the biggest wear scar area, closely followed by the 304L, Nitronic 60 and the chromized plate, which showed a half mean area worn with a high variance. The AlTiN coated stainless steel showed a third of the previous, closely followed by Nitrocarburizing 1, Nitrocarburizing 2, CrN and the Stellite 6 plate showing half of the area. The smallest wear scar area was attributed to the T400 plate.

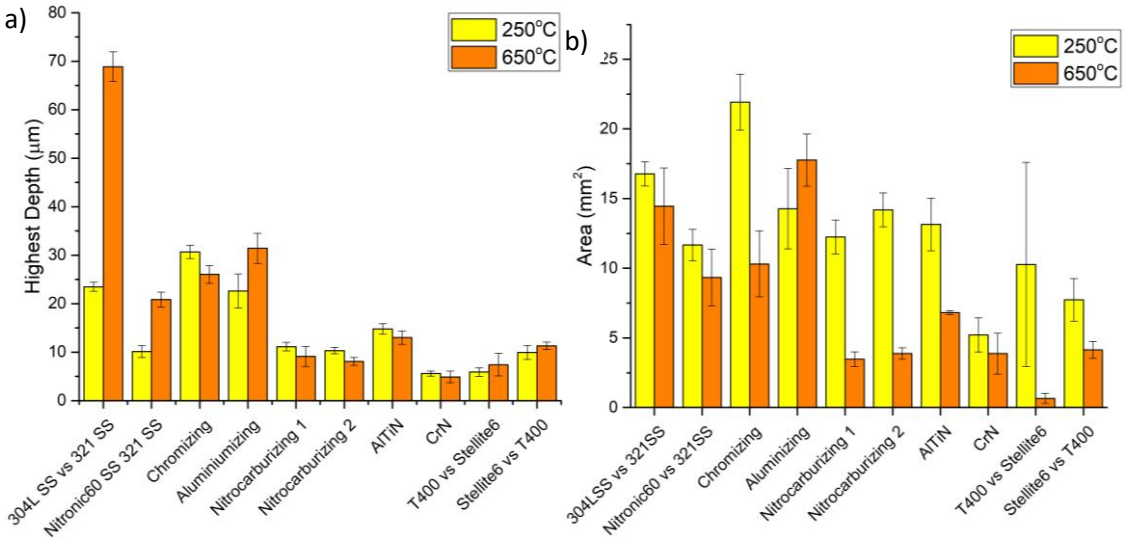

Figure 5.3. Pin wear depth (a) and pin affected area (b) for the different material pairs after testing at 250°C and 650°C.

As with the plates, most of the pins showed a reduction in the wear-affected area at the higher temperature, except the aluminized stainless steel, which showed a higher worn area. For the three stainless steel pairs, the 304L vs 321 pair showed a slight reduction in the worn area compared to the aluminized pair, while the Nitronic 60 vs 321 stainless steel and the chromized pair showed values lowered by nearly a factor of 2. As previously, the stainless steels are followed by the AlTiN coated pin, where the worn area was nearly half of that of the chromized pair. Nitrocarburizing 1, Nitrocarburizing 2, CrN and the T400 pin, from the Stellite 6 plate vs T400 pin test, showed a worn area that was half of the AlTiN pin. The pin with the lowest area affected by the wear process, with a worn area nearly seven times smaller than the second smallest, was the Stellite 6, from the T400 plate vs Stellite 6 pin pair.

Comparing the different pin worn area at 650°C to the 250°C tests, all material pairs showed the same trend as for the plate affected areas.

From a pin wear scar depth perspective, the results shown by Figure 5.3 confirm what was observed from the height distribution maps and the 2D surface representations. In comparison to 250°C, the 321 stainless steel pin for both pairs showed an increase in the depth of the wear

scar, a factor of three increase when it was against the 304L plate and factor of two increase against Nitronic 60. The aluminized pin, the Stellite 6 and the T400 all also showed a slight increase in the wear scar depth at 650°C. Finally, the chromized pin, Nitrocarburizing 1, Nitrocarburizing 2, AlTiN and the CrN coated showed a slight decrease.

Comparing the pin depths from the different materials at 650°C, the 321 stainless steel pin that was in contact with the 304L plate showed the deepest scar, followed by the aluminized and chromized pins and the 321 stainless steel pin that was in contact with Nitronic 60; the depth of the wear scar in these three cases was reduced by a factor of 3 compared to the 321 stainless steel. The AlTiN showed a half of the depth observed for the previous pin materials, closely followed by Nitorcarburizing 1, Nitrocarburizing 2 and the T400 pin. Finally, the lowest depth observed was observed for the CrN pin, which showed a value only slightly lower than the Stellite 6 pin.

5.2 Discussion

As in the previous chapter, all the data presented in the previous sections will be used to explain the differences between material pairs from a friction and wear perspective. The materials will be compared using the 304L vs 321 stainless steel pair as the base line. Some pairs, including the nitrocarburizing treatments, the PVD coatings and the Co-base superalloys, will also be compared with respect to each other. In addition, possible explanations for the changes in the friction and wear behaviour between 250°C and 650°C will be given.

5.2.1 Tribological behaviour

For the 304L and 321 stainless steel pair, the changes observed in friction and wear due to the test temperature may be explained by two hypotheses, both of which relate to the loss of mechanical properties, mainly of the 304L stainless steel. The friction and wear on the plate, as well as the groove depth in both materials, were observed to increase at the higher temperature. This was due to an increase in the deformation component, which produced a thermomechanical fatigue failure [86] in the subsurface. The increase in deformation is in turn attributed to the larger volume of material affected by the load, due to the loss of mechanical properties at increased temperatures. This is in addition to the ploughing of harder particles, composed of various Fe- and Cr based oxides and the formation of compacted layers on the 304L mechanical mixed layer on the pin. Hypothesis one assumes the compacted layer lasted the throughout the test and contributed significantly to further reduce the total wear; if it did not (hypothesis two) then friction and wear increased due to the continuous abrasion of the deep

grooves formed. Even though the wear increased the scar depth on both the plate and the pin, the area affected was reduced as the wear process was heavily concentrated.

Although the friction and wear behaviours of the Nitronic 60 pin vs 321 stainless steel plate were similar to those of the previous pair, this material pair showed a decrease in the damage done, but also a slight increase in friction as temperature increased. While the ploughing component of friction was reduced due to the formation of compacted layers on both components, it was simultaneously increased due to the formation of Fe- and Cr-based oxides that ploughed on softer areas, in addition to delamination of the compacted layers. The deformation component of friction increased due to the loss of mechanical properties. While the materials themselves lost mechanical properties, the overall wear performance was improved due to the formation of compacted layers and heavily internally oxidized regions

The chromized pin and plate showed a decrease of both CoF and the volume of worn material as the test temperature increased to 650^{o}C. The improvement was attributed to the formation of compacted layers made from Fe- and Cr- based oxides. The improvement in performance in comparison to the stainless steel base material was attributed to the oxide-based compacted layer, which protected the surface during the steady-state. Another hypothesis is that the layer acted as a load carrier, reducing the damage caused during the running-in, evidenced by the reduced depth of the damage.

The aluminized pin and plate showed the same value of the CoF as at the previous temperature, while exhibiting a lower plate wear volume and smaller affected areas for both the plate and the pin. However, the depth of the wear scar was increased. The value of CoF at the higher temperature was similar to that at 250^{o}C due to a balance between the ploughing of hard oxides, which acted to increase the CoF, and a reduction of ploughing in other areas due to the formation of compacted layers composed primarily of Fe_2O_3 oxides. Top layer of the layered system deformation was also observed; as it appeared to be pushed into the substrate material as the stiffness properties of the intermetallic compounds were reduced [119]. The increased abundance of Fe-based oxides, despite the increased stability of Al_2O_3, was attributed to the growth kinetics [225]. The wear of the plate was reduced due to the protective action of the mechanical mixed layers, while the pin material probably underwent similar or higher wear than at the previous temperature. The pin affected area and the scar depth are higher. This was attributed to the amount of material that is compacted, showed to be higher for the base stainless steel pair (from a depth perspective), while from an area perspective was attributed to a less catastrophic failure during the running in.

In comparison to the 304L vs 321 stainless steel, the poor performance of the aluminized pair was not attributed to the loss of mechanical properties; in fact, the CoF slowly increased to a similar value as the stainless steels, and the layers provided a higher load carrying capacity. Instead, it suggested that abrasion had a bigger effect on this material pair, in conjunction with not providing enough load carrying capacity at areas were the mechanical-mixed layers were formed as the top layer seemed to be pushed into the component.

Nitrocarburizing 1 and Nitrocarburizing 2 showed similar changes in the CoF and the wear as the temperature of the test was increased. Both materials showed a better performance in both friction and wear at the higher temperature, attributed to the continuous oxide layer formed of different Fe-based oxides. The grown oxide layer reduced the effect of abrasion, and the number of oxide particles in the contact caused the improved wear performance, while also reducing the ploughing component of friction. Not only did this oxide layer improve performance in comparison to the steel, but the higher hardness of the case-hardened area enabled the increased load carrying capacity of the system and prevented the subsurface material from delaminating.

For AlTiN, the loss of mechanical properties [226] as a consequence of the higher temperature also contributed to the improved performance of the material pair, whether some areas delaminated during running-in or coating was removed by abrasion as the formation of a smooth layer of stainless steel material and different Fe-based oxides on areas covered by the AlTiN coating; in comparison to the previous temperature, this smooth layer aided to reduce abrasion and, if occurred, coating delamination. In comparison to the base stainless steel base pair, the better performance was attributed to the increased hardness and toughness of AlTiN at higher temperatures [149]. This not only helped during the running-in behaviour, but also prevented deep delamination and supported the formation of a mechanical mixed layer.

The CrN coated stainless steel pair at 650^{o}C showed a slight improvement in wear behaviour in comparison to 250^{o}C, as well as a significant reduction in the CoF. This is in spite of potential loss of mechanical properties in the layer as evidenced by the grain increase in the coating layer. The improvement in performance was largely related to formation of the compacted layer composed mainly of Cr_2O_3 oxides. The CrN and Cr_2N phases were found in the uppermost (most recently formed) particles in the compacted layer, or, as observed in the TEM, in areas where compacted layers did not form. It is important to note that the Cr_2N phase existence [159] was possible, but its confirmation is complicated by the proximity of its peak position relative to the Cr_2O_3 peak in the Raman spectra. The compacted layer clearly helped to reduce wear as the

surface was protected from abrasive particles in the contact. It also reduced the number of particles in the system, as they were used to form the layer. From a friction perspective, the number of abrasive particles in the system was reduced to a negligible amount as most of them were compacted. Most of the wear occurred either during the running-in period (hypothesis 1) or through the removal and build-up of the compacted layers, which is a common process in the contact (hypothesis 2).

In comparison to the stainless steel base pair, as for previous pairs, the combination of a hard compacted layer with a layer below with a higher load carrying capacity improved the performance of the CrN coated pair. There are two possible explanations for the different behaviour in this case. The first hypothesis is that there were a higher number of particles on the nitrocarburizing treatments, as the layers were not compacted. There were, therefore, a higher number of loose particles in the system, raising the CoF through a higher ploughing component. Hypothesis 2 suggests the compacted layers for the CrN coated pair showed low shear strength, due to defects in the compacted layer seen in the TEM image as darker regions (voids) in between compacted particles. The surface SEM image showed low compacted layer adhesion and a granulated topography was observed below the delaminated compacted layers. As highlighted by the horizontal red line in the TEM image, there was a change in grain structure between the upper area, where the grain size and morphology were irregular, and the lower region, where grains showed a semi-circular morphology.

As previously, the improvement in friction and wear performance shown by the T400 plate vs the Stellite 6 pin was attributed to the formation of a compacted layer. Again, the compacted layers aided with CoF by reducing the number particles in the contact and providing a similar hardness material in contact (compacted layer).

In comparison to the base stainless steel material, as for the previous materials, the T400 plate and Stellite 6 matrix and hard second phase offered a load carrying capacity that the stainless steel pairs could not provide. It is not known to what extent the load relief was supplied by the layer to the bulk material, as the continuous surface deformation of the bulk material will cause similar failure behaviours as seen in the stainless steel pair, but probably not as severe.

In comparison to the CrN coated pair, the T400 plate and Stellite 6 pin showed a higher CoF; the explanation for this hinge on the efficacy the two hypotheses proposed above for the low CoF of CrN in comparison to the nitrocarburized treatments. If hypothesis 1 above is true, then the higher CoF for this material pair may be attributed to the increased impact of the deformation component on both the surface and subsurface bulk material and to the high-Mo content areas

that were aligned with the direction of the motion. If hypothesis 2 was true, then, in addition to deformation of substrate and subsurface material, the lack of shearing of the glazed layers will provide the higher CoF observed for T400 vs Stellite 6 relative to the CrN coated pair.

For the Stellite 6 plate vs T400 pin material pair, the performance was not only dependent on the formation of the scattered compacted layers, but also the retention of mechanical properties due to the existence of intermetallic (T400) and carbide (Stellite 6) particles. The material pair exhibited an increase in the CoF at the higher temperature, attributed to an increase in ploughing at the areas not covered by the compacted layers, as well as delamination of material from the T400 pin. However, it should also be noted that the measured value of the volume of lost material was incorrect, as the plate did not appear to suffer significantof wear as observed in at the 2D surface profile; thus part of the observed worn volume is thought to arise from an error in the measurement.

In comparison to the base stainless steel material pair, the better performance of the Stellite 6 plate vs the T400 pin was caused by a combination of the scattered compacted layers, the higher hardness of both the matrices, and the presence of particles. These prevented material failure due to heavy delamination and ensured that abrasion remained the main wear mechanism. The CoF was slightly lower for the same reasons, in addition to the reduction of the deformation component.

The Stellite 6 plate vs the T400 pin performed worst from a friction and wear perspective in comparison to the previously discussed pair (T400 plate vs Stellite 6 pin). This was attributed to the discontinuity of the compacted layer. The discontinuity was obscured, as the near surface chemistry was composed of the same/similar components, and while the Stellite 6 component suffered less from the mechanisms acting on the system in both cases, the layers formed had very similar structures. The differences observed were:

- The T400 layers were more prone to show porosity at the compacted layer. Note that porosity observed at the compacted layer was attributed to the TEM sample preparation. In addition, areas within the compacted layer showed a preference direction at the axis motion.
- This pair showed a 5% increase in the content of Mo and a 10% in the O content at the compacted layer of the T400 pin, while the Stellite 6 layer showed a very similar structure and element concentration at the compacted layer. These differences may be an artefact of the specific areas from which samples were obtained.

- The oxide layer for the T400 pin was below the surface of the matrix material, while it was above the matrix for the T400 plate. This behaviour was observed at the surface, where the T400 particles formed oxides were highly polished at the surface. There was a possibility that the oxide formed at the intermetallic particles had helped the formation of the compacted layer at the beginning of the test, as the T400 was in the pin position, which means more time in contact, those oxides were quickly removed. The particles in these alloys may then have had to sustain most of the load, causing them to fracture and increase the instability of the system (hypothesis 1).
- The affected area became higher as the pin was increasingly worn. Within the contact area, the contact stresses during the test were controlled by the pin geometry [223]. As the pin material is worn, the contact stresses will be reduced, which caused the compacted layers to be more porous and more easily removed (hypothesis 2). This also relates to the position of the material in the contact.
- When the layers were scattered, as opposed to a uniform compacted layer, they suffered from cracking at their edges. The formation of scattered compacted layers could be caused by a non-uniform area wear or by the agglomeration of the particles at certain regions (hypothesis 3).

Finally, there is also the possibility that an unconsidered process or a combination of those listed above was the driver of the behaviour observed.

5.3 Conclusion

Overall, the different material pairs were ranked, in Table 5.1, in order of decreasing friction and wear performance as:

Position	Friction	Wear
1	CrN	T400 plate vs Stellite 6 pin
2	T400 plate vs Stellite 6 pin	CrN
3	Nitrocarburizing 2	Nitrocarburizing 1
4	Chromizing	Nitrocarburizing 2
5	Nitrocarburizing 1	Stellite 6 plate vs T400 pin
6	AlTiN	AlTiN
7	Stellite 6 plate vs T400 pin	Nitronic 60 plate vs 321 SS pin
8	Nitronic 60 plate vs 321 SS pin	Chromizing
9	Aluminising	Aluminising
10	304L SS plate vs 321 SS pin	304L SS plate vs 321 SS pin

Table 5.1. List of best to worst performing materials from a friction and wear perspective.

As in the previous chapter, the list takes into consideration the numerical measurements, but also the stability of the material pair and the mechanisms acting in the contact.

As a summary, materials tend to lose mechanical properties at increased temperatures. As a result, the performance of the material pairs may deteriorate as the system becomes more unstable and more detrimental behaviours dominate the system, as observed for the base stainless steel pair. However, higher hardness materials, in the formed of oxide layers (compacted or grown) or base material showed an improvement in the behaviour, as the mechanisms observed at the base stainless steel pair had a lower to no impact. This was further improved by increasing the toughness of the system, providing a hard, compacted layer followed by a layer or region of material strong enough to withstand contact stresses and to not deflect under the load, thus improving wear and friction performance. The nitrocarburizing 1 treatment did not have the best friction performance, although it was one of the best from a wear perspective. In the case of the CrN pair, the lightly adhered compacted layer may have aided towards the improvement of the friction performance.

Finally, the table below (Table 5.2) shows the results of the selection process described previously. The best performing treatments, Chromizing and CrN, are immediately taken through to the tribological test at the final temperature, 750^{o}C. The base stainless steel pair and the Co-based superalloys also go forward as they are being used as baselines, to which the

performance of the coated/treated materials will be compared to understand their potential at the different temperature ranges. The last two materials put through to the next test were Nitrocarburizing 1, as it is used as a baseline material for coated and surface treated stainless steel, and Nitrocarburizing 2, as it is more environmentally friendly and, at the potential point of introducing the treatment to current technologies using Nitrocarburizing 1, will have lower probable development costs. Aluminising was removed from the selection process due to its lower overall performance and worst performance from a tribological perspective, and AlTiN was removed due to its lower engineering performance.

Rating of Importance to Customer (low 1- high 10)	10	7	5	9	8	7	7	10	7	9	10	8	9	7	2	
Inputs	Life of Coating	Corrosion Resistance	Thermal Shock Resistance	Thermal Capability	Surface treatment uniformity	Base Material Surface Finish Requirement	Changes to Final Component Dimensions	Tribological Characteristics	Proprietary Technology	Sensitivity of Process to Component Geometry	Environmental Compliance Risk of Process and Components	Cost	Dual Source and Global Availability	Risk of Supplier Design Control	Intregation of Manufacturing Technology into Cummins Facility	Total
Boronizing	3	1	9	1	1	9	1	-	9	9	9	9	9	3	1	579
Chromizing	3	3	9	9	9	9	9	1	9	9	9	9	9	3	1	795
Aluminizing	3	3	9	3	9	9	1	1	9	9	9	9	9	3	1	685
Nitriding	1	1	9	1	1	9	9	-	9	9	9	9	9	9	3	661
Nitrocarburizing 1	3	1	9	1	9	9	9	3	1	9	1	3	1	3	0	471
Nitrocarburizing 2	3	1	9	1	9	9	9	3	1	9	3	3	1	3	0	491
AlTiN	3	3	9	3	3	3	9	1	9	3	9	3	9	9	9	607
AlCrN	0	1	0	1	9	3	9	-	9	3	9	3	9	9	9	538
CrN	3	3	9	3	3	3	9	9	9	3	9	3	9	9	9	687
Total	220	119	360	207	424	441	455	180	455	567	670	408	585	357	66	

Table 5.2. C&E matrix used along the EngD showing the scores given to each material for each engineering and purchasing perspective and their scores at the end of this temperature test.

6. Tribology test at 760ºC

Before starting with this section, please note that surface and cross-sections morphology and chemistry can be observed at Submission 4.

6.1 Results

6.1.1 Friction behaviour

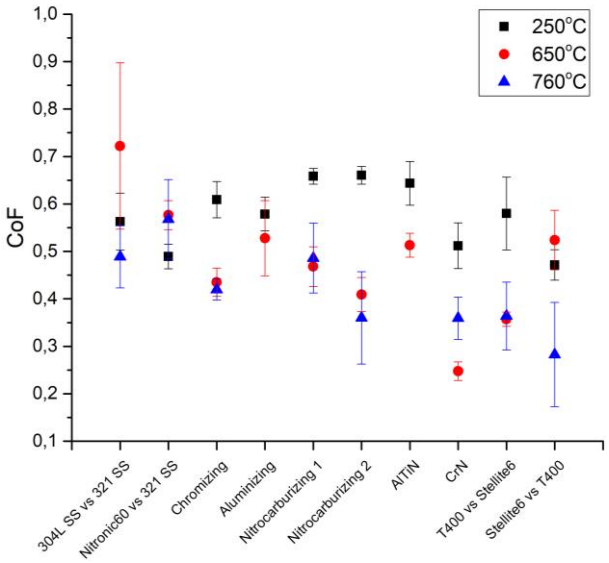

Figure 6.1. Average steady-state CoF of the different material pairs when tested at 250ºC, 650ºC and 760ºC.

At 760ºC, Figure 6.1 sjowed the 304L stainless steel vs the 321 stainless steel decreased its CoF from the previous temperature. The Nitronic 60 vs 321 stainless steel showed a similar CoF of 0.59; however, its variation was higher. Similarly, the chromized steel pair had a similar CoF with a value of 0.43. Nitrocarburizing 1 and Nitrocarburizing 2 also showed relatively similar CoFs in comparison with the previous temperature, with values of 0.49 and 0.39 respectively, with a higher variation attributed to the variation between tests. The CrN coated steel experienced an increase in the CoF up to 0.37, again with a higher variation due to differences between the tests. The T400 plate vs the Stellite 6 pin showed the same value of 0.37 with a higher variation at 760ºC attributed to test differences. Finally, the Stellite 6 plate vs the T400 showed a lower average CoF of 0.3 with a high variation due to test variations.

6.1.2 Wear behaviour

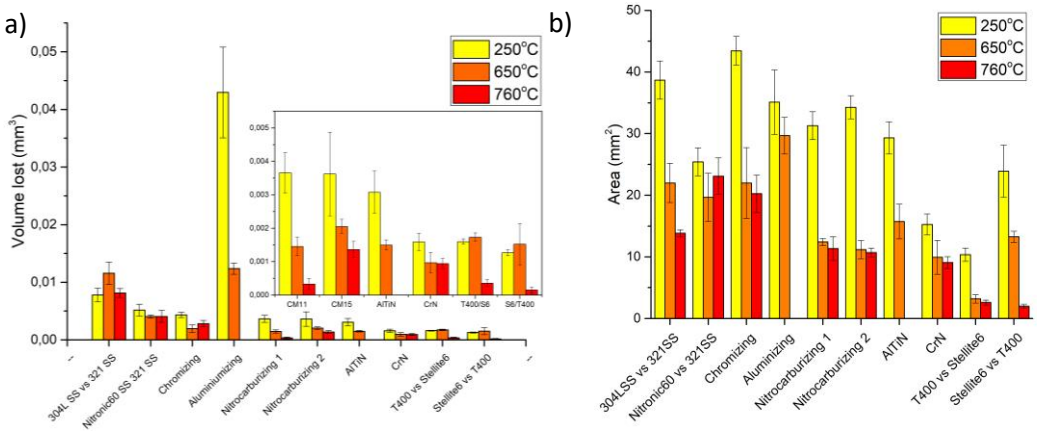

Figure 6.2. Plate worn volume (a) and plate affected area (b) for the different material pairs after testing at 250°C, 650°C and 760°C.

As the test temperature was increased, most materials showed a decrease in the plate volume lost when compared to the 650°C tests. The biggest reductions were observed for the 304L vs 321 stainless steels, which showed a factor of three reduction in lost material, and both Co-superalloy plates and Nitrocarburizing 1, which showed four times less material volume was lost. The Nitrocarburizing 2 plate also experienced a reduction of a third in the volume of material lost by the plate. Both the CrN coated plate and the Nitronic 60 plate were found to have lost the same volume in comparison to the volume lost at 650°C. Finally, the chromized plate showed a slight increase in the material lost from the plate.

When comparing the plate volume lost from the different material plates tested at 760°C, the 304L plate lost the largest volume, followed by the Nitronic 60 and the chromized plate, which lost similar volumes. Nitrocarburizing 2 and the CrN coated plate followed, showing a two times reduction relative to the chromized plate. These are followed by the Nitrocarburizing 1 and the T400 plate showing, where the volume of material lost is again reduced by half, in comparison to Nitrocarburizing 2 and CrN. Finally, the Stellite 6 plate lost the smallest volume of material, which was half that of the previous two plates.

When comparing the worn affected area of the tested plates at 760°C with the 650°C plates, all plates showed either a relatively similar or reduced affected area. The Nitronic 60, chromized, Nitrocarburizing 1, Nitrocarburizing 2, CrN coated and T400 plate showed a similar affected area to the previous temperature, while the 304L and Stellite 6 plate showed around 2 times and 5 times less worn area, respectively.

The worn area of the plate did differ, however, when comparing the different materials at 760°C. The materials that showed the highest area were the Nitronic 60 and chromized plate, closely followed by the 304L plate. The Nitrocarburizing 1, Nitrocarburizing 2 and CrN plates showed a third of the area affected from the wear process in comparison to the 304L plate. Finally, the T400 and Stellite 6 plates had the least area affected by the wear process, which was around three times less than the previous plates.

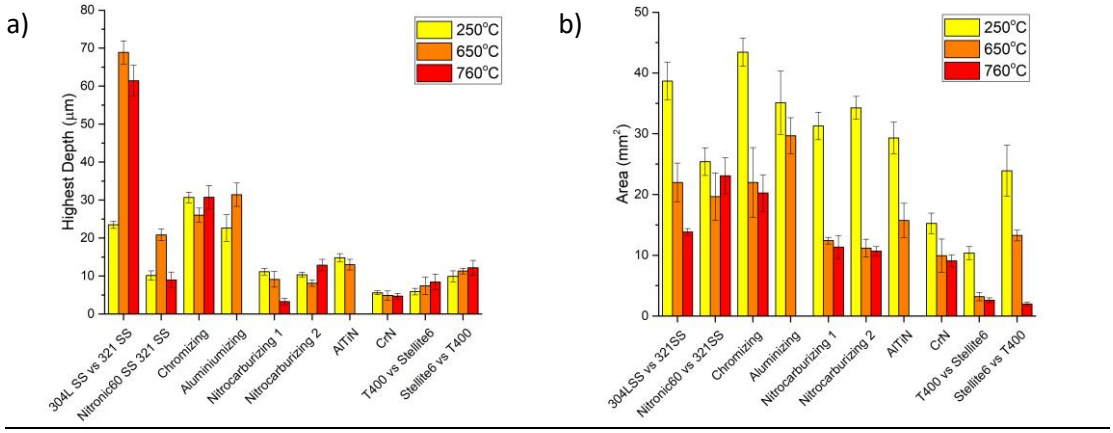

Figure 6.3. Pin wear depth (a) and pin affected area (b) for the different material pairs after testing at 250°C, 650°C and 760°C.

In comparison to the previous temperature (650°C), the pin worn area observed at the 760°C showed similar trends as the ones observed when comparing the plate worn area at 650°C and 760°C.

For the pin worn area at this temperature (760°C), most of the pin materials followed the same trend as at 650°C, except the stainless steels and the chromized pair. For the pins, the 321 stainless pin that ran against the 304L plate showed a slightly less worn area than that run against the Nitronic 60 plate; however, due to the variation in the measurement, the observed reduction was less significant. On the other hand, the chromized pin showed a higher affected area than the 321 stainless steel pin that ran against the Nitronic 60 plate, even though the uncertainty range overlaps for both the pin and the plate. In comparison to the previous temperature, the trend observed for the plate materials was also observed for the pins, except for the metallic pairs where the error ranges overlap, creating uncertainty.

When looking at the maximum depth of the wear scar on the pin, shown in figure 6.3, there was no correlation observed between the depths at 760°C and those of the previous temperatures. Both the 321 stainless steel and Nitrocarburizing 1 pin showed a decrease in the depth of the wear scar; the difference was small for the 321 stainless steel that ran against the 304L stainless steel plate, but the depth was lower by a factor of for the 321 pin run against the Nitronic 60

plate and the Nitrocarburizing 1 pin. The chromized and the Nitrocarburizing 2 pins showed a slight increase in the depth at this temperature, while the CrN coated, Stellite 6 and T400 pins showed very similar depths.

When comparing the different materials at 760°C, the 321 stainless steel pin running against the 304L stainless steel plate showed the highest depth. The depth shown by the chromized pin was roughly half as high, followed by the 321 stainless steel pin ran against the Nitronic 60 plate and the Nitrocarburizing 2, the T400 and Stellite 6 pins, each showing around three times less depth than the 321 stainless steel pin. Finally, CrN showed a third of the depth than the previous pairs, while the depth for the Nitrocarburizing 1 was lowest, at half that of the CrN pin.

6.2 Discussion

As in the previous chapter, all the data presented in the previous sections will be used to explain the differences between material pairs from a friction and wear perspective. The materials will be compared using the 304L vs 321 stainless steel pair as the base line. Some pairs, including the nitrocarburizing treatments, the PVD coatings and the Co-base superalloys, will also be compared with respect to each other. In addition, possible explanations for the changes in the friction and wear behaviour between 650°C and 760°C will be given.

6.2.1 Tribological behaviour

As with the previous temperature, the high CoF found during running-in for the 304L v 321 stainless steel pair was caused by the loss of mechanical properties, which promoted thermo-mechanical fatigue failure [86]. Following the failure, deep grooves were formed where particles produced from the failure were compacted; this compaction probably occurred more quickly at this temperature due to the further reduction in mechanical properties, therefore, the running-in time was reduced. As for the previous temperature, it is unknown whether most of the damage of the plate and pin was caused during the running-in, producing a wear-resistant compacted layer (hypothesis 1) or if additional damage was caused at the grooves due to the failure of the compacted layers (hypothesis 2). From an inspection of all the data, the deep grooves appeared to be mostly covered by a compacted layer that suffered from abrasion and not large-scale delamination. The surrounding areas may have suffered from mild abrasion and material delamination, indicated by the small cracks that were growing in mildly internally oxidized regions (hypothesis 3). From a wear perspective, this explains the lower wear-affected area and the lower volume lost on the plate, while the similar depth on the wear scar can be explained by the formation of compacted layers. From a friction perspective, two of the tests displayed slow increases and decreases of the CoF which may be attributed to a build-up of particles or an increase in the deformation component in certain regions of the wear scar.

Alternatively, an artefact caused by the higher temperature may have affected the measured traction force. Meanwhile, one of the tests showed a more stable CoF with smaller increases and decreases in magnitude. It was thus believed that though the external oxide provides benefits to the friction behaviour as a compacted layer, it does not provide further advantages.

The Nitronic 60 vs the 321 stainless steel showed the same average CoF as the previous temperature, while showing differences in its variation. At 650^{o}C, the decreases in CoF were attributed to delaminated material breaking down into smaller particles. At 760^{o}C, there was a continuous instability, believed to be caused by cracking of material from the compacted layer in combination with hard oxide particles ploughing areas where the compacted material was removed, mostly at the edges of the wear scar. While the ploughing component was probably reduced as no large particles seemed to be formed during the steady-state, it was believed that the material pair suffered from heavy deformation. This can be seen on the 2D topography plots, as the pin material completely lost its original shape and the plate showed a significant increase in height at the edges of the wear scar.

In comparison to the 304L stainless steel plate and 321 stainless steel pin, for the Nitronic 60 plate vs the 321 stainless steel pin, the difference in friction and wear behaviour is caused by the difference was attributed to plate material and the running-in behaviour. The increase of the average CoF and instability of the Nitronic 60 plate pair was attributed to the thinner compacted layer (relative to the 304L plate compacted layer) that formed in the middle of the wear scar, which served as the load carrying element of the pair. Despite this, small chucks of material were expelled by delamination from the compacted layer, causing the system to heavily deform under the load as particles were ploughing on areas uncovered by these compacted layers. On the contrary, less wear was experienced by the pin and plate in the Nitronic 60 pair, as shown by the reduced amount of material delaminated via to thermo-mechanical fatigue failure [86] or simply heavy abrasion. The maximum depth of the wear scar was also less, as Nitronic 60 retains its mechanical properties at the higher temperature; for this reason, the material wear mechanism was mainly abrasive, while the 304L plate pair experienced additional material delamination.

For the chromized pair, the average CoF was similar to that at 650^{o}C, but it showed a slightly higher variability. Observing that the pin surface looked very similar at both temperatures while differences were observed on the plate, this increased variability is attributed to the plate behaviour. Two main differences were observed on the plate; firstly, the compacted layer seemed to be better compacted and was continuous across the contact area when compared to

the pin, and secondly, the material from the chromized plate did not delaminate, as it was observed to do at 650°C. Based on the magnitude of the CoF, it is believed that particle ploughing was more important at 650°C. At 760°C the ploughing component was reduced as material did not delaminate and the areas in contact were covered by the compacted layer. It may be noted, however, that the cross-sections showed the formed layer being pushed inwards, which may mean that the regions in contact undergo deformation.

Relative to the base stainless steel pair, the lower CoF observed for the chromized pair was believed to be due to a lower ploughing component, which was reduced due to less material being present at the contact (lower wear) and fewer delaminated particles. From a wear perspective, the chromized plate showed overall better wear performance as the wear volume and depth of the pin worn area are much lower than those of the base material pair. While the worn area was larger, less material was lost due to the lower amount of material delaminated during running-in.

For Nitrocarburizing 1, the friction behaviour at the increased temperature was similar to 650°C. The failure mechanisms observed on the surface of the pin and the plate were similar, supporting the observation of a similar CoF. However, the Raman spectra showed a greater number of regions containing a higher abundance of Fe_3O_4. The reduction in wear was attributed to the faster growth of the oxides at higher temperatures.

The average CoF of the three tests on the Nitrocarburizing 1 pair was similar to the CoF of the base stainless steel pair. However, if the Nitrocarburizing 1 test that showed a CoF of 0.6 is excluded due to machine/software issues or test variation (hypothesis 1), the average CoF for Nitrocarburizing 1 is now lower than for the stainless steel pair. This could be explained by the thick oxide layer, as it possesses similar mechanical properties to the oxidized particles and is thus less susceptible to ploughing. If the higher CoF value of 0.6 is a true effect attributable to material pair behaviour (hypothesis 2), a possible explanation could be that the ploughing component of this pair is increased due to the compaction of particles in the Nitrocarburizing 1 pair, which does not occur in the stainless steel. From a wear perspective, the higher load carrying capacity and the higher mechanical properties of the thick, continuous oxide layer reduced the wear of the system; as the stainless steel pair had areas where oxides were not present and it is believed that the major damage was inflicted at the beginning of the test.

Similar to Nitrocarburizing 1, the Nitrocarburizing 2 pair had a similar average CoF to the previous temperature due to the high variation between tests; however, two of the three tests achieved a lower CoF than the base stainless steel pair. Unlike at the previous temperature, two

of the tests showed a gradual reduction in the CoF as the test time increased, before reaching a plateau. A potential explanation for this behaviour is that most of the damaged to the surface in contact was caused during the running-in, as indicated by the fact that most of the areas from where the material pulled out had been filled; therefore, as less particles were in the contact friction was reduced.

As previously discussed for Nitrocarburizing 1, the reduction in the CoF and wear for Nitrocarburizing 2 in comparison to the base stainless steel material was due to the higher load carrying capacity and the hardness of the layer and sublayer. In comparison to Nitrocarburizing 1, Nitrocarburizing 2 performed slightly better from a friction perspective. One of the tests showed a higher CoF, for the other two tests the CoF was lower and decreased as test time increased until a plateau was reached. This was not observed for the Nitrocarburizing 1. This behaviour was previously explained as a loss of particles in the contact as few particles were generated due to less oxide breaking and delaminating in the contact (hypothesis 1). Further studies are required in order to understand whether: the oxide layer is structured differently and have a significant impact on the performance, or the ratio between the different Fe-base oxides impacted on the behaviour of the oxide layer. In terms of the wear behaviour, Nitrocarburizing 2 showed a similar area affected by the wear process, but it showed a higher plate worn volume and increased pin depth wear. This was attributed to the oxide spalling off during sample cleaning after the test. This induced additional uncertainty in the interpolation of the surface performed in MATLAB.

The CrN coated stainless steel pair showed an increase in the CoF at this temperature but exhibited a similar wear performance in all the categories. As at the previous temperature, the friction and wear behaviours were controlled by the oxide layer that formed pre-test. Compacted layers were not believed to be formed (proving it will require some more characterization) and most of the coating was still protected by the oxide layer that formed pre-test. The increase in CoF could then have been caused by particles with higher O content increasing ploughing at oxide-free areas (hypothesis 1) or the action of high shear strength oxide regions in the contact (hypothesis 2). Note that it is also unknown how phase transformations [159] occurring at the CrN layer and the layer itself in combination with the loss of mechanical properties attributed the the increase in grain size [169] and the diffusion of N into the substrate material contribute towards the CoF. From a wear perspective, the similar performance was attributed to the pre-formed oxide layer for 760^{o}C and compacted oxide layer at 650^{o}C formed during the test. The cross-sections of both the pin and plate at 650^{o}C showed a large areas of oxidised surface, while those at 760^{o}C showed a thicker layer of Cr_2O_3 that formed pre-testing.

In comparison to the base stainless steel pair, as with the nitrocarburizing treatments, the improvement in friction and wear performance of the CrN pair was attributed to the higher load carrying capacity and the higher hardness of both the oxide layer and the coating. When comparing CrN against the nitrocarburizing treatments, the CoF of CrN was lower than that of Nitrocarburizing 1. In the case of CrN, a large number of oxide particles fell into and became trapped within the machining mark valleys with most of the oxide removed by abrasion. From a wear perspective, the wear-affected area for both material pairs was similar, while the wear volume was less. This may have been due to the faster formation of oxides refilling any regions where material was lost but could also be an artefact caused by the difficulty in measuring the wear on the Nitrocarburizing 1 due to the fracture and loss of the oxide layer, as explained above.

The T400 plate vs the Stellite 6 pin showed very similar average CoF, pin and plate worn areas, and pin wear scar depth relative to the previous temperature (650^{o}C) however, a lower volume of material was lost from the plate. From a friction perspective, though the average CoF value was similar to that at 650^{o}C, one test at this temperature gave a CoF value of 0.6, while the other two were below 0.4. In addition, the instability during the steady-state was smaller than at 650^{o}C. The reduction of the instability was attributed to the smeared areas not delaminating from the compacted layers. From a wear perspective, the area affected by the wear scar and the pin depth were similar to the values at the previous temperature. This was due to the rapid formation of the compacted layers, which occurred when the Stellite 6 underwent a failure at the beginning of the test. A similar argument can be used to explain the reduction in material lost from the T400 plate.

In comparison to the base stainless steel pair, the better wear and friction performance was attributed to the formation of the compacted layers and the higher load carrying capacity of these alloys. However, it may be noted that the Stellite 6 pin underwent a significant delamination event early in the test due to the increase of brittleness of the alloy caused by carbide precipitation [227]. In comparison to the other materials such as Nitrocarburizing 1 or CrN, the better wear performance was attributed to the compaction of the material into a layer. The higher observed pin depth was attributed to difficulties in measuring the depth due to the geometry of the pin. From a friction perspective, if the two tests below 0.4 CoF are considered, the CoF value is similar to that of CrN. This is attributed to low particle accumulation, as most of the material was compacted at the beginning, and particle formation was reduced, relative to Nitrocarburizing 1, as the material did not delaminate.

Finally, the Stellite 6 plate and the T400 pin showed slightly different behaviours in comparison to the previous tested temperature. The decrease in CoF and in most of the measured wear properties was attributed to the formation of a compacted layer during the 760°C test that covered the whole wear scar. The maximum depth measure at this temperature was the same as that at 650°C.

In comparison to the base stainless steel pair, the improvement in the tribological performance of the Stellite 6 plate and the T400 pin was again attributed to the formation of the compacted layer and the higher load carrying capacity of the alloys during running-in and steady-state. In comparison to the previous material pair, T400 plate vs Stellite 6 pin, both showed a very similar performance from a wear perspective, but the friction behaviour showed some slight differences. These differences are related to mechanisms observed in these materials at higher temperatures, which are:

- Hardening of the Stellite 6 due to carbide precipitation [227]. This is likely to be the reason behind Stellite 6 showing a drastic microstructural change, as it caused the material to break off before subsequently compacting again. When the Stellite 6 was the pin, at the subsurface the higher Cr regions also showed a higher O content, while the surface sometimes showed the formation of the Co_3O_4 layer previously observed at lower temperatures. However, the layer did not cover the whole surface, as shown by the polished appearance of Cr-based oxide regions, and the growth of a Co, Mo and O-based compound, probably a $CoMoO_4$, which was detected in the Raman spectrum and had a high content across the wear scar. When the Stellite 6 was the plate, the subsurface particles appeared more rounded and were widely spread through the matrix with a large range of grain sizes. The surface was composed of a Co_3O_4 layer, with the Raman showing some degree of $CoMoO_4$ formation, followed by a Cr-base oxide layer.
- The oxidation occurring at the intermetallic particles, followed by diffusion of Mo ions from Mo-based oxides, which are unstable at higher temperatures [230], enabled the formation of $CoMoO_4$ [229]. When the T400 was the plate, the spread of higher relative Mo content areas observed for both the T400 plate and the Stellite 6 pin was immediately noticeable. Meanwhile when T400 was the pin, both materials exhibited more concentrated regions of high relative Mo contents at the intermetallic particles for T400 pin and more randomly located for the Stellite 6 plate.

Exchanging the positions of the alloys induced a change in the structure of the compacted layer though it is currently unknown how this structural change may act to reduce the CoF of the system, but it is believed to be related to the mechanisms discussed above.

An alternative explanation for the different behaviour of the Stellite 6 plate vs T400 pin may be the reduction in the area of contact caused by the failure of the Stellite 6 plate and the subsequent formation of scattered compacted layers above the damaged areas on the plate.

6.3 Conclusion

Overall, the different materials tested at this temperature can be ranked as shown in Table 6.4

Position	Friction	Wear
1	Stellite 6 plate vs T400 pin	Stellite 6 plate vs T400 pin
2	CrN	T400 plate vs Stellite 6 pin
3	T400 plate vs Stellite 6 pin	Nitrocarburizing 1
4	Nitrocarburizing 2	CrN
5	Chromizing	Nitrocarburizing 2
6	Nitrocarburizing 1	Chromizing
7	304L SS plate vs 321 SS pin	Nitronic 60 plate vs 321 SS pin
8	Nitronic 60 plate vs 321 SS pin	304L SS plate vs 321 SS pin

Table 6.1. List of best to worst performing materials from a friction and wear perspective.

As in the previous chapter, the list takes into consideration both numerical values and the mechanisms acting on the system to rank the material pairs.

In summary, as at the previous temperature, the loss of mechanical properties at higher temperatures caused the material performance to decrease during running-in. As the load carrying capacity of the system increases or kept good enough due to the increased in thickness of oxide regions or due to being composed of a layer with the wear particles that could carry this function, the wear and friction behaviour during running-in and steady-state improve or stayed similar. Oxidation behaviour is highly important as oxide layers can aid during the wear, but the reduction of wear does not mean an improvement in friction performance, as observed with CrN. Also, the position of the material in the system (i.e. pin or plate) can change the structure of the compacted layers that form. Although this did not seem to affect the wear performance, it can have a significant impact on the friction behaviour, as observed with the Co-based superalloy pairs.

7. Conclusions, Personal Reflection and Recommendations for Future Work

7.1 Tribology conclusions

During this Project, a range of bulk materials, surface treated stainless steels and coatings were characterized from a range of purchasing and engineering requirements. During this thesis a focus was taken into their tribological performance at 250°C, 650°C and 760°C characterizing the behaviour changes from a structural, mechanical and chemical perspective.

The 304L plate vs 321 stainless steel pin behaviour at lower temperatures (250°C) was mainly attributed to the work-hardening behaviour of the 304L attributed to a low SFE showing a typical galling behaviour observed by particle delamination on the surface and spike CoF increases, while the 321 the most significant behaviour was the formation of oxide regions with a semi-circular pattern near surface. As temperature increased (650°C), the behavioured observed was attributed to the lost of mechanical properties of the steels suffering from thermo-mechanical fatigue causing a high CoF during running-in reaching a steady state due to the cell-like particle compaction and surface hardening due to internal oxidation. At 760°C, the running in behaviour experienced was similar to the previous temperature, but the improved performance observed was attributed to the faster oxidation of the subsurface and the cell-like compacted particles improving the system stability.

The Nitronic 60 vs 321 stainless steel showed the same behaviours as the previous pair at 250°C, but the improvement in performance was attributed to the higher hardness and the higher SFE of the Nitronic 60 reducing the both the work-hardening tendency and the size of the delaminated particles as the defects formed during the work-hardening process occured closer to the surface. At 650°C, this pair showed a lower runing-in CoF than the previous pair attributed to the higher mechanical properties retentation of Nitronic 60, while the pin showed similar behaviours in comparison to the previous pair, the Nitronic 60 plate still showed some internal cracking and semi-circular patterned internal oxidation. While at 760°C it still showed a better wear performance attributed to the less rough running-in and the higher mechanical properties at higher temperatures, the slightly higher CoF was attributed to particle ploughing at uncovered areas and thinner compacted/oxidized regions reducing the load carrying capacity of the system.

The chromized 304L stainless steel plate vs chromized 321 stainless steel pin also, showed an improvement in wear performance in comparison to the base material pair at the whole temperature range, but CoF showed fluctuatuations. At 250°C, this material pair showed a

higher CoF than the base material pair, but as temperatura increased the CoF of the system was reduced attributed to the formation of compacted layers.

The aluminized pair worst performance at lower temperature (250^{o}C) was attributed to the brittleness of the layer causing the layer to crack and delaminate followed by the heavy abrasión of the harder intermetallic particles into the softer intermetallic. Even though the performance improved at higher temperatures (650^{o}C) as the intermetallic phases become more ductile due to lost of hardness, the similar performance to the base stainless steel was attributed to the formation of mechanical mixed layer which not provided enough load carrying capacity.

Both Nitrocarburizing 1 and Nitrocarburizing 2 showed very similar behaviours at all temperatures. Higher temperature behaviour was attributed to the oxide growth instead to particle compaction. The CoF at higher temperatures achieved lower values for the Nitrocarburizing 2, which did not change significantly between 650^{o}C and 760^{o}C, due to unknown reasons. At 760^{o}C Nitrocarburing 1 showed lower wear values attributed to the delamination of the oxide produced during testing when cleaning the samples before doing the measurements.

For the AlTiN coated stainless steel pair, at 250^{o}C, showed the coating removed at the end of the tribology test. Even though there is the possibility of the coating being removed by the abrasive action in the contact, it is belived that the coating failed during running in as no drastic changes in CoF were observed along the test. The failure of the oating during running in was attributed to its brittleness in comparison to the other coatings and/or surface treatments studied during this EngD. At 650^{o}C the coating was completely remove at some areas of the pin and the plate as the pin was fully covered by substrate material in the formed of a mechanical mixed layer and some areas of the plate were also covered by substrate material.

The CrN pair showed one of the lowest CoF's and material lost at 250^{o}C due to being a hard, but tough enough to not give up under the loads experienced during running in. At 650^{o}C, this pair still showed high wear resistance and low CoF attributed both to the constant removal of the oxide/compacted layer that had low shear strength due to por adherance to the surface or high porosity due to poor compaction. At 760^{o}C the increase in CoF and the high wear resistance was also attributed to the durable oxide layer.

The T400 plate vs Stellite 6 pin showed a good resistance as the alloy is composed of hard particles that protect these alloys agaisnt abrasion. As the temperature increased, the particles formed mostly from the Co matrix created a compacted layer of a Co-base oxide that protect the surface of the material agaisnt abrasion and helped keeping a more stable CoF.

Stellite 6 plate vs T400 pin also showed high wear resistance due to the intermetallic, but also showed one of the lowest CoF's from the material pairs under study attributed to a lower particle accumulation in comparison to the previous pair. As the temperatura increased (650^{o}C), the wear volumen was similar to the previous temperature but the CoF increased attributed to the loss of mechanical properties of the matrix and the ploughing of oxide particles on the surface as non-continuous compacted layers were formed on the materials surface. At 760^{o}C. the formation of a continuous compacted layer improved both wear and friction performance of the material pair.

Overall, for the bulk materials both Co-superalloy pairs showed the best performance, while from the coating/surface treatments it was believed that CrN performed best as it provided a high wear resistance similar or just slightly higher than the Co-superalloys (temperature dependent) and just Nitrocarburizing 1 showed just a slighly better wear resistance. Therefore, from the materials observed, hardness (with enough toughness to no fracturing under the loads experience during running-in or steady-state) and high load bearing capacity of the surface/subsurface system was key for the reduction of wear. At lower temperatures, these properties need to be inherent to the material or to the system, while at higher temperatures, the oxidation mechanisms and particle compaction can create the surface required to prevent more damaging process and keeping the system to wear by a light oxidative or abrasive type of wear. From a friction perspective, at lower temperatures, the lowest wear performances obtained were linked to a better wear performance as less particles in the contact and lower subsurface deformation aided to improve friction. At higher temperatures, two of the material pairs, the CrN coated stainless steel pair at 650^{o}C and the Stellite 6 plate vs T400 pin at 760^{o}C, showed relatively low friction for a dry contact. For the CrN material pair was speculated to be due to a low shear strength compacted layer due to poor layer adherence or high defect concentration, while it was unknown why the Stellite 6 plate vs T400 pin achieved those values. Last thing to note was that most materials with a higher bearing capacity at high temperatures and the formation relatively thicker oxides or compacted layer showed very similar CoF values even thought the composition of those was very different.

7.2 Selection process conclusions

In conclusion, the selection processe developed during this project took into account a variety of engineering and purchasing requirements, that included a series of filtering tests in order to narrow down the number of materials along the testing period. The number of materials removed were dependent on time and budget.

As mentioned in Section 4, before starting with the tribology test, boronizing and nitriding were removed from the process. While boronizing was ranked 3rd last from the rest of materials, therefore removed, nitriding did much better than the PVD coatings, but it was still removed due to its poor engineering performance on the filtering tests. After the 250^{o}C and 650^{o}C tribology test, Aluminising and AlTiN were removed from the selection process as they were the worst by the selection criteria established. Nitrocarburizing 1 went through the whole process as it is the current used treatment. Nitrocarburizing 2 went also through, even though it showed to be one of the worst treatments from the begining when judge under the described criteria. Nevertheless, both treatments showed a high wear resistance at all the temperatures and relatively good friction behaviour. The CrN pair showed to be second best as it performs relatively good in all aspects and excelled on its wear and friction performance. Finally, the chromized stainless steel pair, showed to be the best coating/surface treated stainless steels under the discribed criteria as, even though it showed a lower wear resistance and higher or similar CoF than the previous materials, it excelled at the other categories.

The reason behind the outcome was due to the high Importance rating in all the sections as the process was aimed for a high performance material for all the engineering and purchasing requirements. Therefore, in this case the results obtained were not taken as absolute, but used as a guide and a way to compare and contrast the different materials, while applying engineering judgement to try an obtain a better solution.

Because of the previous reasons, it will be recommended to change the way the importance criteria is evaluated, as looking for the a treatment that excelled at all the categories could be rare. A way to improve it can be to take a similar approach as with the scoring criteria, e.i. 9, 3, 1 and 0, in which the criteria are divided into four categories, the highest one giving a relatively higher value, while reducing the change in importance as the category has a lower importance, as an example 10, 5, 3 and 1.

7.3 Personal Reflection

An EngD is a degree granted due to innovative achievements and to provide a meaningful piece of work to the sponsor company that could be used for both current product and future research.

Innovation is oftern used as a buzzword and depending on who defines it, its meaning can slightly differ. One thing that does not change is innovation is an idea, process, service, product,… that keeps a company relevant in their market or new market by providing a

solution that gives value to their costumer. Taking that idea, the following points provide the innovative achievements obtained along this EngD:

- Provided a selection process for high temperature tribology for turbocharger applications that take into consideration both purchasing and engineering requirements.
- The tribological performance of a range of materials at a temperature range in the environment that replicates as much as possible the conditions experienced by a CTT VG mechanism. In addition, alike materials were tested at all temperature knowing fully that chemical affinity can be detrimental form a tribological perspective. The reason behind this decision was the unknown knowledge of how the different possible mechanisms could contribute to the friction and wear performance. Also, other limiting factors played a role, such as commercial availability coatings and the environment at which will be subjected.
- Finally, a alike material pair showed an improve performance from a friction and wear performance and could be offered as a product. Before that point, more testing is required.

Apart from the previous points, other points were believed to provide a meaningful result of the EngD to the sponsor company. These points are:

- Encourage other groups into investing in researching coating technology to improve future performance of turbocharger.
- Knowledge on why materials offer the performance observed.
- Knowledge related on how the technology suppliers work, what they can offer and how they keep control on their product. In addition, knowledge about coating technology, including different ways and tricks to perform the analsys of the different characteristics surface characteristics.
- A base research that can be taken forward in order to produce a final product with optimum performance from a tribological or cost efficiency perspective.

7.4. Future Work

7.4.1 Observation base

This future work section is related to problems encountered or could be encountered while going through the EngD, in addition to observed behaviour changes of the different material pairs. These projects are:

- **Surface Topography**

  - Objective: Friction reduction by surface texturing/machining methods
  - Approach: Texture density within an area, depth and material (coating/surface treated vs no coated).

- **Load bearing capacity of layers**

  - Objective: understanding whether the different layer system could be used for higher load purposes
  - Approach: Tribology test information and scratch test

- **Coating/layer system adhesion studies**

  - Objective: understanding the influence of coating/layer system, substrate, topography and internal stresses in adhesion of mechanical bonded layers.
  - Approach: internal stresses measurement, topography (key parameter identification), and different indentation techniques.

- **Duplex systems/multilayer systems**

  - Objective: Obtain thicker layers and compare performance for applications were higher thicknesses are required.
  - Approach: Use of different ways of manufacturing the ''same'' product in order to keep the same performance over the component life. Tribology testing

-High temperature performance of coatings/treatments for tribological applications

- Objective: increase library and knowledge of materials for high temperature tribological applications for future applications
- Approach: Tribology testing

7.4.2 Interest base

These concentrate on continuing the current EngD work in order to understand the behaviour observed.

- Nanoindentation and nanoindentation scratch testing studies to understand how the different surfaces structure and layers may behave under specific load conditions.

- Running-in studies in order to try to understand the behaviour the of the different material pairs during this friction regime as it was believed that most of the behaviour observed were caused by the mechanisms ocurring at this stage.
- Long duration testing to understand the behaviour of the different materials in situations not observed during this Project, such as compacted layer failure or substrate material being exposed after coating removal.
- From the materials observed, such as the PVD coatings, obtain different versions of a similar product from different suppliers as the production method and parameters may have an impact on their performance.

References

1. **European Parliment**. (2009). REGULATION (EC) No 595/2009 OF THE EUROPEAN PARLIAMENT AND OF THE COUNCIL of 18 June 2009. *Official Journal of the European Union*. 1 (188), 1-13.
2. **IRTE**.(2017).*Nextgeneration.*Available:http://www.transportengineer.org.uk/article-images/153145/ Next_generation.pdf. Last accessed 6th Aug 2018.
3. **Patil, C.; Varade, S. and Wadkar, S.** (2017). A Review of Engine Downsizing and its Effects. *International Journal of Current Engineering and Technology*. 7 (1), 319-324.
4. **Rodriguez, F.; Muncrief, R.; Delgado, O. and Baldino, C.** (2017). *Market penetration of fuel-efficiency technologies for heavy-duty vehicles in the European Union, the United States, and China* [White paper]. Retrieved August 8, 2018 from The International Council on Clean Transportation: https://www.theicct.org/publications/cost-effectiveness-of-fuel-efficiency-tech-tractor-trailers.
5. **Cummins, Inc**. (2018).*Holset Turbochargers.* Available: https://www.cummins.com/components/holset-turbo-technologies/holset-turbochargers. Last accessed 7th Aug 2018.
6. **Carter, J.; Sharp, N.K. and Tennant, H.** (2010). Turbocharging technologies for heavy-duty diesel engines. In: Zhao, H. *Advanced Direct Injection Combustion Engine Technologies and Development*. New York: Woodhead Publishing. 318-357.
7. **Vikström J.** (1994). Galling resistance of hardfacing alloys replacing Stellite. Wear. 179(1-2),143-146.
8. **Ocken H.** (1995) The galling wear resistance of new iron-base hardfacing alloys: a comparison with established cobalt- and nickel-base alloys. Surface and Coatings Technology.76-77,456-461.
9. **Kim, J.; Ma, H.; Cha, H.; Lee, H.; Sung, J.; Seo, M.; Oh, P.; Park, M. and Cho, J.** (2018). A highly stabilized nickel-rich cathode material by nanoscale epitaxy control for high-energy lithium-ion batteries. *Energy and Environmental Science*. 1 (11), 1449-1459.
10. **NavinSek, B.** (1992). Improvement of cutting tolos by TiN PVD hard coating. *Materials and Manufacturing Processes.* 7(3), 363-382.
11. **Burakowski T, Wierzchoń T.** (1999). Surface engineering of metals. Boca Raton, Fla.: CRC Press.
12. **Cummins Inc.** (2017). *Annual Report Pursuant to Section 13 or 15(d) of the Securities Exchange Act of 1934.* Columbus, IN: Cummins, Inc. Available from: http://investor.cummins.com/phoenix.zhtml?c=112916&p=irol-reportsannual (accessed 12 November 2018)
13. **Besanoon, R**. (1990). *The Encyclopaedia of Physics*. 3rd Ed. New York: Springer Science+Business Media. 497.
14. **Suh, N.P.; Saka, N.; Jahanmir, S.; Randall, N.X. and Wedeven, V.** (2016), *Tribology: Friction, Wear and Lubrication.* Massachusetts Institute of Technology, Cambridge.
15. **Leonardo Da Vinci**. (1508). Rollers for Friction Studies. *Manoscritto L. Foglio 11 V*.
16. **Hutchings, I.M.** (1992). Tribology: Friction and Wear of Engineering Materials, Edward Arnold.
17. **Rabinowicz, E.** (1995). *Friction and Wear of Materials*. New York: John Wiley & Sons, Inc.
18. **Barwell, F.T.** (1957). Wear of Metals. *Wear*. 1, 317-332.
19. **Saka, N.** (2015), 'On the Laws and Theories of Sliding Friction', *IMECE 2015*, Houston, Texas, pp 1- 10.
20. **Hutchings, I.M.** (1992). *Tribology: Friction and Wear of Engineering Materials*. Edward Arnold.
21. **Bowden, F.P. and Tabor, D** (1974). *Friction: An Introduction to Tribology*. London: Doubleday & Company Inc.1
22. **Bowden, F.P. and Tabor, D.** (1950). Friction and lubrication of solids. Part I, Oxford, Oxford U.P., Oxford.
23. **Ernst, H. and Merchant, E.** (1940). Chip Formation, Friction and Finish. *The Cincinati Milling machine Co.* Ohio. Cincinati.

24. **Shaw, M.C. and Macks, E .F** (1949). *Analysis and lubrication of bearings*. Michigan: McGraw-Hill Book Co.
25. **Buckley, D.H.** (1978). Definition and effect of chemical properties of surfaces in friction, wear, and lubrication. *NASA Technical Memorandum*. 1 (1), 1-41.
26. **Buckley, D.H.** (1981). Surface Effects in Adhesion, Friction, Wear and Lubrication, Elsevier.
27. **Suh, N.P.** (1986). *Tribophysics*. New Jersey: Prentice-Hall. 1.
28. **Green, A.P.** (1954). Friction between unlubricated metals: a theoretical analysis of the junction model. *Royal Society Publishing*. 228, 191-204.
29. **Hartweck, W. and Grabke, H.J.** (1979). Effect of Absorbed Atoms on the Adhesion of Iron surfaces, *Surface Science*. 89, 206-212.
30. **Suh, N.P. and Sin, H.C.** (1981). The Genesis of Friction. *Wear*. 69, 91-114.
31. **Sin, H.; Saka, N. and Suh, N.P.** (1979). Abrasive wear Mechanisms and the Grit Size Effect. *Wear*. 55 (1), 163-190.
32. **Barwell, F.T**. (1957). Report on papers on wear presented at the Institution of Mechanical Engineers Conference. *Wear*. 1, 418-445
33. **Arthard, J. F. and Hirst, W.** (1956). The wear of metals under unlubricated Conditions. Proc. R. Soc. London, 236A, 397-410.
34. **Ludema, K.C.** (1991). Third Bodies in Wear Models – Wear Particles: From the Cradle to the Grave. *Proceedings of the 18th Leeds-Lyon Symposium on Tribology*, Lyon, France, Ed. D. Dowson, Publ. Elsevier, 155-160
35. **Gates, J.D.** (1998). Two-Body and three-body abrasion: A critical discussion. *Wear*. 214 (1), 139-146.
36. **Stachowiak, G. W. and Batchelor, A. W.** (2005). *Engineering Tribology*. Oxford: Elsevier, Inc.
37. **Hutchings, I.M.** (1992). *Tribology: friction and wear of engineering materials*. London: Edward Arnold.
38. **Rabinowicz, E.; Dunn, L.A. and Russell, P.G.** (1961). A study of abrasive wear under three-body conditions. *Wear*. 4 (1), 345-355.
39. **Zum Gahr, K.H.** (1961). A study of abrasive wear under three body conditions. *Wear*.4, 345-355.
40. **Quinn, T.F.J.** (1971). Oxidational Wear. *Wear*. 18, 413-419.
41. **Jiang, J.; Stott, F.H. and Stack, M.M.** (2004). A generic model for dry sliding wear of metals at elevated temperatures. *Wear*. 256, 973-985.
42. **Rose, S.** (2003) *Studies of the High Temperature Tribological Behaviour of Some Superalloys*. PhD Thesis. Northumbria University.
43. **Stott, F.H.; Glascott, J. and Wood, G.C.** (1984). Factors affecting the progressive development of wear-protective oxides on iron-base alloys during sliding at elevated temperatures. *Wear*. 97, 93-106
44. **Iwabuchi, A.; Kubosawa, H. and Hori, K.** (1988). The effect of oxide particles supplied at the interface before sliding on the severe - mild wear transition. *Wear*. 128, 123-137.
45. **Rice, S.L.** (1991). The role of wear particles in modifying coefficients of friction. *Proceedings of the 18th Leeds-Lyon Symposium on Tribology*, Lyon, France, Ed. D. Dowson, Publ. Elsevier, 463-467.
46. **Suh, N.P. and Saka, N.** (1987). Surface Engineering. *CIRP Annals*. 36, 403-408.
47. **Tian, H.; Saka, N. and Suh, N.P.** (1989). Boundary Lubrication Studies on Undulated Titanium Surfaces. *STLE Tribology Transactions*. 32 (3), 289-296.
48. **Pauschitz, A.; Roy, M. and Franek, F.** (2008). Mechanisms of sliding wear of metals and alloys at elevated temperatures. *Tribology International*. 41 (1), 584-602.
49. **Subramanian, C.** (1991). Effects of sliding speed on the unlubricated wear behaviour of Al-12.3 wt. % Si alloy. *Wear*, 151, 97-110.

50. **Subramanian, C.** (1991). Wear of Al-12.3 wt. % Si alloy slid against various counterfaces materials. *Scripta metallurgica.* 25, 1369-1374.
51. **Subramanian, C.** (1993). On mechanical mixing during dry sliding of aluminium 12.3wt. % silicon alloy against copper. *Wear*. 161, 53-60.
52. **Green, A.P.** (1954). Friction between unlubricated metals: a theoretical analysis of the junction model. *Royal Society Publishing*. 228, 191-204.
53. **Bowden, F.P. and Tabor, D.** (1950). Friction and lubrication of solids. Part I, Oxford, Oxford U.P., Oxford.
54. **Jahanmir, S.** (1980). On the wear mechanisms and the wear equations. In: Fundamentals of Tribology, Suh, N.P. and Saka, N. (Eds), The MIT Press, London. 455-467.
55. **Molgaard, J.** (1976). A discussion of oxidation, oxide thickness and oxide transfer in wear. *Wear*. 40, 277-291
56. **Archard, J.F.** (1958/59). The temperature of rubbing surfaces. *Wear*. 2, 438-455.
57. **Quinn, T.F.J.** (1983). Review of oxidational wear. Part 2: Recent developments and future trends in oxidational wear research. *Tribology International*. 16, 305-314.
58. **Suh, N.P.** (1973). The Delamination Theory of Wear. *Wear*. 25, 111-124.
59. **Stott, F.H.** (1998). The role of oxidation in the wear of alloys. *Tribology International*. 31, 61-71.
60. **Inma, I.A.** (2003). Compacted oxide layer formation under conditions of limited debris retention at the wear interface during high temperature sliding wear of superalloys. PhD Thesis. Northumbria University.
61. **Sttot, F.H.; Glascott, J. and Wood, G.C.** (1984). Factors affecting the progressive development of wear-protective oxides on iron-base alloys during sliding at elevated temperatures. *Wear*. 97, 93-106.
62. **Burkinshaw, M. and Blacker, D.** (2014). *The high temperature tribological performance of turbocharger wastegate materials.* Available: http://www.cumminsturbotechnologies.com/CTT/CTTContent/CTTUS/SiteContent/en/BinaryAsset/PDFs/Downloads/The_High_Temperature_Tribological_Performance_of_Turbocharger_Wastegate_Materials.pdf. Last accessed 26th May 2016.
63. **Wood, P.D.; Datta, P.K.; Burnell-Gray, J.S. and Wood, N.** (1997). Investigation into the high temperature wear properties of alloys contacting against different counterfaces. *Material Science Forum*. 251-254, 467-474.
64. **Wood, P.D.** (1997). The Effect of the Counterface on the Wear Resistance of Certain Alloys at Room Temperature at 750oC. PhD Thesis. Northumbria University.
65. **Pauschitz, A.; Roy, M. and Franek, F.** (2008). Mechanisms of sliding wear of metals and alloys at elevated temperatures. *Tribology International*. 41 (1), 584-602.
66. **Stott, F.H.; Lin, D. S. and Wood, G.C.** (1973). 'Glazes' Produced on Nickel-based Alloys during High Temperature Wear. *Nature Physical Science.* 242 (1), 75-77.
67. **Stott, F.H., Lin, D.S. and Wood, G.C.** (1973). The structure and mechanism of formation of the 'glaze' oxide layer produced on nickel based alloys during wear at high temperature. *Corrosion Science.* 13 (1), 449-469.
68. **Jiang, J.; Stott, F.H. and Stack, M.M.** (1995). A mathematical model for sliding wear of metals at elevated temperatures. *Wear.* 181-183 (1), 20-31.
69. **Hsu, K.L.; Ahn, T.M. and Rigney, D.A.** (1980). Friction, Wear and Microstructure of Unlubricated Austenitic Stainless Steels.*Wear.*60 (1), 13-37.
70. **Talonen, J. and Hänninen, H.** (2007). Formation of shear bands and strain-induced martensitic during plastic deformation of metastable austenitic stainless steels. *Acta Materialia.* 55 (1), 6408-6118.
71. **Lee, Y.-K.; Lee, S.-J. and Han, J.** (2016).Critical assessment 19: stacking fault energies of austenitic steels. *Materials Science and Technology.*32 (1), 1-8.

72. **Vitos, L.; Nilsson, J.O. and Johansson, B.** (2006). Alloying effects on the stacking fault energy in austenitic stainless steels from first-principles theory. *Acta Materialia.* 54 (1), 3821-3826.
73. **Das, A.; Sivaprasad, S.; Ghosh, M.; Chakraborti, P.C. and Tarafder, S.** (2008).Morphologies and characteristics of deformation induced martensite during tensile deformation of 304LN stainless steel. *Materials Science and Engineering A.*486 (1), 283-286.
74. **Lo,K.H.; Shek,C.H. and Lai,J.** (2009). Recent developments in stainless steels. *Materials Science and Engineering R Reports.* 65 (4-6), 39-104.
75. **Breedis, J.F. and Kaufman, L.** (1971). Formation of HCP and BCC phases in austenitic iron alloys. *Metall. Trans.* 2, 2359 - 2371.
76. **Shimizu, K. and Tanaka, Y.** (1978). The y + E + a' martensitic transformations in a Fe-Mn- C alloy. *Trans. Jpn Inst. Met*. 19, 685 - 693.
77. **Sin,H.C. and Suh,N.P.** (1984). Subsurface Crack Propagation Due to Surface Traction in Sliding Wear. *Applied Mechanics Transactions.* 51 (1), 317-323.
78. **Rigney,D.A. and Glaeser,W.A.** (1978). The Significance of Near Surface Microstructure in the Wear Process. *Wear.* 46 (1), 241-250.
79. **Rigney, D.A.** (2000). Transfer, Mixing and Associated Chemical and Mechanical Processes during the Sliding of Ductile Materials. *Wear*.245 (1), 1-9.
80. **Korshunov, L.G. and Mints, R.I.** (1969). Investigation of the wear resistance of metastable austenitic steels under dry sliding friction conditions. *Fiziko-Khimicheskaya Mekhanika Materialov.*5 (5), 569-572.
81. **Dumbleton, J.H. and Douthett, J.A.** (1977). The unlubricated adhesive wear resistance of metastable austenitic stainless steels containing silicon. *Wear.* 42 (2), 305-332.
82. **Bressanelli, J.P. and Moskowitz, A.** (1966). Effects of strain rate, temperature, and composition on tensile properties of metastable austenitic stainless steel. *AMS Transactions Quarterly.* 59, 223-239.
83. **Shende,V.** (1980). A study of the effect of metastability on the unlubricated sliding wear of austenitic stainless steels. Master Thesis. Department of Metallurgical Engineering, The Ohio University.
84. **Singer, I.L.; Vardiman, R.G. and Bolste r, R.N.** (1988). Polishing wear resistance of ion-implanted 304 steel. *Journal of Materials Research*. 3 (6), 1134-1143.
85. **Stott, F.H. and Jordan, M.P.** (2001). The effects of load and substrate hardness on the development and maintenance of wear-protective layers during sliding at elevated temperatures. *Wear.* 250 (1), 391-400.
86. **Hirsch, M.R. and Neu, R.W.** (2013). Influence of temperature on the fretting response between AISI 301 stainless steel and AISI 52100 steel. *Tribology International.* 68, 77-84.
87. **Smith, A.F.** (1985). The sliding wear of 316 stainless steel in air in temperature range 20-500^{o}C. *Tribology International.* 18 (1), 35-43.
88. **Dautzenberg, J.H. and Zaat, J.H.** (1973). Model of strain distribution by sliding wear. *Wear.* 26, 105-119.
89. **Newman, P.T. and Skinner, J.** (1986). The high temperature sliding wear of stainless steel in a CO_2 atmosphere-The effect of adding low concentrations of O_2. *Wear.* 112 (3-4), 291-325.
90. **Roy,M.; Pauschitz, A.; Wernisch, J. and Franek, F.** (2004). Effect of mating surface on the high temperature wear of 253 MA alloy. *Materials and Corrosion.* 55 (4), 259-273.
91. **Nature research.** (2018). *A nanomaterial to make your phone battery last.* Available: https://www.nature.com/articles/d41586-018-04884-w. Last accessed September 27th.
92. **Favre, J.** (2012). Recrystallization of L-605 Cobalt Superalloy during Hot-Working Process. PhD Thesis. Tohoku University.

93. **Kapoor, S.** (2012) High Temperature Hardness and Wear Resistance of Stellite Alloys. Phd Thesis. Carleton University.
94. **Sebastiani, M; Mangione, V.; De Felicis, D.; Bemporad, E. and Carassiti, F.** (2012).Wear mechanisms and in-service surface modifications of a Stellite 6B Co-Cr alloy.*Wear.*290-291 (1), 10-17.
95. **Liu, R.; Xu, W.; Yao, M.X.; Patnaik, P.C. and Wu, X.J.** (2005). A newly developed Tribaloy alloy with increase ductility. *Scripta Materialia.* 53 (1), 1351-1355.
96. **Renz, Alexander; Prakash, B.; Hardell, J. and Lehmann, O.** (2018). High-temperature sliding wear behaviour of Stellite®12 and Tribaloy®T400. *Wear.* 402-403 (1), 148-159.
97. **Nsoesie, S.; Liu. R.; Jiang, K. and Liang, M.** (2013). High-temperature Hardness and Wear Resistance of Cobalt-based Tribaloy Alloys. *International Journal of Material and Mechanical Engineering*. 2 (3), 48-56.
98. **Hull, M.** (2008). Tom Bell. *Surface Engineering. 24 (3), 167-169.*
99. **Holmberg, K. and Matthews A.** (1994). Tribology of Coatings. In: Holmberg, K. and Matthews A. *Coatings Tribology: Properties, Techniques and Applications in Surface Engineering.* Amsterdam: Elsevier. 33-124.
100. **Shepard, S.R. and Suh, N.P.** (1982). The effects of ion implantation on friction and wear of metals. *Journal of lubrication technology.* 104, 29-38.
101. **Bull, S.J. and Rickerby, D.S.** (1990). Compositional, microstructural and morphological effects on the mechanical and tribological properties of chromium nitrogen films. *Surface and Coatings Technology.* 43-44, 732-744.
102. **Leroy, J.M. and Villechaise, B.** (1990). Stress determination in elastic coatings and substrate under both normal and tangential loads. In: Downson, D. *Mechanics of coatings.* Amsterdam: Elsevier. 195-201.
103. **Sainsot, P.; Leroy, J.M. and Villechaise, B.** (1990). Effect of surface coatings in a rough normally loaded contact. In: Downson, D. *Mechanics of coatings.* Amsterdam: Elsevier. 151-156.
104. **Blomberg, A.; Erickson, L.; Lu, J.; Hogmark, S. and Olsson, M.** (1993). Improved wear resistance of ceramics through the use of coatings. *Surface and Coatings Technologies.* 57, 51-59.
105. **Burakowski, T. and Wierzchon, T.** (1999). *Surface Engineering of Metals: Principles, Equipment and Technologies*. London: CRC Press.
106. **Matijevic, B. and Stupnišek, M.** (2008). Novelty in Diffusion Coating Technology. *Materials and Manufacturing Processes*. 24 (1), 887-893.
107. **Behrani, V.** (2007). Surface Modifications of Steel to Improve Corrosion Resistance in Sulfidizing-Oxidizing Environments. *PhD Thesis.* Georgia Institute of Technology.
108. **Mervel, R.; Duret, C. and Pichoir, R.** (1986). Pack cementation processes. *Materials Science and Technology.* 2 (3), 201-206.
109. **Zandrahimi, M.; Vatandoost,J. and Ebrahimifar, H.** (2012). Pack Cementation Coatings for High-Temperature Oxidation Resistance of AISI 304 Stainless Steel. *Journal of Materials Engineering and Performance.* 21, 2074-2079.
110. **Stein, F.** (2009). Summer School on Iron Aluminides Part 1: The binary Fe-Al system*. In Proceedings of the 5th Discussion Meeting on the Development of Innovative Iron Aluminum Alloys in Prague*. Prague, Czech Republic.
111. **Zamanzade, M.; Barnoush, A. and Motz, C.** (2016). A review on the properties of Iron Aluminide Intermetallics. *Crystals.* 6(10), 1-29.
112. **McKamey, C.; Horton, J. and Liu, C.** (1989) Effect of chromium on properties of Fe3Al. *Journal of Materials Research*. 4, 1156–1163
113. **Koster, W. and Godecke, T.** (1982). Physical measurements on iron-aluminium alloys between 10 and 50 at.-% Al. Iv.—The modulus of elasticity of the alloys. *International Journal of Materials Research*. 73, 111–114.

114. **Sharma,G.; Limaye, P.K, Ramanujan, R.V.; Sundararaman, M. and Prabhu,N.** (2004). Dry-sliding wear studies of Fe3Al-ordered intermetallic alloy. *Material Science and Engineering A.* 386, 408-414.
115. **Yang, J.; La, P.; Liu, W. and Xue, Q.** (2004). Tribological properties of FeAl intermetallics under dry sliding. *Wear*. 257, 104-109.
116. **Zhang, Q.Y.; Zhou, Y.; Liu, J.Q.; Chen, K.M.; Mo, J.G.; Cui, X.H. and Wang, S.Q.** (2015). Comparative research on dry sliding wear of hot-dip aluminized and uncoated H13 steel. *Wear.* 344-345, 22-31.
117. **Kato, H.** (2003). Severe-mild wear transition by supply of oxide particles on sliding surface. *Wear.* 255 (1-6), 426-429.
118. **Ahmadi, H. and Li, D.Y.** (2003). Beneficial effects of yttrium on mechanical properties and high-temperature wear behaviour of surface aluminized 1045 steel. *Wear.* 255 (7-12), 933-942.
119. **Davis, J.R.** (2002). *Surface Hardening of Steels: understanding the basics*. USA: ASM International.
120. **Carbucicchio, M.; Bardani, L. and Sambogna, G.** (1983). On the early stages of high purity iron boriding with crystalline boron powder. *Journal of Materials Science.* 18, 3355-3362.
121. **Campos-Silva, I.E. and Rodriguez-Castro, G.A.** (2015). Boriding to improve the mechanical properties and corrosion resistance of steels. In: Mittemeijer, E.J. and Somers, M.A.J. *Thermochemical Surface Engineering of Steels.* London: Woodhead Publishing. 651-702.
122. **Factsage**. (2006). *Fe-B*. Available: http://www.factsage.cn/fact/documentation/BINARY/B-Fe.jpg. Last accessed 16th October 2018.
123. **Tabur, M.; Izciler, M.; Gul,F. and Karacan, I.** (2009). Abrasive wear behaviour of boronized AISI 8620 steel. *Wear.* 266, 1106-1112.
124. **Wang, A.G. and Hutchings, I.M.** (1988). Mechanisms of abrasive wear in a boronized alloy. *Wear.* 124, 149-163.
125. **Jain, V. and Sundararajan, G.** (2002). Influence of the pack thickness of the boronizing mixture on the boriding of steel. *Surface Coating Technology.* 149, 21-26.
126. **Motallebzadeh, A.; Dilektasli, M.; Baydogan, M.; Atar, E. and Cimenoglu, H.** (2015). Evaluation of the effect of borided layer structure on the high temperature wear behaviour of borided steels *Wear.* 328-329, 110-114.
127. **Cimenoglu, H.; Atar, E. and Motallebzadeh, A.** (2014). High temperature tribological behaviour of borided surfaces based on the phase structure of the borided layer. *Wear.* 309 (1-2), 152-158.
128. **Taktak, S.** (2006). Tribological behaviour of borided bearing steels at elevated temperatures. *Wear.* 201, 2230-2239.
129. **Kaluba, W. and Foct, J.** (1986). Structural and Physicochemical Factors Controlling the Formation of Chromium Carbide Cases During Chromizing. *Proceedings of the AST World Conference Advances in Surface Treatments and Surface Finishing.* 5, 93-110.
130. **Castle, A.R. and Gabe, D.R.** (2013). Chromium diffusion coatings. *International Materials Reviews.* 44 (2), 37-58.
131. **Lin, N.; Xie, F.; Yang, H, Tian, W.; Wang, H. and Tang, B.** (2012). Assessments on friction and wear behaviours of P110 steel and chromizing coating sliding against two counterparts under dry and wet conditions. *Applied Surface Science.* 258 (11), 4960-4970.
132. **Lee, J.W.** (2005). Microstructures and mechanical properties of hard chromized austenitic Fe-Mn-Al alloys. *Applied Surface Science.* 244 (1-4), 248-251.
133. **Taktak, S.; Ulker, S. and Gunes, I.** (2008). High temperature wear and friction properties of duplex surface treated bearing steels. *Surface and Coatings Technology.* 202 (14), 3367-3377.
134. **Hakami, F.; Sohi, M.H. and Ghani, J.R**. (2011) Duplex surface treatment of AISI 1045 steel via plasma nitriding of chromized layer. *Thin Solid Films.* 519 (20), 6792-6796.

135. **Korwin, M.J.; Morawski, C.D.; Tymowski, G.J. and Liliental, W.K.** (2016). Nitrided and Nitrocarburized Materials: Design. In Totten, E.G. and Colas, R. *Encyclopaedia of Iron, Steel, and Their Alloys.* Boca Raton: CRC Press. 2317-2356.

136. **Schneider. R.S.E.** (2015). Austenitic nitriding and nitrocarburizing of steels. In: Mittemeijer, E.J. and Somers, M.A.J. *Thermochemical Surface Engineering of Steels.* London: Woodhead Publishing. 373-391.

137. **Somers, M.A.J.** (2015). Development of the compound layer during nitriding and nitrocarburizing of iron and iron-carbon alloys. In: Mittemeijer, E.J. and Somers, M.A.J. *Thermochemical Surface Engineering of Steels.* London: Woodhead Publishing. 341-372.

138. **Wahl, G.** (1995). Component Properties after Salt-bath Nitrocarburizing by the Tufftride Process. *Heat Treatment of Metals.* 22 (3), 65-73.

139. **Jacquet, P.; Coudert, J.B. and Lourdin, P.** (2011). How different steel grades react to a salt bath nitrocarburizing and post-oxidation process: Influence of alloying elements. *Surface and Coatings Technology.* 205 (16), 4064-4067.

140. **Sola, R.; Giovanardi, R.; Veronesi, P. and Poli, G.** (2011). Improvement of wear and corrosion resistance of ferrous alloys by post-carburizing treatments. *Metallurgical Science and Technology.* 29 (2), 14-24.

141. **Psyllaki, P.; Kefalonikas, G.; Pantazopoulos, G.; Antoniou, S. and Sideris, J.** (2003). Microstructure and tribological behaviour of liquid nitrocarburised tool steels. *Surface and Coatings Technology.* 162 (1), 67-78.

142. **Heydarzadeh Sohi, M.; Ebrahimi, M.; Honarbakhsh Raouf, A. and Mahboubi,F.** (2010). Effect of plasma nitrocarburizing temperature on the wear behaviour of AISI 4140 steel. *Surface and Coatings Technology.* 205 (1), S84-S89.

143. **Qiang, Y.H.; Ge, S.R. and Xue, Q.J.** (2000). Microstructure and tribological properties of complex nitrocarburized steel. *Journal of Materials Processing Technology.* 101 (1-3), 180-185.

144. **Emami, M.; Ghasemi, H.M. and Rassizadehghani, J.** (2010). High temperature tribological behaviour of 31CrMoV9 gas nitride steel. *Surface Engineering*. 26 (3), 168-172.

145. **Pellizzari, M.** (2011). High temperature wear and friction behaviour of nitride, PVD-duplex and CVD coated tool steel against 6082 Al alloy. *Wear.* 271 (9-10), 2089-2099.

146. **Tanaka, Y.; Gur, T.M.; Kelly, M.; Hagstrom, S.B.; Ikeda, T.; Wakihira, K. and Satoh, H.** (1998). Properties of ($Ti_{1-x}Al_x$)N coatings for cutting tools prepared by the cathodic arc ion plating method. *Journal of Vacuum Science & Technology A.* 10, 1749.

147. **Wahlstrom, U.; Hultman, L.; Sundgren, J.-E.; Adibi,F.; Petrov, I. and Greene, J.E.** (1993). Crystal growth and microstructure of polycrystalline Ti1-XalXN alloy films deposited by ultra-high-vacuum dual-target magnetron sputtering. 235, 62-70.

148. **Chen, L.; Chang, K.K.; Du, Y.; Li, J.R. and Wu, M.J.** (2011). A comparative research on magnetron sputtering and arc evaporation deposition of Ti-Al-N coatings. *Thin Solid Films.* 519 (11), 3762-3767.

149. **Hörling, A.; Hultman, L.; Oden,M.; Sjölén, J. and Karlsson, L.** (2005). Mechanical properties and machining performance of $Ti_{1-x}Al_xN$-coated cutting tools. *Surface and Coatings Technology.* 191 (2-3), 384-392.

150. **Rodriguez, R.J.; Garcia, J.A.; Medrano, A.; Rico, M.; Sanchez, R.; Martinez, R.; Labrugere, C.; Lahaye, M. and Guette,A.** (2002). Tribological behaviour of hard coatings deposited by arc-evaporation PVD. *Vacuum.* 67 (3-4), 559-566.

151. **Aihua, L.; Jianxin, D.; Haibing, C.; Yangyang, C. and Jun, Z.** (2012). Friction and wear properties of TiN, TiAlN, AlTiN and CrAlN PVD nitride coatings. *International Journal of Refractory Metals and Hard Materials.*31, 82-88.

152. **Hsieh, J.H.; Tan, A.L.K. and Zeng. X.T.** (2006). Oxidation and wear behaviours of Ti-based thin films. *Surface & Coatings Technology.* 201, 4094-4098.
153. **Mayrhofer P.H.; Hörling, A.; Karlsson, L.; Sjölén, J.; Larsson, T.; Mitterer, C. and Hultman, L.** (2003). Self-organized nanostructures in the Ti-Al-N system. *Applied Physics Letters.* 83 (10), 2049-2051.
154. **Liu, A.H. and Deng, J.X.** (2015). Elevated temperature tribological properties of AlTiN up to 700oC. *Surface Engineering.* 31 (1), 17-23).
155. **Dejun, K. and Haoyuan, G.** (2015). Friction-wear behaviours of cathodic arc ion plating AlTiN coatings at high temperatures. *Tribology International.* 88, 31-39.
156. **Nohava, J.; Dessarzin, P.; Karvankova, P. and Morstein. M.** (2012). Tribological Characterization and Wear Mechanisms of Novel Oxynitride PVD coatings Designed for Applications at High Temperatures. *13th International Conference on Plasma Surface Engineering*, Germany, 10-14.
157. **Oden, M.; Ericsson, C.; Hakansson, G. and Ljungcrantz, H.** (1999). Microstructure and mechanical behaviour of arc-evaporated Cr-N coatings. *Surface and Coatings Technology.* 114 (1), 39-51.
158. **Mayrhofer, P.H.; Tischler,G. and Mitterer,C.** (2001). Microstructure and mechanical/thermal properties of Cr-N coatings deposited by reactive unbalanced magnetron sputtering. *Surface and Coatings Technology.* 142-144, 78-84.
159. **Lin, J.; Zhang, N.; Sproul, W.D. and Moore, J.J.** (2012). A comparison of the oxidation behaviour of CrN films deposited using continuous dc, pulse dc and modulated pulse power magnetron sputtering. *Surface and Coatings Technology.* 206 (14), 3283-3290.
160. **Mayrhofer, P.H.; Willmann, H. and Mitterer, C.** (2001). Oxidation kinetics of sputtered Cr-N hard coatings. *Surface and Coatings Technology.*146-147, 222-228.
161. **Lee, D.; Lee, Y. and Kwon, S.** (2001). High temperature oxidation of a CrN coating deposited on steel substrate by ion plating. *Surface and Coatings Technology.* 141 (2-3), 227-231.
162. **Kimura, A.; Kawate, M.; Hasegawa, H. and Suzuki, T.** (2003). Anisotropic lattice expansion and shrinkage of hexagonal TiAlN and CrAlN. *Surface and Coatings Technology.*169-170, 367-370.
163. **Makino. Y and Nogi, K.** (1998). Synthesis of pseudobinary Cr-Al-N films with B1 structure by rf-assisted magnetron sputtering method. *Surface and Coatings Technology.* 98 (1-3), 1008-1012.
164. **Lin, J.; Mishra, B.; Moore, J.J. and Sproul, W.D.** (2008). A study of the oxidation behaviour of CrN and CrAlN thin films in air using DSC and TGA analyses. *Surface and Coatings Technology.* 202 (14), 3272-3283.
165. **Apreutesei, M**. (2015) Temperature impact on thermal evolution of advanced PVD ceramic and metallic glass thin films: Physico-chemical and microstructural analysis. PhD Thesis. INSA de Lyon.
166. **Wu, Z.T.; Qui, Z.B.; Zhu, F.P.; Liu, B.and Wang, Z.C.** (2013). Influences of Y Addition on Mechanical Properties and Oxidation Resistance of CrN Coating. *Physics Procedia*. 50, 150-155.
167. **Rovere, F.; Mayrhofer, P.H.; Reinholdt, A.; Mayer, J. and Schneider, J.M.** (2008). The effect of yttrium incorporation on the oxidation resistance of Cr-Al-N coatings. *Surface and Coatings Technology*. 202 (24), 5870-5875.
168. **Rojas, T.C.; Dominguez-Meister.S; Brizuela, M. and Sanchez-Lopez, J.C.** (2018). High-temperature oxidation of CrAlYN coatings: Implications of the presence of Y and type of steel. *Surface and Coatings Technology.* 354, 203-213.
169. **Lembke, M., Titchmarsh, J., Lewis, D., & Münz, W.** (2000). Investigation of The Oxidation Behaviour of A TiAlCrYN Pvd Hard Coating. *MRS Proceedings*, 648, P6.57.

170. **Hones, P.; Martin, N.; Regula, M. and Levy, F.** (2003). Structural and mechanical properties of chromium nitride, molybdenum nitride, and tungsten nitride thin films. *Journal of Physics D: Applied Physics.* 36, 1023-1029.

171. **Reiter, A.E.; Derflinger, V.H.; Hanselmann, B.; Bachmann, T. and Sartory, B.** (2005). Investigation of the properties of $Al_{1-x}Cr_xN$ coatings prepared by cathodic arc evaporation. *Surface and Coatings Technology.* 200 (7), 2114-2122.

172. **Wang, L. and Nie, X.** (2013). Effects of annealing temperature on tribological properties and material transfer phenomena of CrN and CrAlN coatings. *Journal of Materials Engineering Performance.* 23 (2), 560-571.

173. **Ding, X.-Z. and Zeng, X.T.** (2005). Structural, mechanical and tribological properties of CrAlN coatings deposited by reactive unbalanced magnetron sputtering. *Surface and Coatings Technology.* 200 (5-6), 1372-1376.

174. **Hall, E.O.** (1951). The Deformation and Ageing of Mild Steel: III Discussion of Results. *Proceedings of the Physical Society Section B*. 64 (9), 747-753.

175. **Sundgren, J.-E. and Hentzell, H.T.G.** (1986). A review of the present state of art in hard coatings grown from the vapour phase. *Journal of Vacuum Science & Technology.* 4 (5), 2259-2279.

176. **Willmann, H.; Mayrhofer, P.H.; Hultman, L. and Mitterer, C.** (2008). Hardness evolution of Al-Cr-N coatings under thermal load. *Journal of Materials Research.* 23 (11), 2880-2885.

177. **Sanchez, J.E.; Sanchez, O.M.; Ipaz, L.; Aperador, W.; Caicedo, J.C.; Amaya, C.; Hernandez Landaverde, M.A.; Espinoza Beltran, F. Munoz-Saldana, J. and Zambrano, G.** (2010). Mechanical, tribological, and electrochemical behaviour of $Cr_{1-x}Al_xN$ coatings deposited by r.f. reactive magnetron co-sputtering method. *Applied Surface Science.* 256, 2380-2387.

178. **Veprek, S.** (1999). The search for novel, superhard materials. *Journal of Vacuum Science & Technology A.* 17 (5), 2401-2420.

179. **Callister, W.D.** (2010). *Materials Science and Engineering*. London: John Wiley & Sons, Inc.

180. **Su, Y.L.; Yao, S.H.; Leu, Z.L., Wei, C.S. and Wu, C.T.** (1997). Comparison of tribological behaviour of three films-TiN, TiCN and CrN-grown by physical vapour deposition. *Wear.* 213, 165-174.

181. **Yao, S.H. and Su, Y.L.** (1997). The tribological potential of CrN and Cr(C, N) deposited by multi-arc PVD process. *Wear.* 212, 85-94.

182. **Warcholinski, B. and Gilewicz, A.** (2009). Tribological properties of CrN_x coatings. *Journal of Achievements in Materials and Manufacturing Engineering.* 37 (2), 498-504.

183. **Lin, J.; Sproul, W.D. and Moore, J.J.** (2012). Tribological behaviour of thick CrN coatings deposited by modulated pulsed power magnetron sputtering. *Surface and Coatings Technology.* 206 (8-9), 2474-2483.

184. **Bobzin, K.; Lugscheider, E.; Nickel, R.; Bagcivan, N. and Kramer, A.** (2007). Wear behaviour of $Cr_{1-x}Al_xN$ PVD-coatings in dry running environments. *Wear.* 263, 1274-1280.

185. **Mo, J.L. and Zhu, M.H.** (2009). Tribological oxidation behaviour of PVD hard coatings. *Tribology International*. 42, 1758-1764.

186. **Zhang, C.; Gu, L.; Tang, G. and Mao, Y.** (2017). Wear Transition of CrN Coated M50 Steel under High Temperature and Heavy Load. *Coatings.* 202 (7); 1-18.

187. **Polcar, T.; Kubart, T.; Novak, R.; Kopecky, L. and Siroky, P.** (2005). Comparison of tribological behaviour of TiN, TiCN and CrN at elevated temperatures. *Surface and Coatings Technology.* 193 (1-3); 192-199.

188. **Sue, J.A. and Chang, T.P.** (1995). Friction and wear behaviour of titanium nitride, zirconium nitride and chromium nitride coatings at elevated temperatures. *Surface and Coatings Technology.* 76-77, 61-69.

189. **Polcar, T.; Martinez, R.; Vitu, T.; Kopecky, L.; Rodriguez, R. and Cavaleiro, A.** (2009). High Temperature tribology of CrN and multi-layered Cr/CrN coatings. *Surface and Coatings Technology.* 203, 3254-3259.

190. **Gangatharan, K.; Narayanasamy, P. and Selvakumar, N.** (2016). Mechanical analysis and high temperature wear behaviour of AlCrN/DLC coated titanium alloy. *International Journal of Surface Science and Engineering.* 10, 27-40.
191. **Polcar, T. and Cavaleiro, A.** (2011). High-temperature tribological properties of CrAlN, CrAlSiN and AlCrSiN coatings. *Surface and Coatings Technology.*206 (6), 1244-1251.
192. **Pulugurtha, S.R.; Bhat, D.G.; Gordon, M.H.; Shultz, J.; Staia, M.; Joshi, S.V. and Govindarajan, S.** (2007). Mechanical and tribological properties of compositionally graded CrAlN films deposited by AC reactive magnetron sputtering. *Surface and Coatings Technology.* 202, 1160-1166.
193. **Holmberg, K. and Matthews, A.** (2009). *Coatings Tribology: Properties, Mechanisms, Techniques and Applications in Surface Engineering*. 2nd ed. Amsterdam: Elsevier Science.
194. **James, D.H.** (1978). Balancing resources and requirement in surfacing. *Surfacing J*. 9 (3),
195. **Smart, R.F.** (1978). Selection of surfacing treatments. *Tribology International*. 11 (2), 97-104.
196. **AZoM.** (2009). *Grade 304L Stainless Steel for Severely Corrosive Conditions (UNS S30403).* Available: https://www.azom.com/article.aspx?ArticleID =5049. Last accessed 1st Aug 2018.
197. **AZoM.** (2001). *Stainless Steel Grade 321 (UNS S32100).* Available: https://www.azom.com/article.aspx?ArticleID =967. Last accessed 1st Aug 2018.
198. **AZoM.** (2013). *Super Alloy Nitronic 60 (UNS S21800).* Available: https://www.azom.com/article.aspx?ArticleID =9599. Last accessed 1st Aug 2018.
199. **Deloro.** (2016). *STELLITE™ 6 ALLOY.* Available: https://static1.squarespace.com/static/56e079802fe131546a70830d/t/577aa957d2b85735f832e0cd/1467656536896/Deloro+MDS+Stellite6+rev00.pdf. Last accessed 1st Aug 2018.
200. **Deloro.** (2016). *TRIBALOY™ T-400 ALLOY.* Available: https://static1.squarespace.com/static/56e079802fe131546a70830d/t/57d09f37b3db2b37b36455a5/1473290040780/Deloro+MDS+Tribaloy400+rev00.pdf. Last accessed 1st Aug 2018.
201. **Rottenfusser, R.; Wilson, E.E. and Davidson, M.W.** (n.a.). *Illumination and the Optical Train.* Available: http://zeiss-campus.magnet.fsu.edu/articles/basics/opticaltrain.html. Last accessed 1st Aug 2018.
202. **Buehler.** (2007). *Buehler® SumMet™- A Guide to Materials Preaparation & Analysis.* 2nd ed. Illinois: Buehler.
203. **Hariharan, P.** (2007). *Introduction. Basics of Interferometry*. London: Elsevier Science.
204. **Schmit, J.** (2014). *Surface Measurement 101 – Non-contact 3D Optical Metrology.* Available: https://www.bruker.com/fileadmin/user_upload/8-PDF-Docs/SurfaceAnalysis/3D-OpticalMicroscopy/Webinars/Surface_Metrology_101.pdf. Last accessed 1st Aug 2018.
205. **AZoM.** (2017). *Optical Metrology – Understanding Focus Variation.*Available: https://www.azom.com/article.aspx?ArticleID=13893. Last accessed 1st Aug 2018.
206. **Leach, R.K.** (2010) Fundamental Principles of Engineering Nanometrology, Elsevier, Ed. 1, Chapter 6, p. 142.
207. **Goldstein, J.I.; Newbury, D.E.;Michael, J.R.;Ritchie, N.W.M.;Scott,J.H.J. and Joy, D.C.** (2007). *Scanning Electron Microscopy and X-Ray Microanalysis*. 4th ed. New York: Springer Nature.
208. **Shamsudin, S.R.** (2011). *Scanning electron microscope (SEM) & how it works.* Available: http://emicroscope.blogspot.com/2011/03/scanning-electron-microscope-sem-how-it.html. Last accessed 2nd Aug 2018.
209. **University of Glasgow.** (2018). *Scanning Electron Microscopy (SEM).* Available: https://www.gla.ac.uk/schools/ges/researchandimpact/researchfacilities/isaac/services/scanningelectronmicroscopy/. Last accessed 2nd Aug 2018.

210. **Melngailis, J.** (1985). Focus Ion Beam Technology. *VLSI Memo*. 1, 1-15.
211. **Reyntjens, S. and Puers, R.** (2001). A review of focused ion beam applications in microsystem technology. *Journal of Micromechanics and Microengineering*. 11 (1), 287-300.
212. **Song, I.H., Peter, Y. and Meunier, M.** (2007). Smoothing dry-etched microstructure sidewalls using focused ion beam milling for optical applications. *Journal of Micromechanics and Microengineering*. 17 (8), 1593-1597.
213. **Williams, D.B. and Carter, C.B**. (2009). *Transmission Electron Microscopy: A Textbook for Material Science*. 2nd ed. New York: Springer. 1.
214. **Epp, J.** (2016). X-ray diffraction (XRD) techniques for materials characterization. In: Hübschen, G.; Altpeter, I.; Tschuncky, R. and Herrmann, H.G. *Materials Characterization Using Nondestructive Evaluation (NDE) Methods*. Amsterdam: Elsevier. 81-124.
215. **Waseda, Y.; Matsubara, E. and Shinoda, K.** (2011). *X-Ray Diffraction Crystallography*. London: Springer.
216. **Christopher, P**. (2000). Raman microscopic studies of PVD deposited hard ceramic coatings. Doctoral, Sheffield Hallam University (United Kingdom).
217. **Larkin, P.J.** (2011). *IR and Raman Spectroscopy: Principles and Spectral Interpretation*. London: Elsevier.
218. **University of Cambridge.** (2004). *Method (dispersive Raman spectroscopy).* Available: https://www.doitpoms.ac.uk/tlplib/raman/method.php. Last accessed 5th Aug 2018.
219. **Vidakis N, Antoniadis A, Bilalis N**. (2003) The VDI 3198 indentation test evaluation of a reliable qualitative control for layered compounds. Journal of Materials Processing Technology.143-144,481-485.
220. **Kayali, Y. and Taktak, S.** (2015) Characterization and Rockwell-C adhesion properties of chromium-based borided steels, *Journal of Adhesion Science and Technology*, 29:19, 2065-2075
221. **Fischer-Cripps, A.C.** (2011). *Nanoindentation*. 3rd ed. New York: Springer. 1
222. **Fuentes G, Almandoz E, Pierrugues R, Martínez R, Rodríguez R, Caro J.** (2010) High temperature tribological characterisation of TiAlSiN coatings produced by cathodic arc evaporation. Surface and Coatings Technology. 205(5),1368-1373.
223. **Johnson, K.** (1987). Contact mechanics. Cambridge [u.a.]: Cambridge Univ. Press.
224. **Wong, M.S.** (1989) Thin diamond films for tribological applications, *Mat. Res. Soc. Symp. Proc*. 140, 483-488
225. **Brunetti, C.; Belotti, L.P.; Miyoshi, M.H.; Pintaude, G. and D'Oliveira A.S.C.M.** (2014). Influence of Fe on the room and high-temperature sliding wear of NiAl coatings. *Surface and Coatings Technology.* 258, 160-167.
226. **Fox-Rabinovich, G.S.; Beake, B.D.; Endrino, J.L.; Veldhuis, S.C.; Parkinson, R.; Shuster, L.S. and Migranov.** (2006). Effect of mechanical properties measured at room and elevated temperaturas on the wear resistance of cutting tools with TiAlN and AlCrN coatings. *Surface & Coatings Technologies.* 200, 5738-5742.
227. **Derow, H. and Bleil, H.E**. (1970). Elevated Temperature Instability of Stellite 6B. *NASA.* https://ntrs.nasa.gov/search.jsp?R=19700016385. Last visited in 03/01/2019.
228. **Peng, J.; Fang, X.; Marx, V.; Jasnau, U. and Palm, M.** (2018). Isothermal oxidation behavior of Tribaloy T400 and T800. *Nature Partner Journals Materials Degradation*.1, 1-7.
229. **Zhang, Y. D. & Yang, Z**. (2007) Structure and oxidation behavior of Tribaloy alloy with iron and aluminum additions. J. Iron Steel Res. Int. 14, 30–34.
230. **Gulbransen, E. A., Andrew, K. F. & Brassart, F. A**. (1963) Oxidation of molybdenum 550° to 1700 °C. J. Electrochem. Soc. 110, 952–959.